ISBN: 978-81-69967-27-3

# RESEARCH AND REVIEWS IN MATHEMATICAL AND STATISTICAL SCIENCE



Editors:
Dr. Chakrala Sreelatha
Dr. Sudha Bishnoi
Dr. Paban Dhar

Bhumi Publishing, India
First Edition: November 2026

**Research and Reviews in Mathematical and Statistical Science**

**(ISBN: 978-81-69967-27-3)**

**DOI: https://doi.org/10.5281/zenodo.24341862**

## Editors

**Dr. Chakrala Sreelatha**

Assistant Professor and Head,

Department of Statistics,

Rajendra University,

Balangir, Odisha

**Dr. Sudha Bishnoi**

Assistant Scientist (Statistics),

Department of Mathematics and Statistics,

Chaudhary Charan Singh Haryana

Agricultural University, Hisar, Haryana

**Dr. Paban Dhar**

Assistant Professor,

Department of Mathematics,

Karimganj College, Sribhumi, Assam

Bhumi Publishing

**November 2026**

Copyright © Editors

Title: Research and Reviews in Mathematical and Statistical Science

Editors: Dr. Chakrala Sreelatha, Dr. Sudha Bishnoi, Dr. Paban Dhar

First Edition: November 2026

ISBN: 978-81-69967-27-3




DOI: https://doi.org/10.5281/zenodo.24341862

All rights reserved. No part of this publication may be reproduced or transmitted, in any form or by any means, without permission. Any person who does any unauthorized act in relation to this publication may be liable to criminal prosecution and civil claims for damages.

***Published by Bhumi Publishing,***

***a publishing unit of Bhumi Gramin Vikas Sanstha***

Bhumi Publishing

**Nigave Khalasa, Tal – Karveer, Dist – Kolhapur, Maharashtra, INDIA 416 207**

**E-mail: bhumipublishing@gmail.com**

**Disclaimer:** The views expressed in the book are of the authors and not necessarily of the publisher and editors. Authors themselves are responsible for any kind of plagiarism found in their chapters and any related issues found with the book.

## *PREFACE*

Mathematics and statistics are fundamental disciplines that provide the theoretical foundations and analytical tools for understanding complex phenomena, solving practical problems, and advancing scientific knowledge. Their applications extend across science, technology, engineering, economics, healthcare, business, and social sciences. With the growing importance of computational methods, data analysis, and quantitative research, mathematical and statistical approaches continue to evolve, creating new opportunities for innovation and interdisciplinary investigation. *Research and Reviews in Mathematical and Statistical Science* brings together diverse scholarly perspectives that highlight contemporary developments, research findings, and emerging applications in these disciplines.

This volume encompasses various areas of mathematical and statistical inquiry, including pure mathematics, applied mathematics, algebra, analysis, geometry, differential equations, numerical methods, probability theory, statistical modelling, and data interpretation. Contemporary developments in computational mathematics, optimization techniques, mathematical modelling, machine learning, and statistical inference are expanding the scope of research and providing effective approaches to real-world challenges. These contributions demonstrate how mathematical reasoning and statistical methodologies support evidence-based decision-making, predictive analysis, and scientific discoveries.

The book emphasizes the significance of theoretical exploration alongside practical applications. Mathematical formulations, analytical investigations, experimental data analysis, and computational techniques collectively strengthen research methodologies and encourage innovative problem-solving. Interdisciplinary applications further demonstrate the relevance of mathematical and statistical sciences in addressing emerging challenges across diverse fields of knowledge.

This volume is intended for researchers, academicians, mathematicians, statisticians, teachers, students, and professionals interested in advancing mathematical and statistical understanding. It seeks to promote scholarly communication, encourage critical thinking, and provide opportunities for further research and collaboration. It is hoped that this book will serve as a valuable academic reference and stimulate new investigations in mathematical and statistical sciences.

**- Editors**

**TABLE OF CONTENT**


| Sr. No. | Book Chapter and Author(s) | Page No. |
|---|---|---|
| 1. | **A HYBRID DECISION TREE AND FUZZY PETRI NET FRAMEWORK FOR STROKE RISK CLASSIFICATION AND ASSESSMENT**<br>S. Meher Taj and P. Vijayaraj | 1 – 6 |
| 2. | **MATHEMATICAL MODELLING WITH DIFFERENTIAL EQUATIONS: THEORY, COMPUTATION AND EMERGING DATA-DRIVEN DISCOVERY**<br>Yokeshwari Ravi and Balaganesan Palanivelu | 7 – 18 |
| 3. | **MATHEMATICAL MODELLING OF DRUG DELIVERY SYSTEMS: DIFFERENTIAL EQUATIONS AND STATISTICAL OPTIMIZATION**<br>Venkatesan R, Shobika P, Pradeep U,<br>Purusothaman R and Subash S | 19 – 30 |
| 4. | **KEYED JULIA-POTENTIAL FIELDS: A PARAMETER-SENSITIVE FRACTAL CARRIER FOR BLIND IMAGE WATERMARKING**<br>S. Ramaswami and Salahuddin | 31 – 36 |
| 5. | **INDUSTRIAL WASTE VALORIZATION AND SUSTAINABLE MATERIAL DESIGN: A DATA-DRIVEN STATISTICAL APPROACH**<br>Sthitadhi Das | 37 – 83 |
| 6. | **UNCERTAINTY MODELLING WITH ADVANCED FUZZY LOGIC SYSTEMS**<br>Vicky B. Watkar | 84 – 88 |
| 7. | **STATISTICAL ANALYSIS OF POPULATION GROWTH USING DIFFERENTIAL EQUATIONS: A MATHEMATICAL AND STATISTICAL MODELLING APPROACH**<br>S. Revathi | 89 – 96 |
| 8. | **ON THE SOLVABILITY OF AN INFINITE SYSTEM OF THREE POINT BOUNDARY VALUE PROBLEM IN THE SEQUENCE SPACES $\mathbf{m}(\Phi)$ AND $\mathbf{m^B}(\Phi)$ USING MEIR-KEELER CONDENSING OPERATORS**<br>Washmin Ara Begum and Rituparna Das | 97 – 115 |

*Research and Reviews in Mathematical and Statistical Science*
*(ISBN: 978-81-69967-27-3)*

# A HYBRID DECISION TREE AND FUZZY PETRI NET FRAMEWORK FOR STROKE RISK CLASSIFICATION AND ASSESSMENT

**S. Meher Taj* and P. Vijayaraj**
Department of Mathematics,
AMET Deemed to be University, Chennai -603112, Tamil Nadu
*Corresponding author Email: mehertaj.s@ametuniv.ac.in

**Abstract**

This study presents an interpretable hybrid framework that combines a supervised decision tree with a Fuzzy Petri Net (FPN) for stroke classification and assessment. The decision tree is trained on demographic and health-related attributes, and its root-to-leaf paths are extracted as IF–THEN rules. These rules are mapped into an FPN in which condition places represent antecedent evidence, transitions represent extracted rules, and output places accumulate stroke-class evidence. To introduce graded evidence around numerical split boundaries, sigmoid membership functions are used for numerical predicates, while one-hot categorical predicates are evaluated crisply. The supplied dataset contains 5,110 records, including 249 stroke-positive records (4.87%); missing body-mass-index values are imputed using the training-set median. In a stratified 80:20 holdout experiment, a depth-limited, class-weighted decision tree achieved ROC-AUC 0.830 and stroke recall 0.840. The FPN rule-execution score achieved ROC-AUC 0.831 and stroke recall 0.840, with modestly higher accuracy, F1 and average precision at a 0.5 threshold. The results demonstrate a reproducible proof of concept for combining rule interpretability with fuzzy evidence aggregation. The model is not clinically validated; class imbalance, false positives, dataset provenance and lack of external validation limit clinical interpretation.

**Keywords:** Stroke Classification, Decision Tree, IF–THEN Rule Extraction, Fuzzy Petri Net, Fuzzy Inference, Explainable Machine Learning, Imbalanced Data

## 1. Introduction

Stroke is a serious health event for which early recognition of risk factors is important. Machine-learning models can identify patterns in structured health data, but a prediction score alone may be difficult for a practitioner or researcher to interpret. Decision trees offer a transparent structure of feature tests and class-labelled leaves. Their paths can be written as IF–THEN rules, providing a direct route from data-driven learning to a symbolic knowledge representation.

Fuzzy Petri Nets extend rule-based representations by associating places with propositions or conditions, transitions with inference rules, and tokens with truth or confidence values. This structure can represent the activation of multiple conditions and the propagation of graded

evidence. The present work uses a decision tree as the rule-generation mechanism and an FPN-inspired execution layer to evaluate the extracted rules. The intended contribution is a reproducible computational workflow, not a claim that the model can diagnose stroke or replace medical assessment.

## 2. Literature Review

Machine learning techniques have been widely applied to stroke classification using clinical attributes such as age, hypertension, heart disease, glucose level, and body mass index. Daeechini *et al.* (2024) reviewed machine learning algorithms for stroke prediction and highlighted the importance of selecting appropriate models and evaluation metrics for imbalanced datasets. Their findings indicate that no single algorithm consistently outperforms others across all datasets.

Decision trees are useful in healthcare classification because they generate interpretable IF–THEN rules. Breiman *et al.* (1984) discussed tree-based methods for classification and prediction, providing a foundation for decision-tree modelling. These rules help identify relationships between patient characteristics and stroke outcomes; however, model performance may be affected by data variations and class imbalance.

Zadeh (1965) introduced fuzzy set theory to represent uncertainty through degrees of membership. Fuzzy Petri Nets integrate fuzzy reasoning with Petri net structures, representing conditions, inference rules, and conclusions. Jensen (1997) described Petri nets as a formal framework for modelling systems involving states and transitions, supporting their use in structured rule-based decision-making.

Stroke datasets often contain considerably fewer stroke-positive cases than non-stroke cases. Saito and Rehmsmeier (2015) demonstrated the importance of precision–recall curves when evaluating classifiers on imbalanced datasets. Therefore, metrics such as precision, recall, F1-score, ROC-AUC, and average precision provide a more comprehensive assessment than accuracy alone.

Although machine learning, decision trees, and fuzzy reasoning have been investigated in healthcare, integrating decision-tree rule extraction with Fuzzy Petri Net inference offers a promising approach to interpretable stroke classification. Accordingly, this study proposes a hybrid Decision Tree–Fuzzy Petri Net framework that extracts rules from clinical data and uses them for structured inference. The framework is evaluated using multiple classification metrics, although further clinical validation is necessary before practical medical application.

## 3. Dataset and Preprocessing

The supplied CSV contains 5,110 rows and 12 columns: an identifier, ten predictor fields, and the binary target stroke. The target contains 249 positive records and 4,861 negative records, so the positive class represents approximately 4.87% of the data. BMI has 201 missing values

(approximately 3.93%); other columns in this file have no missing values. The identifier column is removed because it is not a meaningful clinical predictor.

| Item | Value | Handling |
|---|---|---|
| Records | 5,110 | All supplied rows |
| Target positives | 249 (4.87%) | Stroke = 1 |
| Target negatives | 4,861 (95.13%) | Stroke = 0 |
| Missing BMI | 201 | Median imputation fitted on training data |
| Categorical fields | gender, ever_married, work_type, Residence_type, smoking_status | Most-frequent imputation if needed, then one-hot encoding |
| Split | 80% train / 20% test | Stratified; random_state = 42 |

Preprocessing is fitted only on the training partition and then applied to the test partition. This avoids estimating imputation and category-encoding parameters from the test data. The split is stratified to preserve the low positive-class proportion. A class-weighted decision tree is used to reduce the training penalty for missing minority-class examples. Because class weighting can increase false positives, precision, recall, and the confusion matrix are reported alongside accuracy.

## 4. Proposed Hybrid Methodology

### 4.1 Fuzzy Petri Nets

Petri Nets (PN), which are mathematical and graphical modeling tools that can be used for a variety of systems, include fuzzy Petri Nets (FPN). Concurrent, asynchronous, distributed, parallel, nondeterministic, and stochastic information processing systems can all be modeled and studied using promising methods (Liu and Shi, 2000). There are two kinds of nodes in fuzzy Petri nets: transitions and locations, which are shown by rectangles and circles, respectively. Every location denotes a predecessor or consequent, and it may or may not have a token that indicates the degree of confidence (zero to one). A certainty factor value between 0 and 1 is given to each transition that expresses a rule. The degree of confidence in the rule is indicated by the certainty factor (Kouzehgar *et al.,* 2011).

### 4.2 Decision-Tree Learning

A DecisionTree Classifier is fitted with maximum depth 4, minimum leaf size 20, class_weight='balanced', and random_state 42. The depth limit encourages a compact, inspectable rule set. Each path from the root to a terminal leaf becomes a rule. For example, a path containing age > 67.5, age <= 73.5, and avg_glucose_level <= 176.97 becomes an IF–THEN rule whose consequent is the leaf's stroke-class membership/probability. Exact rule conditions and leaf statistics are generated by the accompanying Python script.

### 4.3 Decision-Tree-To-Rule Extraction

For every internal node, the algorithm records the tested feature, threshold, and branch operator (<= for the left branch and > for the right branch). Traversal continues until a leaf is reached. The accumulated conditions are joined with AND to form the antecedent. The leaf class distribution supplies the consequent membership. Thus, a rule can be represented as IF A1 AND A2 AND ... AND Ak THEN stroke-membership = c, where c is the proportion of stroke-positive training examples at that leaf. These are learned associations and must not be interpreted as causal statements.

R1: IF age <= 47.50 AND age <= 37.50 AND age <= 1.36 AND bmi <= 19.85 THEN class 0

R2: IF age <= 47.50 AND age <= 37.50 AND age <= 1.36 AND bmi > 19.85 THEN class 1

R3: IF age <= 47.50 AND age <= 37.50 AND age > 1.36 THEN class 0

R4: IF age <= 47.50 AND age > 37.50 AND bmi <= 45.70 AND avg_glucose_level <= 59.03 THEN class 0

R5: IF age <= 47.50 AND age > 37.50 AND bmi <= 45.70 AND avg_glucose_level > 59.03 THEN class 0

R6: IF age <= 47.50 AND age > 37.50 AND bmi > 45.70 THEN class 1

R7: IF age > 47.50 AND age <= 67.50 AND bmi <= 27.25 AND bmi <= 26.45 THEN class 0

R8: IF age > 47.50 AND age <= 67.50 AND bmi <= 27.25 AND bmi > 26.45 THEN class 0

R9: IF age > 47.50 AND age <= 67.50 AND bmi > 27.25 AND bmi <= 28.55 THEN class 1

R10: IF age > 47.50 AND age <= 67.50 AND bmi > 27.25 AND bmi > 28.55 THEN class 1

R11: IF age > 67.50 AND age <= 73.50 AND avg_glucose_level <= 176.97 THEN class 1

R12: IF age > 67.50 AND age <= 73.50 AND avg_glucose_level > 176.97 THEN class 1

R13: IF age > 73.50 AND bmi <= 34.20 THEN class 1

R14: IF age > 73.50 AND bmi > 34.20 THEN class 1

## 5. Experimental Setup

Experiments were run on the supplied CSV with a stratified 80:20 split (4,088 training records and 1,022 test records), random_state 42, a maximum tree depth of 4 and minimum leaf size 20. The fitted tree has 14 leaves, producing 14 root-to-leaf rules. The metrics below are computed on the held-out test partition. ROC-AUC and average precision use continuous scores; the other listed classification metrics use the 0.5 threshold.

## 6. Results

**Table 1: Performance comparison of Decision Tree and Fuzzy Petri Net Rule execution models**

| Model | Accuracy | Precision | Recall | F1 | ROC-AUC | PR-AUC / AP |
|---|---|---|---|---|---|---|
| Decision Tree | 0.6487 | 0.1069 | 0.8400 | 0.1896 | 0.8300 | 0.1977 |
| FPN rule execution | 0.6771 | 0.1154 | 0.8400 | 0.2029 | 0.8306 | 0.2034 |

Confusion matrices (TN, FP, FN, TP): Decision Tree = (621, 351, 8, 42); FPN rule execution = (650, 322, 8, 42). There are 50 stroke-positive records in the test set.

The FPN score has slightly higher accuracy (0.677 versus 0.649), stroke precision (0.115 versus 0.107), F1 (0.203 versus 0.190), ROC-AUC (0.831 versus 0.830) and average precision (0.203 versus 0.198) in this single split. Both systems identify 42 of the 50 positive test cases, giving recall of 0.84, while missing eight. However, both produce many false positives: 322 for the FPN threshold score and 351 for the tree. These results indicate a minority-class sensitivity/false-positive trade-off, not clinical readiness. The small difference in AUC should not be interpreted as a statistically significant improvement without repeated validation and uncertainty estimates.

## 7. Construction and Structuring of the Fuzzy Petri Net

A Fuzzy Petri Net (FPN) is constructed by integrating fuzzy logic with Petri net theory to represent uncertainty in stroke classification. In the proposed framework, places represent clinical attributes such as age, hypertension, heart disease, average glucose level, and body mass index (BMI). Transitions represent the IF–THEN rules extracted from the decision tree, while fuzzy weights indicate the strength of the associated rules. Membership functions are used to represent the degrees to which clinical attributes satisfy specific conditions. The model is then executed by firing transitions according to the input conditions and aggregating the resulting rule activations to classify stroke and non-stroke cases. This approach combines interpretable decision-tree rules with fuzzy inference to support stroke classification under uncertainty.

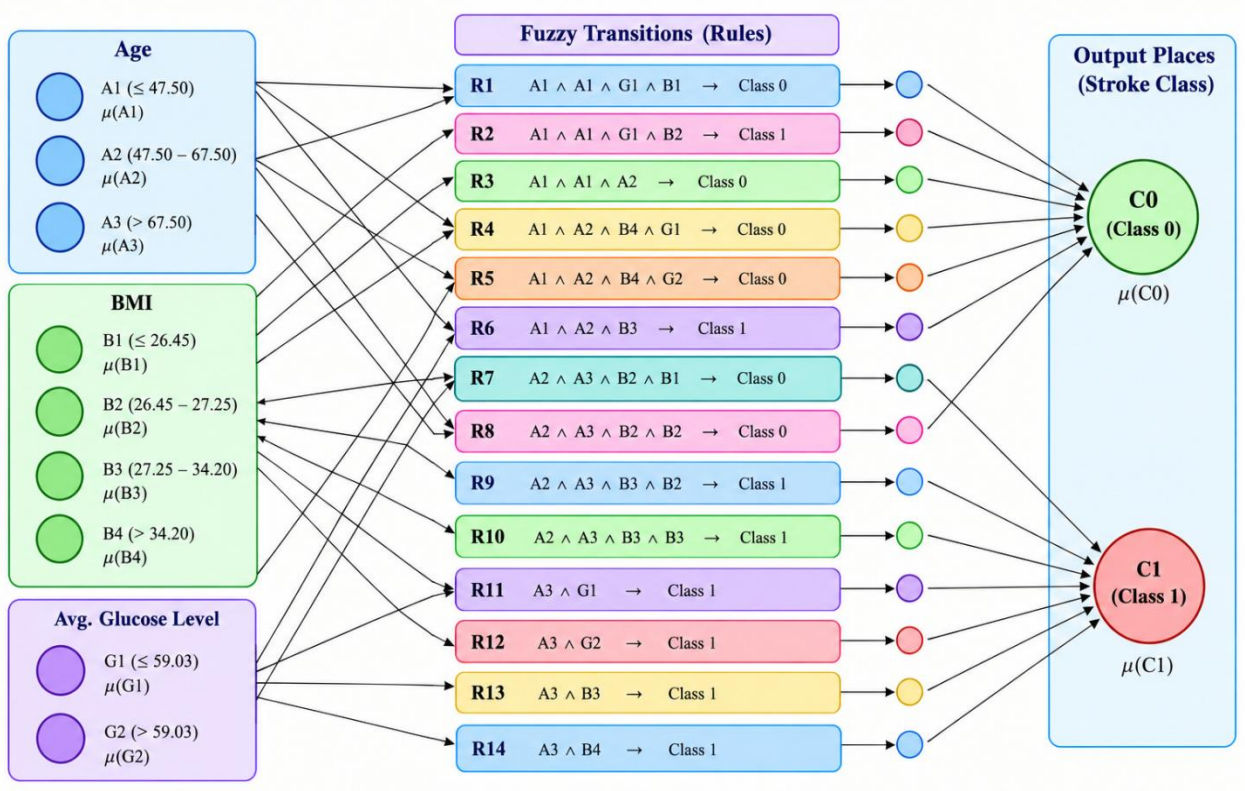



**Figure 1: Fuzzy Petri Net Representation of Decision-Tree Rules for Stroke Classification**

## Conclusion

This paper developed a hybrid Decision Tree–Fuzzy Petri Net workflow for stroke classification using a supplied tabular dataset. The decision tree was trained in Python, its root-to-leaf paths were extracted as IF–THEN rules, and those rules were executed as fuzzy transitions that aggregate graded evidence. On a stratified holdout test set, FPN rule execution produced slightly higher accuracy, F1, ROC-AUC and average precision than the baseline tree, with equal stroke recall. The high false-positive count and absence of external validation prevent clinical conclusions. Future work should include repeated validation, transparent threshold selection, calibration, sensitivity analysis, independent datasets and expert review of the extracted rules.

**Acknowledgement:**

The authors express their sincere gratitude to the management of AMET Deemed to be University for their invaluable support throughout this research study.

## References

1. Breiman, L., Friedman, J. H., Olshen, R. A., & Stone, C. J. (1984). *Classification and regression trees*. Wadsworth International Group.
2. Daeechini, A. H., *et al.* (2024). The most efficient machine learning algorithms in stroke prediction: A systematic review. *Health Science Reports, 7*(10), e70062.
3. Jensen, K. (1997). *Coloured Petri nets: Basic concepts, analysis methods and practical use*. Springer.
4. Saito, T., & Rehmsmeier, M. (2015). The precision-recall plot is more informative than the ROC plot when evaluating binary classifiers on imbalanced datasets. *PLOS ONE, 10*(3).
5. Zadeh, L. A. (1965). Fuzzy sets. *Information and Control, 8*(3), 338–353.
6. Liu, M. Y., & Shi, P. (2008). Verification and validation of fuzzy rules-based human behavior models. In *Proceedings of the 7th International Conference on System Simulation and Scientific Computing* (pp. 813–819).
7. Kouzehgar, M., Badamchizadeh, M. A., & Khanmohammadi, S. (2011). Fuzzy Petri nets for human behavior verification and validation. *International Journal of Advanced Computer Science and Applications, 2*(12), 106–114.

# MATHEMATICAL MODELLING WITH DIFFERENTIAL EQUATIONS: THEORY, COMPUTATION AND EMERGING DATA-DRIVEN DISCOVERY

**Yokeshwari Ravi and Balaganesan Palanivelu***
Department of Mathematics,
AMET Deemed to be University, Chennai, Tamilnadu, India
*Corresponding author E-mail: yogiravi010@gmail.com

**Abstract**
Assumptions about the way a system changes are translated into mathematical equations that can be analyzed, simulated and compared to data. This chapter is a review of that translation in a very short and practice-oriented manner. It starts with the modelling cycle and a classification of the equation types, introduces ordinary differential equation models of growth and epidemics, establishes theory of equilibria and stability, and reaction-diffusion models of spatial spread. The following problems are addressed: the numerical integration, stiffness and control of error, parameter estimation, and identifiability. The latter parts provide a brief overview of two current research areas in the sparse and physics-informed learning of governing equations and fractional-order models with memory. Accompanying the text are worked examples, a simulated epidemic as well as two comparison tables, highlighting open challenges for researchers getting into the field.

**Keywords:** Differential Equations, Mathematical Modelling, Stability Analysis, Numerical Methods, Parameter Estimation, Reaction-Diffusion, Fractional Calculus.

## 1. Introduction

A differential equation states how fast something changes in terms of what it currently is, where it is, and what acts upon it. That compact statement is enough to describe a cooling cup of tea, the concentration of a drug in the bloodstream, the spread of an infection through a city or the voltage across a neuron. Because so many natural and engineered processes are governed by local rules of change, differential equations have become the standard language through which quantitative science is written, and the discipline of mathematical modelling is in large part the craft of choosing the right equation for the question at hand.

Modelling is never merely a matter of solving an equation that someone else has supplied. A modeller must decide which quantities matter, which can be neglected, what form the interactions between variables should take, and how much complexity the available data can support. The resulting model is then analysed, computed, fitted and challenged, and the cycle is repeated when it fails. Classic texts such as Murray [1] and Strogatz [2] present this process through biological and physical case studies; the present chapter instead takes a methodological

view and follows a single thread, from formulation to analysis to computation to calibration, while pointing to recent developments that change how each step is carried out.

The chapter has three aims. The first is to give researchers from neighbouring fields a coherent map of the main equation classes and the questions each is suited to answer. The second is to illustrate the core analytical tools, equilibrium and stability analysis, threshold behaviour and travelling-wave estimates, on short worked examples. The third is to describe the numerical and statistical machinery that connects a model to measurements, and to outline how machine learning is beginning to take part in this connection. Throughout, emphasis is placed on what can go wrong, because understanding the limits of a model is as important as understanding its predictions.

**2. The Modelling Cycle and Types of Equations**

It is useful to regard modelling as a loop with six stages. In formulation, verbal or conceptual hypotheses are written as balance laws, for example “rate of change of a stock equals inflow minus outflow”. In simplification, variables are scaled to dimensionless form so that the number of free parameters is reduced and small effects can be identified and dropped. In analysis, one must figure out what the equations mean, such as which states are steady, whether they are stable, and how behavior changes as the parameters change. In simulation, one solves numerically those regimes which are too complex to be done by hand. In calibration, one estimates the parameters based on observations. And finally, in validation, one checks the model against data that were not used for the calibration, and if there is a systematic discrepancy, one goes back to step one. A model that has survived a few iterations of the loop is not “true,” only useful for a given purpose.

Scaling needs an example since it is usually skipped. In the logistic equation introduced below, the substitution $u = N/K$ and $\tau = rt$ removes both parameters and leaves $du/d\tau = u(1-u)$, showing that every logistic population follows the same curve once population is measured in units of capacity and time in units of the growth period. Likewise, the epidemic model of Section 3.2 depends on its two rates only through $R_0$ once time is measured in units of the infectious period. Dimensionless groups of this kind tell us which parameter combinations can matter at all and prevent wasted effort on separately tuning quantities that only act together.

The choice of equation class encodes a hypothesis about the system itself. Table 1 summarises five classes that cover most applications. Ordinary differential equations (ODEs) assume that the state is described by a finite number of quantities that are well mixed in space. Partial differential equations (PDEs) are required when position matters. Delay equations represent finite lags such as maturation or transmission times, stochastic equations represent random fluctuation that cannot be averaged away, and fractional equations represent memory effects that decay as a power law rather than exponentially.

**Table 1: Principal classes of differential-equation models**

| Class | Generic form | Typical applications | Main analytical tools | Class |
|---|---|---|---|---|
| ODE | $\mathrm{dx/dt} = \mathrm{f(x, \theta)}$ | Population growth, reaction kinetics, epidemics | Phase plane, linearisation, Lyapunov functions | ODE |
| Reaction–diffusion PDE | $\partial \mathrm{u}/\,\partial \mathrm{t} = \mathrm{D}\nabla^2\mathrm{u} + \mathrm{f(u)}$ | Invasion fronts, pattern formation | Travelling waves, Turing analysis | Reaction–diffusion PDE |
| Delay equation | $\mathrm{x'(t)} = \mathrm{f(x(t), x(t-\tau))}$ | Blood-cell production, gene regulation | Characteristic equations | Delay equation |
| Stochastic equation | $\mathrm{dX} = \mathrm{f\,dt} + \sigma\,\mathrm{dW}$ | Finance, small populations, noise-driven switching | Itô calculus, Fokker–Planck equation | Stochastic equation |
| Fractional equation | ${}^{\mathrm{C}}\mathrm{D}^{\alpha}\mathrm{x} = \mathrm{f(t, x)}$ | Anomalous diffusion, viscoelastic media | Mittag–Leffler functions, Laplace transform | Fractional equation |

## 3. Ordinary Differential Equation Models

### 3.1 Single-species growth

The simplest dynamic model assumes that a population grows at a per-capita rate that falls linearly as the population approaches the carrying capacity $K$ of its environment. With $N(t)$ denoting population size and $r$ the intrinsic growth rate, this gives the logistic equation

$$dN/dt = rN(1 - N/K)$$

which can be integrated in closed form after separating variables:

$$N(t) = K/[1 + ((K - N_0)/N_0)\, e^{-rt}]$$

Two equilibria exist, $N = 0$ and $N = K$. Evaluating the derivative of the right-hand side of (1) shows that the first is unstable, with slope $r$, and the second is stable, with slope $-r$, so every positive initial population converges to $K$. Despite its simplicity, the logistic law has served as a building block for models of tumour growth, fisheries and microbial cultures, and it demonstrates a feature seen repeatedly below: the long-term behaviour is dictated by the equilibria and their stability, not by the details of the transient.

### 3.2 Epidemic dynamics

A landmark application of ODE modelling is the compartmental theory of epidemics introduced by Kermack and McKendrick [3]. A population of fixed size is divided into susceptible ($S$), infectious ($I$) and removed ($R$) individuals, expressed as fractions of the total. Susceptibles

become infectious on contact with an infectious person at rate $\beta$, and infectious individuals are removed at rate $\gamma$, which gives

$$\begin{aligned} \mathrm{dS/dt} &= -\beta \mathrm{SI} \\ \mathrm{dI/dt} &= \beta \mathrm{SI} - \gamma \mathrm{I} \\ \mathrm{dR/dt} &= \gamma \mathrm{I} \end{aligned}$$

Adding the three equations shows that $S + I + R$ is constant, so the system is effectively two-dimensional. In equation (4), the infection grows initially if and only if $\beta S > \gamma$. Writing the basic reproduction number as $R_0 = \beta/\gamma$ and setting $S \approx 1$ at the start of an outbreak, the condition reads $R_0 > 1$: an infectious person must replace themselves with more than one new case on average. This threshold phenomenon, a sharp qualitative change at a critical parameter value, is one of the most influential insights produced by mathematical modelling in public health.

Dividing (3) by (5) and integrating gives an implicit relation for the final epidemic size $z$, the fraction of the population ever infected, in the form $z = 1 - \exp(-R_0 z)$ when the initial infection is negligible. Figure 1 shows both the timing and the relationship for a disease where $\beta = 0.3$ and $\gamma = 0.1$ per day, giving $R_0 = 3$. The fraction of the population that is infectious peaks at about 30%, and almost 94% of the population gets infected if there is no intervention. Figure (b) shows how quickly the final size saturates as $R_0$ becomes greater than the threshold, which is the reason why even small decreases in transmission can prevent many cases near $R_0 = 1$, but not when $R_0$ is large.

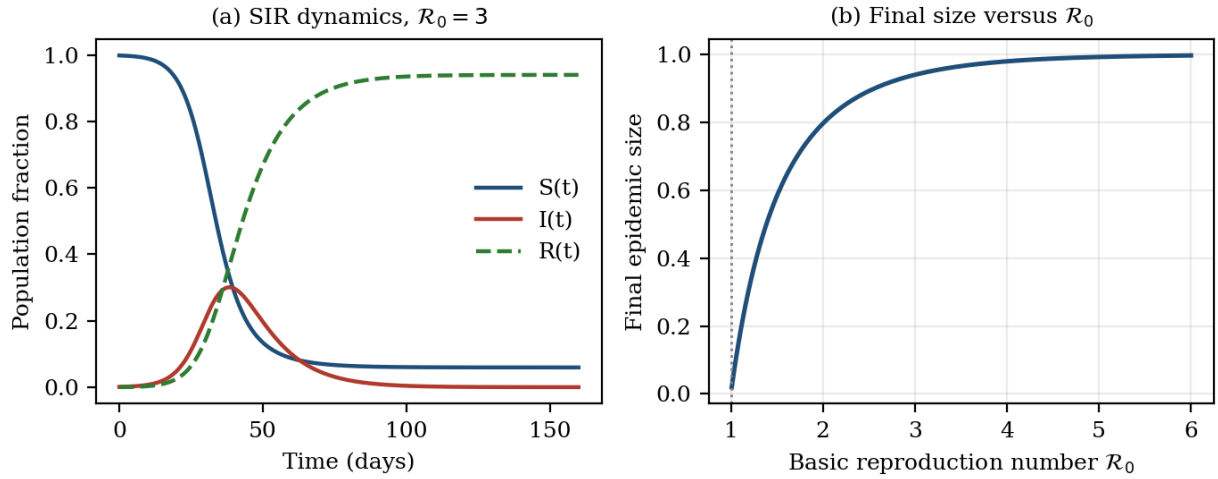



**Figure 1: (a) Numerical solution of the SIR model (3)–(5) with $\beta = 0.3$, $\gamma = 0.1$ and $I(0) = 0.001$. (b) Final epidemic size as a function of the basic reproduction number**

The SIR model is based on several strong assumptions, such as homogeneous mixing, constant rates, and exponentially distributed infectious period. For these reasons, practical models are built on extensions of SIR with a latent class (SEIR model), age or contact structure, vaccination, waning immunity, spatial coupling, or time-varying transmission. Each of these extensions

introduces additional parameters and changes the qualitative behaviour; that is why it is crucial to use the analytical methods from the next section, even though the resulting model has to be solved numerically.

In addition, this model allows for basic policy analysis. If a fraction $p$ of the population gets vaccinated prior to the outbreak, the initial fraction of susceptibles will be $1-p$. As a result, the effective reproduction number equals $R_e = R_0(1-p)$, and the disease cannot take off when $R_e \leq 1$, that is, when

$$p_c = 1 - 1/R_0$$

With $R_0 = 3$, the threshold is 2/3, while in the case of the less transmittable agent, $R_0 = 1.5$, the threshold is only 1/3. As mentioned before, the herd immunity threshold is a lower bound based on some idealistic assumptions because it does not take into account heterogeneities in the contact rate, inefficiency of the vaccine, and clustering of the unvaccinated population, all of which increase the threshold of coverage. Nevertheless, one can see from the above example that even the simplest ODEs may give us quantitative targets.

### 3.3 Delays and randomness

Two important modifications of the ODE model are time delays and randomness. First, we have delays. If the process of maturation, incubation, or signal transmission takes a fixed period of time $\tau$, then the growth rate is determined by the state of the system in the past, and our model becomes $x'(t) = f(x(t), x(t-\tau))$. As the initial condition is now a function defined on an interval of length $\tau$, the phase space becomes infinite-dimensional, and the stability is determined by the roots of a transcendental characteristic equation. Delays provide a well-known example of a method of producing oscillations: a stable feedback loop, when there is no delay, becomes an oscillation after a critical threshold of delay is crossed.

The other important aspect is that of randomness. In the case of very small populations, either early in an outbreak or within one cell, the smooth dynamics of an ODE represent only the mean population behavior. By adding a noise term, we get a stochastic differential equation in the form $dX = f(X)\,dt + \sigma(X)\,dW$, whose solutions exhibit random paths, and the evolution of their probability density obeys a Fokker-Planck equation. The difference is a significant one. A deterministic ODE model with $R_0 > 1$ will always imply an epidemic outbreak. However, for the stochastic model, there is a chance that the outbreak will be extinct by chance before taking off, and this probability is a key one in dealing with outbreaks. The deterministic models are therefore always considered first due to their low cost and the large population limit of the stochastic description.

## 4. Equilibria, Stability and Bifurcations

For an autonomous system $x' = f(x)$, an equilibrium $x^*$ satisfies $f(x^*) = 0$. Its stability is governed, at least when it is hyperbolic, by the Jacobian matrix $J = \partial f / \partial x$ evaluated at $x^*$: the

equilibrium is asymptotically stable if every eigenvalue of $J$ has a negative real part and unstable if any has a positive real part. The Hartman–Grobman theorem justifies replacing the nonlinear system by its linearisation in the hyperbolic case, while non-hyperbolic equilibria need further tools such as centre-manifold reduction or Lyapunov functions [2].

The predator–prey model of Lotka and Volterra shows the method at work, and also its limits. With prey density $x$ and predator density $y$, the equations are

$$dx/dt = \alpha x - \beta xy, \qquad dy/dt = \delta xy - \gamma y$$

and the coexistence equilibrium is $(\gamma/\delta, \alpha/\beta)$. At this point the Jacobian has purely imaginary eigenvalues $\pm i\sqrt{\alpha\gamma}$, so linearisation is inconclusive (Figure 2a shows the resulting closed orbits). The function $V = \delta x - \gamma \ln x + \beta y - \alpha \ln y$ is however constant along every trajectory, which proves that orbits are closed curves around the equilibrium and that populations oscillate with a period that depends on the amplitude. This structural fragility is a known weakness of the model: adding any realistic effect, such as prey self-limitation, converts the centre into a stable spiral and removes the neutral cycles. The moral of this for modellers is that qualitative predictions of the model need to be checked for robustness under small variations in its structure.

Bifurcation theory deals with the way equilibrium points and their stability depend on parameter values. In the SIR model with births and deaths, the disease-free state loses stability as $R_0$ passes through one and an endemic equilibrium appears, an example of a transcritical bifurcation. Hopf bifurcations, in which an equilibrium gives way to sustained oscillations, are central in models of cardiac rhythm, chemical clocks and business cycles. Continuation software that tracks equilibria and periodic orbits as parameters vary has made it routine to map such regimes for systems with dozens of variables.

**5. Spatial Models: Reaction-Diffusion Equations**

When individuals, molecules or cells are not well mixed, position must be added to the state. If the quantity $u(x,t)$ is transported by random motion with diffusivity $D$ and simultaneously reacts locally according to a function $f$, conservation of mass gives the reaction-diffusion equation

$$\partial u/\partial t = D\ \partial^2 u/\partial x^2 + f(u)$$

Choosing logistic kinetics, $f(u) = ru(1 - u/K)$, gives the Fisher–KPP equation, introduced to describe the spread of an advantageous gene and since applied to the invasion of species, the growth of tumours and the propagation of wildfires. Linearising about the unstable state $u = 0$ shows that disturbances move into the unoccupied region as travelling waves whose speed $c$ must satisfy $c \geq 2\sqrt{rD}$, and for compactly supported initial data the front selects this minimal speed. This estimate is useful in practice since it connects the measurable quantities, the growth rate and the dispersal coefficient, to the measurable invasion velocity, and it has been applied to test the feasibility of observed colonisation velocities.

PDE models require for their completeness the specification of initial and boundary conditions, which are part of the scientific hypothesis, not a technicality. The zero-flux (Neumann) boundary conditions correspond to the impossibility of individuals crossing the edge of the domain, the Dirichlet boundary conditions specify the concentration at the boundary, and the Robin boundary conditions correspond to partial exchange with the outside. Well-posedness issues, that is existence, uniqueness and continuous dependence of the solution on the data, must be clarified before computing, since a numerical algorithm can easily provide a smooth solution to an ill-posed problem.

Diffusion may create structure, too, rather than destroy it. Indeed, Turing found that two interacting chemicals with sufficiently unequal diffusivities could drive an initially homogeneous system unstable if it was otherwise stable, thereby generating stripes or spots. These types of instabilities, as described in [1], continue to be one of the main explanations for pattern generation in embryology and ecology. In computation, PDEs are typically replaced by large ODEs through the method of lines; i.e., space is approximated using finite differences, finite elements, or spectral representations, followed by integration in time, so that the next discussion also pertains to them.

**6. Numerical Solution of Differential Equations**

Most models of realistic complexity have no closed-form solution, and numerical integration is therefore the everyday tool of the modeller. The simplest scheme is the explicit Euler method, which advances the solution of $y' = f(t, y)$ by a step $h$ according to

$$y_{n+1} = y_n + hf(t_n, y_n)$$

Its local truncation error is $h^2$ while its global error is $h$, and hence its error is halved whenever the step size is halved. Higher-order Runge–Kutta methods make multiple evaluations of $f$ in each step, and in the case of the classical fourth-order method, the global error is $h^4$. In adaptive techniques, an embedded pair of methods (of different orders) is used, and the difference between the solutions gives an estimate of the error. Thus, the accuracy of the method is controlled automatically and the user need not choose $h$ [6].

Error is not the only thing to worry about, as stability is very important. In case of the test equation $y' = \lambda y$ with $\mathrm{Re}\,\lambda < 0$, explicit Euler multiplies the solution by $(1 + h\lambda)$ at each step, and it will decay only if $h < 2/\lambda$ in case of $\lambda$ being real. Problems in which fast and slow processes coexist, common in chemical kinetics and in method-of-lines discretisations of diffusion, are called stiff, because the fastest timescale forces an explicit method to take tiny steps long after the corresponding transient has died out. Implicit methods, such as backward Euler with amplification factor $1/(1 - h\lambda)$, remain stable for any step size when $\mathrm{Re}\,\lambda < 0$ and are therefore preferred for stiff problems despite requiring a nonlinear solve at every step. Table 2 compares frequently used choices.

**Table 2: Commonly used integration methods and their characteristics**

| Method | Order | Stability Behaviour | Suitable For |
|---|---|---|---|
| Explicit Euler | 1 | Conditionally stable; step limited by fastest timescale | Teaching, quick prototypes |
| Classical Runge – Kutta (RK4) | 4 | Conditionally stable; larger region than Euler | Smooth non-stiff problems |
| Adaptive Dormand – Prince pair | 4(5) | Conditionally stable with automatic step control | General-purpose non-stiff solving |
| Backward Euler | 1 | A-stable; no step restriction for decaying modes | Stiff problems, robust baseline |
| BDF / implicit Runge–Kutta | 1–5 | Stiffly stable; variable order | Stiff kinetics, discretised PDEs |

Verification of numerical output should be routine. Convergence under step refinement, conservation of known invariants, such as the constant total population in (3) – (5), and comparison with special cases that can be solved exactly provide inexpensive checks. For Hamiltonian or conservative systems, structure-preserving integrators that retain energy or symplectic structure give qualitatively correct long-time behaviour where general-purpose methods drift.

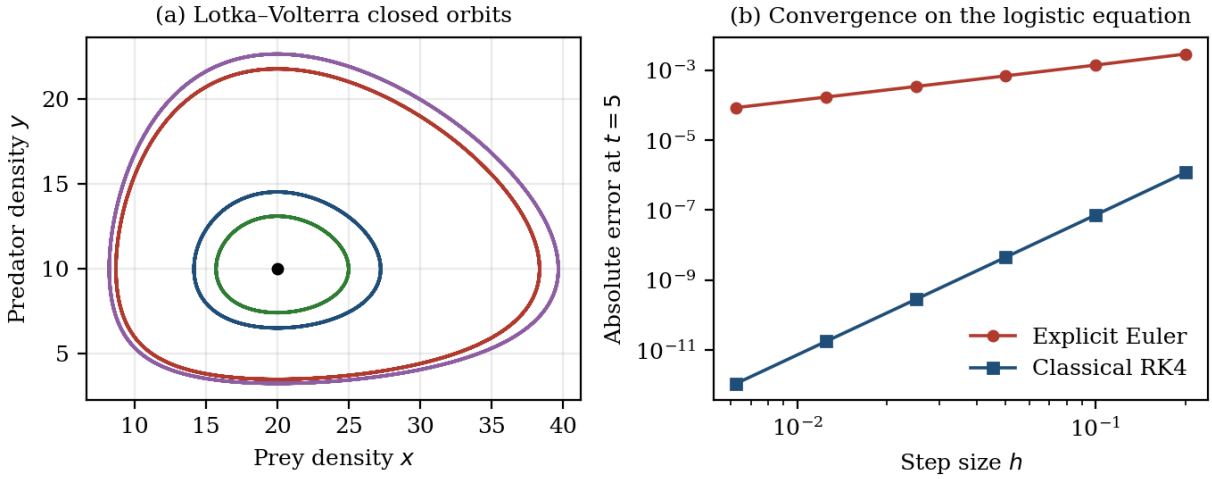



**Figure 2: (a) Closed orbits of the Lotka–Volterra system (7) for $\alpha = 1, \beta = 0.1, \gamma = 1.5, \delta = 0.075$; the dot marks the equilibrium (20, 10). (b) Global error at $t = 5$ of explicit Euler and classical RK4 for the logistic equation with $r = K = 1$ and $N(0) = 0.1$**

Figure 2b gives a concrete check of the order claims above. On the logistic equation, whose exact solution (2) is known, the Euler error decreases with a fitted slope of about 1.0 on logarithmic axes, whereas the RK4 error falls with a slope of about 4.0. At a step size of 0.2, RK4 already has a smaller error (about $1 \times 10^{-6}$) than Euler has at a step 32 times smaller

(about $9 \times 10^{-5}$), which shows that order matters far more than raw step count once the required tolerance is demanding. Such convergence plots are a simple diagnostic that every modeller can produce for a new code.

**7. Parameter Estimation and Identifiability**

A model is only as informative as its parameters are credible. Suppose a model produces trajectories $x(t;\theta)$ depending on a parameter vector $\theta$, and observations $y_i$ are made at times $t_i$ through an observation function $g$. Under independent Gaussian errors, maximum likelihood estimation reduces to the nonlinear least-squares problem

$$J(\theta) = \sum_{i=1}^{n} | y_i - g(x(t_i;\theta))|^2$$

The estimate is the value of $\theta$ that minimises the total squared distance between observed values and model predictions over all observation times. Because $J$ depends on $\theta$ through the numerical solution of the differential equation, gradients are obtained by finite differences, by forward sensitivity equations or by adjoint methods, and the last of these scales well to models with many parameters.

Estimation presupposes that parameters can in principle be recovered. A parameter is structurally identifiable if different values always yield different outputs for noise-free, continuous data, and practically identifiable if it can be pinned down with acceptable uncertainty from the finite, noisy data actually available. In the SIR model, for example, case counts early in an outbreak constrain the growth rate $\beta - \gamma$ much better than $\beta$ and $\gamma$ separately, so confidence intervals for the individual rates can be very wide even when the fit looks excellent. Profile likelihood, the Fisher information matrix and Bayesian posterior sampling reveal such problems by exposing flat directions in parameter space. If identifiability is not achieved, additional data on more compartments can be taken, a parameter can be fixed with prior knowledge or the model can be simplified.

The connection between model and data is as important as the model and data themselves. The number of cases reported is not usually the state variables themselves. They are delayed, aggregated on a weekly or daily basis, are under-reported, and influenced by testing policies. A calibration that is defendable, then, must contain a definite observation model, for example, reported incidence as a fraction of the reported incidence plus a count-distribution error term like Poisson or negative binomial noise for which parameters are estimated with the dynamical parameters. The failure to take this layer into account can cause errors in the rates even when the dynamical equations are correct.

Last but not least, it is not a proof of validation if goodness of fit. A flexible model can mimic nearly any set of data, and agreement with data used to fit has little to do with predictive ability. Out-of-sample data, future forecasting for a later time frame and comparison with simple

baselines provide a much more accurate estimate, while information criteria can be used to compare fit and parsimony when multiple model structures are considered.

## 8. Contemporary Developments

### 8.1 Learning governing equations from data

Classical modelling starts from theory and uses data for calibration. Data-driven discovery reverses the order. The sparse identification of nonlinear dynamics (SINDy) of Brunton and colleagues [4] assumes that the right-hand side of the unknown system is a sparse combination of candidate terms. Measured states and their estimated time derivatives are stacked in matrices, and one solves

$$\dot{X} \approx \Theta(X)\Xi$$

where the columns of $\Theta(X)$ are candidate functions such as constants, polynomials or trigonometric terms, and the coefficient matrix $\Xi$ is made sparse by sequential thresholded least squares or an $l^1$ penalty. The surviving terms form an interpretable differential equation, and the method has recovered known laws from simulated data of fluid and chemical systems. Its weaknesses are sensitivity to noise in the estimated derivatives and dependence on a well-chosen library of candidates, so weak-form and ensemble variants have been proposed to improve robustness.

### 8.2 Physics-informed neural networks

Physics-informed neural networks (PINNs) [5] solve the differential equation using the neural network $u_\theta(x,t)$ and optimise the following composite cost function. One of the parts is aimed at penalising the discrepancy between the data and another penalises the governing equation's residual taken at numerous points (collocation) via automatic differentiation. This makes it possible to force the neural network to converge to physically sensible functions even in the regions devoid of measurements. The PINN methodology may also be used to find unknown coefficients, thereby converting the inverse problem into a standard optimisation one. Issues discussed by practitioners include slow/unstable optimisation for stiff/multiscale problems and lack of the same guarantees on the accuracy that classical methods possess. For forward problems that are well-posed, standard discretisation is preferable. The method is most appealing for inverse problems, complex geometries, and cases where modeling and data have to be combined.

### 8.3 Fractional-order models

Media have memory. The relaxation of polymers follows a power-law delay instead of an exponential one, while tracers diffuse in a porous or crowded medium either slower or faster than predicted by the Brownian motion model. The fractional calculus approach takes into account such behavior through the replacement of the first derivative with a memory-dependent operator. For $0 < \alpha < 1$, the Caputo derivative is defined by

$$^{C}D^{\alpha}x(t) = \frac{1}{\Gamma(1-\alpha)}\int_{0}^{t}(t-s)^{-\alpha}x'(s)\,ds$$

As $\alpha \to 1$ the ordinary derivative is recovered. The linear equation with Caputo derivative, $D^{\alpha}x = -\lambda x$, has the solution $x(t) = x_0 E_{\alpha}(-\lambda t^{\alpha})$, where $E_{\alpha}$ is the Mittag–Leffler function, and for large $t$ this decays like a power law, $t^{-\alpha}$, instead of the exponential decay of the classical case [7]. Fractional models therefore describe heavy-tailed relaxation with few parameters, but they bring costs. The order $\alpha$ has to be estimated and is difficult to interpret mechanistically, and numerical schemes must store or approximate the full history, which raises the computational cost from linear to quadratic in the number of steps unless fast convolution techniques are used.

**9. Challenges and Future Directions**

There were several problems that spanned the topics listed above. Uncertainty quantification: Predictions should always have credible ranges that take into account parameter uncertainty, structural uncertainty, and observational uncertainty; structural uncertainty—the uncertainty that the equations themselves may be incorrect—is not usually addressed in a principled fashion. The second is multiscale modelling, when processes from molecular to population scale interact, and one equation or one step size is not enough. The third is that of the mechanistic and learned parts. Hybrid approaches that retain the trusted physical structure and use a neural network to represent unknown closure terms are promising, but the questions of identifiability, extrapolation and interpretability that remain unanswered by classical theory are raised.

Another difficulty is the reproducibility. The reported simulations are often hard to repeat due to a lack of documentation of solver settings, tolerances, initial conditions or code. It is inexpensive and greatly enhances trust in published results to share model files, fixed random seeds, and a record of solver versions and tolerances. The barrier to entry is now low: There are well-developed open-source solver libraries for every major scientific language. The risk is simply to use the default values. The most helpful habit for students and newcomers is to take the simplest model that can answer the question, understand it as analytically as possible, and add complexity where data and/or question call for it. The preceding discussion can be applied to nearly any study of a differential equation, and is summarized in the checklist of questions and diagnostics in Table 3.

**Table 3: A practical checklist for model construction and model testing for a model of a differential equation**

| **Stage** | **Guiding question** | **Useful diagnostic** |
|---|---|---|
| Formulation | Does each term correspond to a stated mechanism? | Unit and dimension check; conservation laws |

**Conclusion**

This chapter has taken the journey from a modelling hypothesis to a calibrated and validated differential equation model. The closed form solutions and phase plane techniques uncover the thresholds, equilibria and oscillations, such as those found in the logistic, epidemic and predator-prey models. Reaction-diffusion theory bridges local dynamics to the speed and pattern of spread. Numerical analysis provides the rigor that simulations require and statistical inference helps us understand what the data can tell us. New techniques such as sparse regression, physics-informed learning and fractional operators do not supplant this framework but augment it, particularly when the laws of the system are partially unknown or possess memory. Those researchers that have analytical insight, computational rigor and validation are most suited to take advantage of these advances.

**References**

1. Murray, J. D. (2002). *Mathematical biology I: An introduction* (3rd ed.). Springer.
2. Strogatz, S. H. (2015). *Nonlinear dynamics and chaos: With applications to physics, biology, chemistry, and engineering* (2nd ed.). Westview Press.
3. Kermack, W. O., & McKendrick, A. G. (1927). A contribution to the mathematical theory of epidemics. *Proceedings of the Royal Society of London. Series A, 115*(772), 700–721.
4. Brunton, S. L., Proctor, J. L., & Kutz, J. N. (2016). Discovering governing equations from data by sparse identification of nonlinear dynamical systems. *Proceedings of the National Academy of Sciences, 113*(15), 3932–3937.
5. Raissi, M., Perdikaris, P., & Karniadakis, G. E. (2019). Physics-informed neural networks: A deep learning framework for solving forward and inverse problems involving nonlinear partial differential equations. *Journal of Computational Physics, 378*, 686–707.
6. Hairer, E., Nørsett, S. P., & Wanner, G. (1993). *Solving ordinary differential equations I: Nonstiff problems* (2nd ed.). Springer.
7. Podlubny, I. (1999). *Fractional differential equations*. Academic Press.

# MATHEMATICAL MODELLING OF DRUG DELIVERY SYSTEMS: DIFFERENTIAL EQUATIONS AND STATISTICAL OPTIMIZATION

**Venkatesan R, Shobika P, Pradeep U*, Purusothaman R and Subash S**
Department of Biomedical Engineering,
E.G.S. Pillay Engineering College, Nagapattinam, Tamil Nadu, India
*Corresponding author E-mail: deep090407@gmail.com

**Abstract**
Drug delivery systems are dynamic processes in which formulation structure, transport physics, biological barriers, and patient variability interact over time. Mathematical modelling provides a language for connecting these layers. Differential equations can represent diffusion through a polymer matrix, dissolution and degradation, interfacial transfer, cellular uptake, tissue distribution, and systemic elimination. Statistical optimization complements the mechanistic model by identifying controllable formulation variables and quantifying their influence on critical quality attributes. This chapter develops a practical modelling framework that begins with mass balance and boundary conditions, advances through compartmental and spatially distributed models, and concludes with design-of-experiments strategies for formulation optimization. The discussion emphasizes model purpose rather than equation selection by habit. A Higuchi-type approximation can be useful when diffusion dominates and geometry is simple, whereas a reaction–diffusion or moving-boundary model is more defensible when polymer erosion, binding, or swelling changes the transport domain. Similarly, an empirical release curve may interpolate observations, but it should not be mistaken for a mechanistic explanation. Recent open-access research illustrates these distinctions: fractional pharmacokinetic models can represent memory-like trapping; magnetic nanoparticle simulations can expose the role of particle size and field direction; and statistical comparisons show why goodness-of-fit must be balanced with parsimony and predictive performance.

**Keywords:** Drug Delivery, Differential Equations, Diffusion, Pharmacokinetics, Reaction–Diffusion, Nanoparticle Transport, Release Kinetics, Design of Experiments, Response Surface Methodology, Quality by Design.

## 1. Introduction: Why Mathematical Models Matter in Drug Delivery

A drug delivery system is not merely a container that releases an active pharmaceutical ingredient. It is a time-dependent system in which the drug may dissolve, partition, diffuse, bind, degrade, or be removed by flow. The measured concentration at a sampling point is therefore the result of several coupled processes. A model is useful when it separates those processes sufficiently to answer a decision question: How long will the system maintain a target concentration? Which formulation variable controls the burst phase? Does a magnetic field alter

the spatial distribution of a carrier? Which combination of excipients achieves small particle size without sacrificing entrapment?

The first modelling decision is the scale of description. A zero-dimensional model tracks average drug mass in compartments and is efficient for pharmacokinetic prediction. A one-dimensional model resolves concentration across a film or membrane. A two- or three-dimensional model becomes necessary when geometry, anisotropy, external fields, or heterogeneous tissue structure drives the outcome. Scale should follow the question, not the sophistication of the software.

A second decision concerns the role of data. Mechanistic models use parameters such as diffusivity, partition coefficient, degradation rate, clearance, and binding affinity. These parameters can be estimated from experiments, literature values, or Bayesian updating. Empirical models use a smaller number of curve-fitting coefficients. Neither class is automatically superior. The defensible choice is the model whose assumptions are visible and whose parameters can be identified from the available observations.

### 1.1 The mass-balance starting point

For a control volume, the conservation statement is written as accumulation = inflow − outflow + generation − consumption. In a spatial domain, the concentration C(x,t) commonly satisfies a conservation equation of the form:

$$\partial C/\partial t = -\nabla \cdot J + R(C,x,t), \quad \text{where} \quad J = -D\nabla C + uC \qquad \text{……..(1)}$$

Here, J is the flux, D is the diffusion tensor, u is the advective velocity, and R represents reaction, dissolution, degradation, binding, or cellular uptake. This compact equation is valuable because each term has a physical interpretation. If a term cannot be measured, bounded, or justified, it becomes a source of structural uncertainty rather than a harmless mathematical decoration.

## 2. Differential-Equation Models for Release and Transport

### 2.1 Diffusion through a delivery matrix

For a homogeneous slab with negligible convection and reaction, the classical Fickian model reduces to $\partial C/\partial t = D\partial^2 C/\partial x^2$. The initial condition specifies the amount and distribution of drug at t = 0. Boundary conditions describe the receiving environment. A perfect sink assumes C = 0 at the surface, while a finite-volume receiver is better described by a mass-transfer condition, $-D\partial C/\partial n = k(C_{surface} - C_{receiver})$. The distinction is important: sink conditions often accelerate the predicted release and can hide the influence of receiver depletion.

The Higuchi relationship, $M_t/M_\infty \approx kH\, t^{1/2}$, is a useful early approximation for diffusion-controlled release from a planar matrix. Its square-root dependence is interpretable, but it is not universal. Swelling, pore formation, polymer erosion, drug solubility, and changing diffusivity can all produce deviations. A fitted Higuchi slope should therefore be reported as a regime descriptor, not as proof that diffusion is the only mechanism.

### 2.2 Reaction–diffusion and moving boundaries

When the carrier degrades or the drug reacts with the matrix, the transport equation needs a reaction term. A simple first-order loss model is $R = -kC$. A more realistic formulation may include a dissolved fraction, an immobilized fraction, and a reversible binding state. The resulting system may contain several coupled ordinary differential equations at each spatial location. If the polymer surface recedes, the domain itself becomes time-dependent, producing a moving-boundary or Stefan-type problem.

Supramolecular delivery systems illustrate why boundary conditions deserve as much attention as the differential equation. Release occurs at interfaces, and the interface can change as dissolution, swelling, or matrix erosion progresses. Mircioiu and colleagues emphasize that the same diffusion equation can generate very different release profiles when geometry and boundary conditions are changed. This is a practical reminder that model specification begins before numerical solution.

### 2.3 Numerical solution and identifiability

Finite differences, finite volumes, and finite elements are common numerical methods. The solver is not the model: a stable numerical solution can still represent a physically incorrect system. Mesh independence, time-step sensitivity, mass conservation, and parameter identifiability should be tested. If two parameters always appear as a product, the data may identify only that product rather than each parameter separately. In that situation, adding more decimal places does not create information.

## 3. Pharmacokinetic Compartment Models and Patient Variability

Compartmental pharmacokinetics represents the body as connected spaces with average concentrations. For a one-compartment intravenous bolus model, $dA/dt = -kA$ and $C = A/V$. A two-compartment model adds a peripheral space and intercompartmental exchange. For an infusion rate Rin, the central balance becomes $dA1/dt = Rin - (k10+k12)A1 + k21A2$, while $dA2/dt = k12A1 - k21A2$. These equations are simple enough to solve rapidly and rich enough to support dose-regimen design. The parameter k10 is not the same as clearance, although they are related through volume. Confusing microconstants, macroconstants, and physiological clearance can lead to incorrect interpretation. The model should state whether parameters are normalized to body weight, lean body mass, or another covariate. Covariate modelling is especially important when inter-patient variability is part of the clinical question.

The following figure illustrates the difference between classical and fractional-order pharmacokinetic models in predicting the decline of drug concentration in the central compartment. It highlights how memory-dependent behaviour may influence drug trapping and patient-specific pharmacokinetic responses. Fractional-order extensions replace an integer derivative with an operator that retains information about prior states. This can be useful when tissue trapping, anomalous diffusion, or delayed release creates a history-dependent response.

The attraction of the approach is conceptual: the model can represent memory without adding many discrete compartments. The risk is interpretive: the fractional order must be estimated and validated, not treated as a universal property of the drug. A clinically useful workflow is iterative. Concentration measurements update the model, an error threshold triggers recalibration, and the updated model informs the next infusion decision. That loop is more defensible than a single fit performed once at the beginning of a long treatment period.

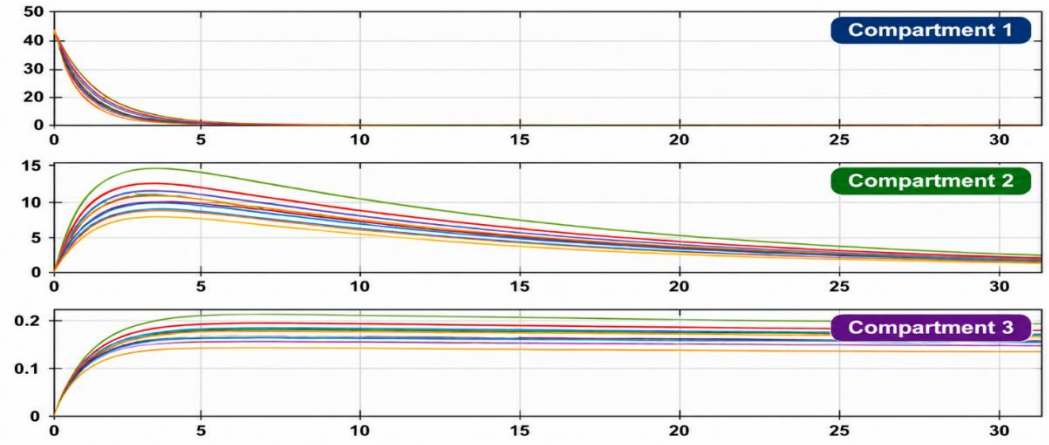



**Figure 1: Classical and fractional-order simulations of propofol compartmental dynamics, illustrating how memory-like behaviour can alter the predicted decline in the central compartment [1].**

## 4. Spatially Distributed Nanoparticle Transport

Nanoparticle delivery introduces a second spatial scale. A carrier may undergo Brownian motion, magnetic drift, hindered diffusion, adsorption, cellular uptake, and clearance. In a porous tissue, the diffusion coefficient can be a tensor rather than a scalar because the local microstructure makes movement easier in one direction than another. The flux can be written $J = -D\nabla C + v_{mag} C$, where $v_{mag}$ represents an effective field-driven velocity. Yuan and colleagues modelled magnetic nanoparticle trajectories in brain white matter and showed how particle size, axon tortuosity, magnetic force density, and field direction alter the distribution. Their work is valuable as a modelling example because the simulation is tied to a concrete design question: how can a desired distribution be obtained in anisotropic tissue?

The following figure illustrates the simulated movement and spatial distribution of magnetic nanoparticles in brain white matter under different magnetic-field conditions. It demonstrates how magnetic force and particle transport characteristics can influence the final nanoparticle distribution. The figure also illustrates a validation principle. A transport model should be compared with measurements or established benchmark cases before it is used for optimization. In the reported work, simulated diffusion behaviour was compared with experimental values from blood and brain white matter. Agreement was useful but not perfect, reminding us that protein interactions and fibre resistance may not be fully represented in a simplified microstructure.

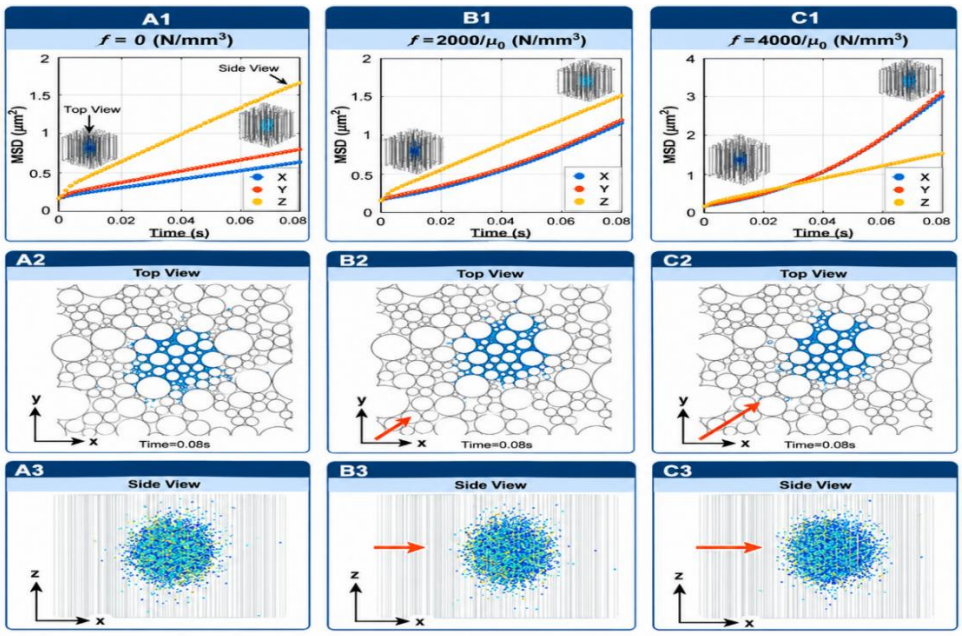



**Figure 2: Simulated mean-squared displacement and final distributions of magnetic nanoparticles under different magnetic-field conditions in brain white matter [2]**

### 4.1 Targeted delivery and coupled biology

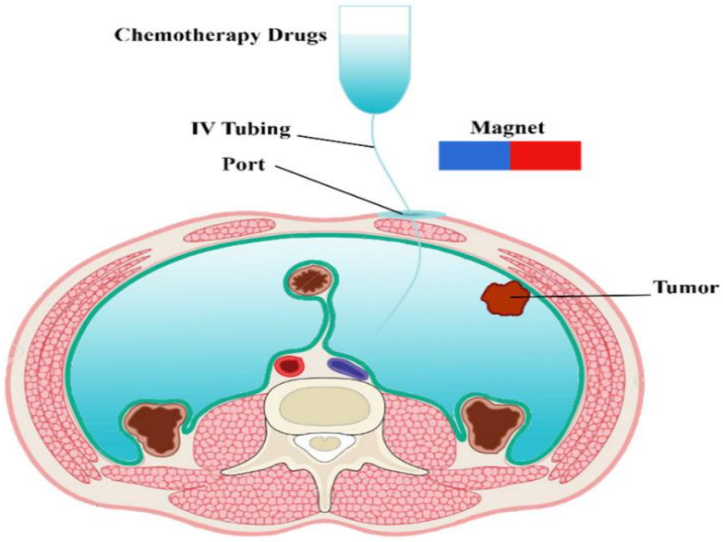



**Figure 3: Schematic representation of magnetic nanoparticle targeting during intraperitoneal chemotherapy [3]**

For tumour-targeted delivery, transport alone is insufficient. The model may need reversible binding, internalization, drug release from the carrier, and cell death. Rezaeian and colleagues combined magnetically controlled transport with binding and internalization to compare magnetic and conventional intraperitoneal chemotherapy. The figure 3 illustrates the basic mechanism of magnetically controlled drug targeting during intraperitoneal chemotherapy. It shows how an external magnetic field can guide drug-loaded nanoparticles towards the tumour region.

## 5. Release-Kinetics Models: Interpretation Before Fit

Release data are often analysed with a family of candidate curves. Zero-order kinetics describes a constant rate, first-order kinetics describes a rate proportional to the remaining drug, and the Higuchi model describes a square-root-time regime under restrictive diffusion assumptions. The Korsmeyer–Peppas equation, $M_t/M_\infty = kt^n$, is commonly used for the early fraction of release. The exponent n is a diagnostic indicator of transport regime only when the geometry and fitting range are appropriate.

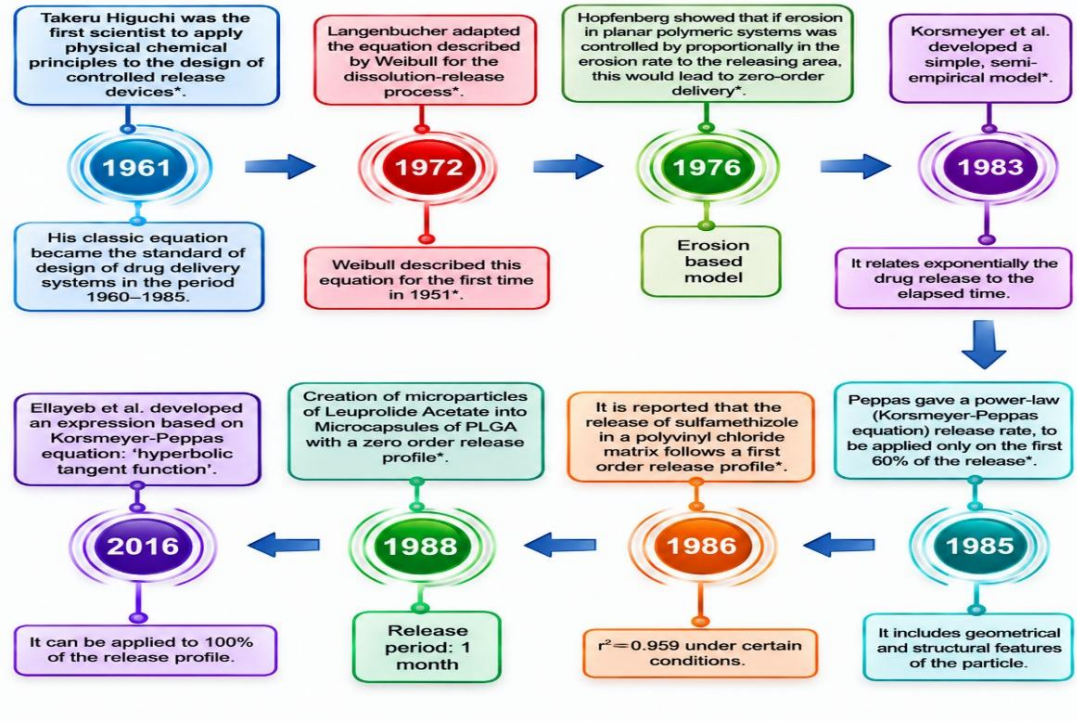



**Figure 4: Comparative release-kinetics modelling for nanoprecipitated PLGA drug-delivery systems [4]**

The Weibull model, $F(t) = 1 - \exp[-(t/\tau)^\beta]$, is flexible and often fits heterogeneous systems well. Its flexibility is both strength and limitation: a good curve fit does not uniquely identify a mechanism. The hyperbolic tangent model has also been proposed for complete release profiles from PLGA nanoparticles. Heredia *et al.* compared several models across 40 datasets and found that the hyperbolic tangent form often performed well by AIC and BIC, while high-order polynomials could overfit.

The following figure illustrates the comparison of different mathematical models used to describe drug-release profiles from PLGA-based nanoparticle systems. It emphasizes the importance of selecting a model that provides both a suitable statistical fit and meaningful predictive performance. The correct comparison therefore includes more than $R^2$. Adjusted $R^2$, AIC, BIC, residual structure, parameter uncertainty, and out-of-sample prediction should be considered. When observations are sparse, bootstrap resampling can help quantify the stability of the comparison, but it cannot replace informative experiments. A model that fits every observed

point may be less useful than a slightly less accurate model that predicts a new batch or a new sampling time.

### 5.1 Practical fitting sequence

First, plot the raw data with uncertainty bars. Second, identify the physically plausible regime and the sampling window. Third, fit a small set of candidate models with comparable weighting. Fourth, examine residuals and parameter confidence intervals. Fifth, validate against an independent batch or a withheld time range. Finally, report the model's intended use: description, interpolation, extrapolation, mechanistic interpretation, or design-space exploration.

## 6. Statistical Optimization and Response-Surface Methodology

Statistical optimization is an important part of drug-delivery development because formulation performance is usually controlled by several factors acting together. Polymer concentration, surfactant level, solvent ratio, stirring speed, processing temperature, and particle size may influence responses such as encapsulation efficiency, particle size, polydispersity, drug release, and stability. Changing one factor at a time may require many experiments and may fail to identify interactions between variables.

Design of experiments (DoE) provides a systematic method for studying several factors simultaneously. Response surface methodology (RSM) is commonly used to develop a mathematical relationship between formulation variables and measured responses. A second-order response model may be expressed as:

$$Y = \beta_0 + \Sigma\beta_i X_i + \Sigma\beta_{ii} X_i^2 + \Sigma\beta_{ij} X_i X_j + \varepsilon \quad \text{.....(2)}$$

where $Y$ is the measured response, $X_i$ and $X_j$ are independent variables, β values are model coefficients, and ε represents experimental error. Linear terms describe the individual effects of variables, squared terms indicate curvature, and interaction terms show whether one variable changes the effect of another. In a study of celecoxib self-microemulsifying drug-delivery systems, the quantities of Labrafil, Labrasol, and Cremophor EL were optimized using a factorial design. Particle size was selected as the main response. The response-surface model showed that the formulation components influenced particle size both individually and through interactions. The predicted particle size was close to the experimentally observed value, demonstrating the usefulness of RSM for formulation development.

The following figure illustrates the agreement between the particle-size values predicted by the response-surface model and the values obtained experimentally. A close relationship between the two values supports the usefulness of the model for formulation optimization.

The relationship between formulation variables and particle size can be further understood through a three-dimensional response-surface plot. Such a plot shows how two factors influence the response while the third factor is kept constant. A curved surface indicates that the response does not change linearly. This information helps researchers identify a practical design region rather than selecting a formulation based only on a single experimental point.

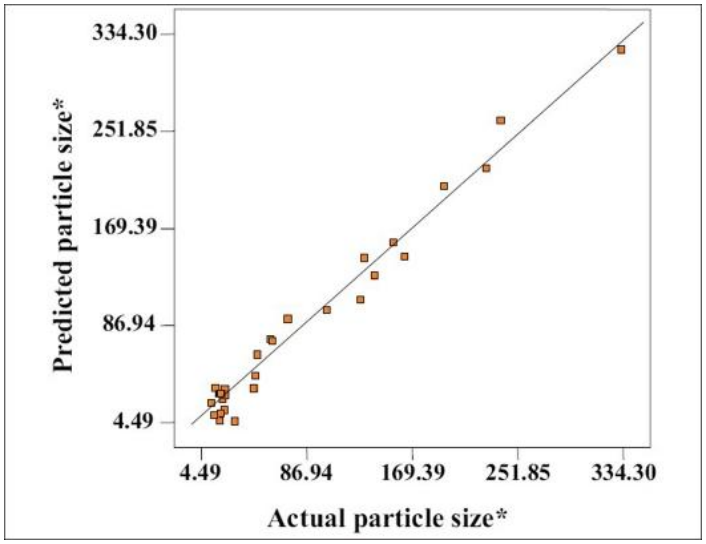



**Figure 5: Predicted versus observed particle size for a celecoxib self-microemulsifying drug-delivery system [5]**

The following figure illustrates the combined influence of Labrafil and Labrasol on the particle size of the self-microemulsifying drug-delivery system while the concentration of Cremophor EL is kept constant. The curved response surface indicates the presence of factor interaction and nonlinear behaviour.

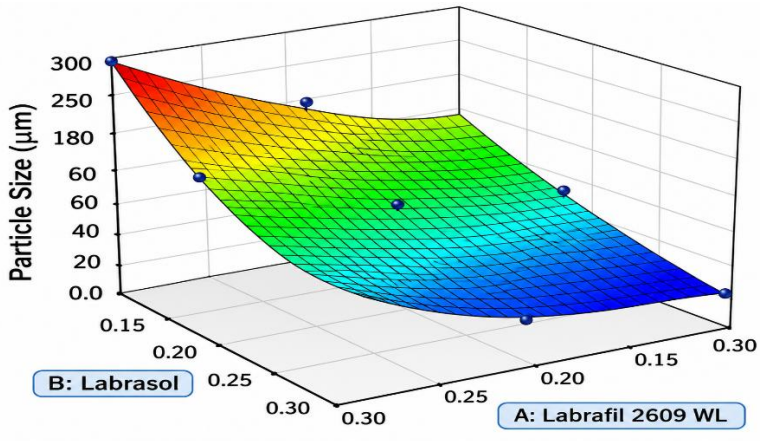



**Figure 6: Response-surface plot showing the combined effect of Labrafil and Labrasol on particle size at a fixed Cremophor EL concentration [5]**

A similar statistical strategy has been used for nanocrystal formulation. In such studies, central composite designs and quadratic models have been applied to optimize encapsulation efficiency and particle size. Analysis of variance, adjusted $R^2$, predicted $R^2$, residual analysis, and desirability functions are useful for evaluating the adequacy of the selected model. The optimized formulation should always be prepared experimentally to compare predicted and observed responses.

Quality by design supports this process by linking formulation objectives with measurable critical quality attributes. The optimized point should remain within the experimentally tested design space. A mathematical optimum outside the validated factor range should not be accepted

without additional experiments. Thus, statistical optimization reduces unnecessary experimentation while maintaining scientific control over formulation development.

**Table 1: A practical map from formulation question to statistical model**

| Design Element | What It Controls | Typical Modelling Output |
|---|---|---|
| Factors | Formulation or process inputs | Coded levels, ranges, constraints |
| Responses | Critical quality attributes | Particle size, EE, release, permeability |
| Model terms | Main effects, curvature, interactions | β coefficients and significance |
| Diagnostics | Adequacy and uncertainty | ANOVA, residuals, lack-of-fit, prediction error |
| Optimization | Trade-offs among responses | Desirability function or Pareto set |

**7. Tables for Study Design and Model Selection**

**Table 2: Model-selection guide for common drug-delivery questions.**

| Model Family | Primary Assumption | Strength | Main Caution |
|---|---|---|---|
| Zero-order | Constant release rate | Simple target profile | Rarely sustained across the full experiment |
| First-order | Rate proportional to remaining drug | Useful for depletion-like release | Mechanism can be ambiguous |
| Higuchi | Diffusion-dominated matrix, suitable geometry | Interpretable square-root scaling | Sensitive to sink and geometry assumptions |
| Korsmeyer–Peppas | Early fractional release follows power law | Regime diagnosis | Exponent is geometry- and range-dependent |
| Weibull | Flexible distribution of release times | Good empirical description | Parameters may lack direct mechanism |
| Reaction–diffusion | Transport and reaction are coupled | Mechanistic interpretation | Needs identifiable parameters and boundary data |
| Compartmental PK | Body represented by connected average spaces | Fast dose and exposure prediction | Spatial heterogeneity is averaged out |
| Fractional-order | History-dependent dynamics | Can represent trapping or memory | Order and kernel need validation |

**Conclusion**

Mathematical modelling becomes most useful when it is treated as a disciplined conversation between mechanism and evidence. Differential equations identify how mass moves and changes;

statistical design identifies which controllable factors shape the response; validation determines whether the combined story travels beyond the original experiment. The best model is not the one with the most parameters. It is the one whose assumptions are visible, whose uncertainty is quantified, and whose predictions support a real formulation or delivery decision.

For future drug-delivery research, the strongest direction is hybrid modelling. Mechanistic transport equations can be coupled to statistical emulators, Bayesian updating, imaging data, and manufacturing constraints. Such systems can shorten formulation cycles without replacing experimental judgement. They can also make failure informative: when a model misses a new batch, the discrepancy points to a missing process, a changed boundary condition, or an unmeasured source of variability.

**References**

1. Copot, D., & Ionescu, C. (2021). Tailored pharmacokinetic model to predict drug trapping in long-term anesthesia. *Journal of Advanced Research, 32*, 27–36. https://doi.org/10.1016/j.jare.2021.04.004
2. Yuan, T., Yang, Y., Zhan, W., & Dini, D. (2023). Mathematical optimisation of magnetic nanoparticle diffusion in the brain white matter. *International Journal of Molecular Sciences, 24*, Article 2534. https://doi.org/10.3390/ijms24032534
3. Rezaeian, M., Soltani, M., Naseri Karimvand, A., & Raahemifar, K. (2022). Mathematical modeling of targeted drug delivery using magnetic nanoparticles during intraperitoneal chemotherapy. *Pharmaceutics, 14*, Article 324. https://doi.org/10.3390/pharmaceutics14020324
4. Heredia, N. S., Vizuete, K., Flores-Calero, M., Pazmiño, K. V., Pilaquinga, F., Kumar, B., & Debut, A. (2022). Comparative statistical analysis of the release kinetics models for nanoprecipitated drug delivery systems based on poly(lactic-co-glycolic acid). *PLOS ONE, 17*(3), e0264825. https://doi.org/10.1371/journal.pone.0264825
5. Shaji, J., & Lodha, S. (2008). Response surface methodology for the optimization of celecoxib self-microemulsifying drug delivery system. *Indian Journal of Pharmaceutical Sciences, 70*, 585–590. https://doi.org/10.4103/0250-474X.45395
6. Bakhaidar, R. B., *et al.* (2022). Response surface methodology powered formulation optimization of nanocrystals. *Polymers, 14*, Article 5184. https://doi.org/10.3390/polymers14235184
7. Mircioiu, C., Voicu, V., Anuta, V., *et al.* (2019). Mathematical modeling of release kinetics from supramolecular drug delivery systems. *Pharmaceutics, 11*, Article 140. https://doi.org/10.3390/pharmaceutics11030140

8. Siepmann, J., & Siepmann, F. (2008). Mathematical modeling of drug delivery. *International Journal of Pharmaceutics, 364*, 328–343. https://doi.org/10.1016/j.ijpharm.2008.09.004
9. Ford Versypt, A. N., Pack, D. W., & Braatz, R. D. (2013). Mathematical modeling of drug delivery from autocatalytically degradable PLGA microspheres. *Journal of Controlled Release, 165*, 29–37. https://doi.org/10.1016/j.jconrel.2012.10.015
10. Arifin, D. Y., Lee, L. Y., & Wang, C. H. (2006). Mathematical modeling and simulation of drug release from microspheres: A review. *Advanced Drug Delivery Reviews, 58*, 1274–1325. https://doi.org/10.1016/j.addr.2006.09.007
11. Higuchi, T. (1963). Mechanism of sustained-action medication: Theoretical analysis of rate of release of solid drugs dispersed in solid matrices. *Journal of Pharmaceutical Sciences, 52*, 1145–1149. https://doi.org/10.1002/jps.2600521210
12. Korsmeyer, R. W., Gurny, R., Doelker, E., Buri, P., & Peppas, N. A. (1983). Mechanisms of solute release from porous hydrophilic polymers. *International Journal of Pharmaceutics, 15*, 25–35. https://doi.org/10.1016/0378-5173(83)90064-9
13. Ritger, P. L., & Peppas, N. A. (1987). A simple equation for description of solute release. *Journal of Controlled Release, 5*, 23–36. https://doi.org/10.1016/0168-3659(87)90034-4
14. Weibull, W. (1951). A statistical distribution function of wide applicability. *Journal of Applied Mechanics, 18*, 293–297.
15. Lansky, P., & Weiss, M. (1998). Is it necessary to use more than one compartment in pharmacokinetic models? *Journal of Pharmacokinetics and Pharmacodynamics, 26*, 761–780. https://doi.org/10.1023/A:1020697826769
16. Macheras, P., & Iliadis, A. (2006). *Modeling in biopharmaceutics, pharmacokinetics, and pharmacodynamics*. Springer.
17. Sheiner, L. B., & Ludden, T. M. (1992). Population pharmacokinetics/dynamics. *Annual Review of Pharmacology and Toxicology, 32*, 185–209. https://doi.org/10.1146/annurev.pa.32.040192.001153
18. International Council for Harmonisation. (2009). *Q8(R2): Pharmaceutical development*. https://www.fda.gov/media/71535/download
19. Yu, L. X., Wu, C., Andrews, L., *et al.* (2014). Understanding pharmaceutical quality by design. *AAPS Journal, 16*, 771–783. https://doi.org/10.1208/s12248-014-9598-3
20. Montgomery, D. C. (2020). *Design and analysis of experiments* (10th ed.). Wiley.
21. Myers, R. H., Montgomery, D. C., & Anderson-Cook, C. M. (2016). *Response surface methodology* (4th ed.). Wiley.
22. Box, G. E. P., & Wilson, K. B. (1951). On the experimental attainment of optimum conditions. *Journal of the Royal Statistical Society: Series B, 13*, 1–45.

23. Nelder, J. A., & Mead, R. (1965). A simplex method for function minimization. *The Computer Journal, 7*, 308–313. https://doi.org/10.1093/comjnl/7.4.308
24. Vandenberghe, L., & Boyd, S. (1996). Semidefinite programming. *SIAM Review, 38*, 49–95. https://doi.org/10.1137/1038003
25. Saltelli, A., Ratto, M., Andres, T., *et al.* (2008). *Global sensitivity analysis: The primer*. Wiley.
26. Kennedy, M. C., & O'Hagan, A. (2001). Bayesian calibration of computer models. *Journal of the Royal Statistical Society: Series B, 63*, 425–464. https://doi.org/10.1111/1467-9868.00294
27. Gelman, A., Carlin, J. B., Stern, H. S., *et al.* (2013). *Bayesian data analysis* (3rd ed.). CRC Press.
28. Atkinson, A. C., Donev, A. N., & Tobias, R. D. (2007). *Optimum experimental designs, with SAS*. Oxford University Press.
29. Puddu, M., *et al.* (2017). Mathematical models for drug diffusion through biological membranes. *Journal of Mathematical Biology*. https://doi.org/10.1007/s00285-017-1114-8
30. Siepmann, J., & Peppas, N. A. (2012). Modeling of drug release from delivery systems based on hydroxypropyl methylcellulose. *Advanced Drug Delivery Reviews, 64*, 163–174. https://doi.org/10.1016/j.addr.2012.09.003
31. Venkatesan, R., Mohamed Harees, M., Surya Prabha, R., & Sharmi, B. (2026). Fabrication and characterisation of free-standing porous and non-porous PCL/PCL-PEO films using spin coating technique. In S. S. Kawar (Ed.), *Nanomaterials: Synthesis, Characterization & Applications* (Vol. 6). AkiNik Publications. https://doi.org/10.22271/ed.book.3872.

# KEYED JULIA-POTENTIAL FIELDS: A PARAMETER-SENSITIVE FRACTAL CARRIER FOR BLIND IMAGE WATERMARKING

**S. Ramaswami[1] and Salahuddin[2]**

[1]Department of Naval Architecture & Offshore Engineer,

[2]Department of Mathematics,

AMET University, Kanathur, Chennai, Tamil Nadu, India

Corresponding author E-mail: sramaswami@ametuniv.ac.in, vsludn@gmail.com

**Abstract**

Quadratic map Julia sets are well-established objects in complex dynamics but have only recently been proposed for applications in signal security, where they have been restricted to generation of chaotic bit streams. We propose Keyed Julia-Potential Fields (KJPF), a structured, 2D, key dependent carrier derived from the potential/smoothed escape time field of the filled Julia set associated with $f_c(z) = z^2 + c$. The complex constant $c$, together with the region of interest/iteration cap parameters forms our secret key. In contrast with typical pseudo random noise carriers used for watermarking, we exploit the self similar multi scale property of these fractals allowing for resilience under mild re-sampling as well as the Fatou-Julia dichotomy inherent to quadratic maps. This allows the designer to choose whether to operate within an easily embeddable connected regime (high correlation) or more entropy rich disconnected regime. We detail both the embedding and detection algorithms and provide an analysis of the key sensitivity/capacity trade-offs as well as a measure of the actual key sensitivity obtained at runtime in this paper. Finally, we specify protocols for evaluating robustness properties which will be implemented in future work.

**Keywords:** Keyed Julia-Potential Fields (KJPF), Parameter-Sensitive Fractal Carrier, Blind Image Watermarking.

## Introduction

Digital watermarking embeds an identifier in the media, so that later he can claim ownership. In spread spectrum techniques (Cox *et al.,* 1997), the watermark is multiplied by a pseudo-random carrier known only to the owner. Two properties are important: *key sensitivity* (an incorrect key must produce an uncorrelated carrier) and *structure tolerance* (a correct key must still be detectable after distortions). Plain random noise is good for the first and bad for the second, because pixel-level noise is destroyed by blur and rescaling.

Julia sets offer a natural compromise: the escape-time images are smooth except at the boundary, richly textured at it, and maximally sensitive to the parameter c, because c is the presiding topography. The paper offers (i) the construction of the KJPF carrier, (ii) a regime selecting rule

based on the Mandelbrot-set inclusion of c, and (iii) a numerical investigation of key-sensitivity (Section 5) resulting in a demonstration of the rate of decay of the carrier correlation with parameter perturbation.

**Preliminaries**

For $f_c(z) = z^2 + c$ with $c \in \mathbb{C}$, the filled Julia set is $K_c = \{z : f_c^n(z) \text{ bounded}\}$ and the Julia set is $J_c = \partial K_c$. By the Fatou–Julia dichotomy, $J_c$ is connected if the critical orbit $\{f_c^n(0)\}$ is bounded (i.e. $c$ lies in the Mandelbrot set $M$) and a Cantor set otherwise (Julia, 1918; Fatou, 1919; Mandelbrot, 1980).

The Green (potential) function of $K_c$ is

$$G_c(z) = \lim_{n\to\infty} 2^{-n} \log\left|f_c^n(z)\right|, \qquad G_c = 0 \text{ on } K_c,\ G_c > 0 \text{ outside.}$$

It is harmonic outside $K_c$ and is approximated numerically by the *smooth escape time*

$$\nu(z) = n + 1 - \log_2\left(\log|z_n| / \log R\right), \qquad n = \text{first index with } |z_n| > R.$$

For small $|c|$, Ruelle's result gives the Hausdorff dimension

$$\dim_H J_c = 1 + \frac{|c|^2}{4 \ln 2} + O(|c|^3).$$

This quantifies how "rough" the carrier boundary is as $c$ moves away from the origin (Fig. 1).

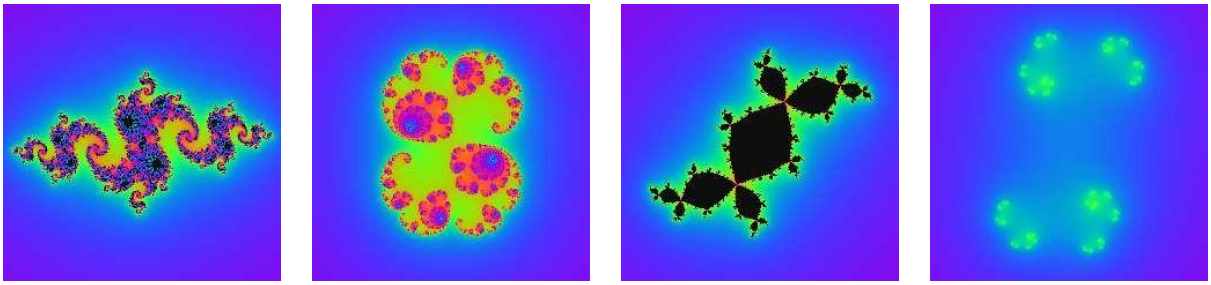


**Figure 1: Smooth escape-time fields for four candidate key parameters: $c = -0.8 + 0.156i$ (filamentary, close to $\partial M$); $c = 0.285 + 0.01i$ (spiral structure, just outside the cusp of $M$, hence a Cantor-type set); $c = -0.123 + 0.745i$ (Douady rabbit, $c \in M$, connected); $c = 0.7 + 0.3i$ (clearly outside $M$, dust-like). Window $[-1.6,1.6]^2$**

**The KJPF Method**

**Key and carrier**

The secret key is $k = (c,w,N)$, where $w$ is a square window in the complex plane and $N$ the iteration cap. For an $H \times W$ host, pixel $(x,y)$ maps to $z_{xy} \in w$. The raw field is $\nu(z_{xy})$, set to $N$ inside $K_c$. We zero-mean and unit-normalise it:

$$s(x,y) = \frac{\nu(x,y) - \mu_\nu}{\sigma_\nu}.$$

**Embedding**

For a watermark bit $b \in \{-1,+1\}$ and host block $X$ (spatial pixels or mid-band DCT coefficients), the marked block is

$$X' = X + \alpha \cdot b \cdot s$$

with strength $\alpha$ chosen for imperceptibility. A multi-bit message uses disjoint blocks, or distinct window offsets $w_j$ per bit, so each bit has its own nearly orthogonal carrier.

**Blind detection**

The detector regenerates $s$ from $k$ and computes the normalised correlation

$$\rho = \frac{\langle X', s \rangle}{\|X'\| \cdot \|s\|}, \qquad \hat{b} = \operatorname{sign}\langle X', s \rangle$$

and declares the mark present if $|\rho|$ exceeds a threshold $\tau$ set from the false-positive target. No original host is required, so detection is blind.

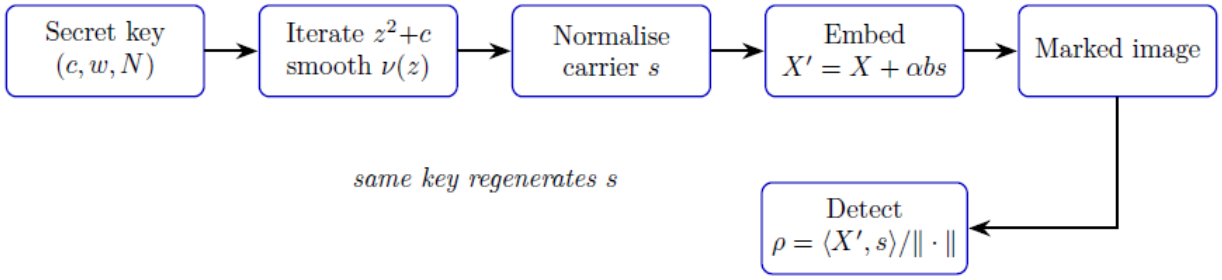



**Figure 2: KJPF embedding (top row) and blind detection (bottom)**

**Theoretical Analysis**

**Regime selection**

If $c \in M$, the field contains a large interior plateau ($v = N$) plus a thin, structured boundary; after normalisation the carrier is dominated by low-frequency content, which resists blur and JPEG-style quantisation but offers lower entropy. If $c \notin M$, $K_c$ is a Cantor dust of measure zero, so almost every pixel escapes and the field is determined by escape speed, giving higher-frequency, higher-entropy texture. We therefore propose: choose $c$ near $\partial M$ for robustness–entropy balance, since the boundary region offers both rich structure and fine parameter sensitivity.

**Key space**

With IEEE-754 doubles, Re$c$ and Im$c$ provide at most $\approx 2^{104}$ distinct mantissa states over a bounded range, before accounting for window and cap. Many of these keys give visually indistinguishable fields, so the *effective* key space is smaller. Section 5 measures the decorrelation scale directly, which is what determines usable key density.

**Sensitivity heuristic**

Escape time depends on the orbit $z_{n+1} = z_n^2 + c$, whose derivative with respect to $c$ satisfies

$$\frac{\partial z_{n+1}}{\partial c} = 2z_n \frac{\partial z_n}{\partial c} + 1.$$

Near $J_c$ this derivative grows exponentially with $n$, so pixels close to the Julia set change escape count under tiny changes of $c$, while pixels far from it change little. Hence we expect *partial* decorrelation: structured regions persist, fine texture does not. This is a feature for tolerance to small perturbations but a limitation for adversarial key-guessing, discussed in Section 7.

**Computed Key-Sensitivity Study**

Using base key $c_0 = -0.8 + 0.156i$, window $[-1.6,1.6]^2$, $N = 200$ and a $160 \times 160$ grid, we regenerate the carrier with $c = c_0 + \delta$ and compute the Pearson correlation with the reference carrier. Fig. 2 shows the carriers and their difference for the largest perturbation; Table 1 is computed by your browser when the page loads.

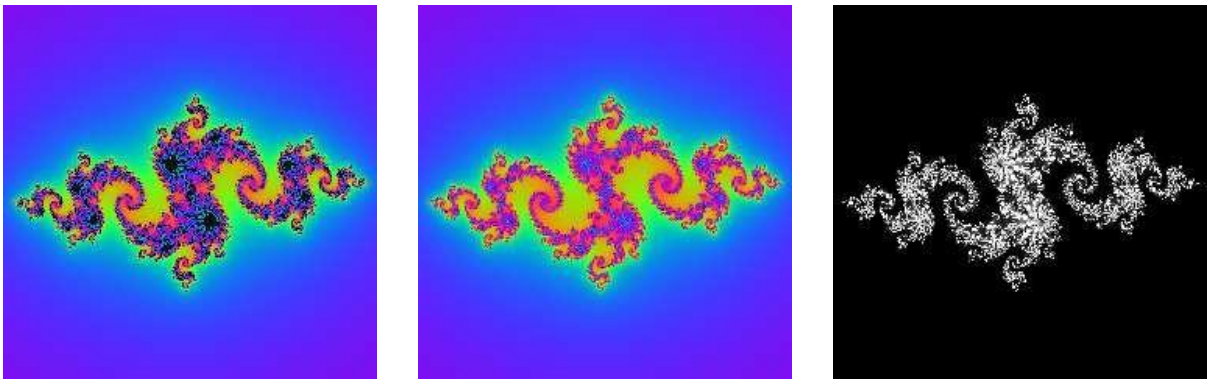


**Figure 2: Left: reference carrier ($c_0$). Middle: carrier with $\delta = 0.01$. Right: absolute difference (brighter = larger change), concentrated near the Julia set**

**Table 1: Carrier correlation versus parameter perturbation (computed live).**

| $\delta$ (added to Re$c$) | Pearson $\rho$ vs reference |
|---|---|
| 0 | 1.0000 |
| $10^{-8}$ | 0.9997 |
| $10^{-6}$ | 0.9954 |
| $10^{-4}$ | 0.9553 |
| $10^{-2}$ | 0.7488 |

The table gives the empirical decorrelation scale for this key region. A watermark scheme should space keys by perturbations well beyond the point where $\rho$ becomes small; this is the practical measure of key density, and it should be recomputed for each chosen $c$ region.

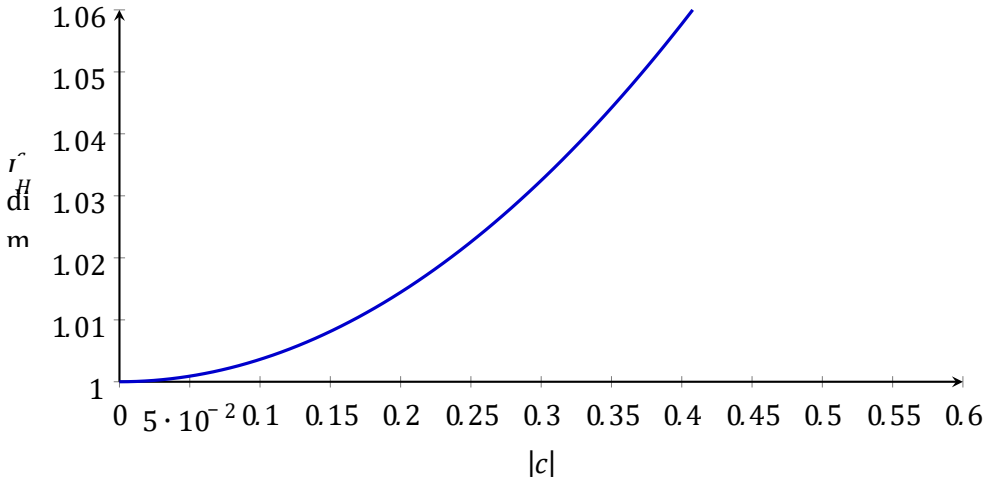



**Figure 3: Small-$|c|$ asymptotic Hausdorff dimension $1 + |c|^2/(4\ln 2)$. The expansion is only valid for small $|c|$; it is plotted on [0,0.6] and should not be extrapolated to the boundary of $M$**

**Proposed Evaluation Protocol**

This paper does not claim detection performance numbers; those require a benchmark run. We specify the protocol so that results are reproducible.

**Data:** standard grey-scale test images (e.g. 512×512 Lena, Baboon, Peppers) plus a naturalimage set of ≥ 1000 images.

**Imperceptibility:** PSNR and SSIM of marked versus original at several $\alpha$.

**Robustness:** JPEG (quality 30–90), Gaussian blur, additive noise, cropping, rescaling 0.5–2×, rotation ±5°.

**Detection:** ROC curves of $\rho$ under correct versus wrong key, with wrong keys drawn at distances $\delta$ from the true key.

**Baselines:** Gaussian spread-spectrum carrier (Cox et al.), logistic-map carrier, and KJPF with $c \in M$ versus $c \notin M$ to test the regime-selection rule of Section 4.1.

**Limitations and Future Work**

(1) Partial decorrelation means that attackers who know the carrier family can search a lowdimensional key space (two real numbers plus window), which is much smaller than a symmetric cipher key; KJPF should therefore be combined with a cryptographic key-derivation step that selects $(c,w,N)$ from a secret.

(2) Geometric attacks require synchronization, which can be achieved by exploiting the self-similarity of the carrier.

(3) The key space would be enlarged by higher-degree maps $z^d+c$, by rational maps, or by two-parameter families.

(4) Cost is $O(HWN)$ per carrier, which is acceptable on GPU or with the cap $N \le 200$ used here.

**Conclusion**

The parameter sensitivity and multi-scale structure of Julia sets are used in KJPF as a keyed watermark carrier with a well-defined detection statistic and a tunable robustness-entropy tradeoff depending on the position of $c$ relative to a Mandelbrot set. The measurements reported here only characterize carrier decorrelation. The protocol in Section 6 is yet to establish end-to-end robustness and security.

**References**

1. Julia, G. (1918). Mémoire sur l'itération des fonctions rationnelles. *Journal de Mathématiques Pures et Appliquées*.
2. Fatou, P. (1919–1920). Sur les équations fonctionnelles. *Bulletin de la Société Mathématique de France*.
3. Mandelbrot, B. (1980). Fractal aspects of the iteration of $z \to \lambda z(1 - z)$ for complex $\lambda$ and $z$. *Annals of the New York Academy of Sciences*.
4. Douady, A., & Hubbard, J. H. (1984). *Étude dynamique des polynômes complexes*. Publications Mathématiques d'Orsay.
5. Ruelle, D. (1982). Repellers for real analytic maps. *Ergodic Theory and Dynamical Systems*.
6. Cox, I. J., Kilian, J., Leighton, F. T., & Shamoon, T. (1997). Secure spread spectrum watermarking for multimedia. *IEEE Transactions on Image Processing*.
7. Falconer, K. (1990). *Fractal geometry: Mathematical foundations and applications*. Wiley.

# INDUSTRIAL WASTE VALORIZATION AND SUSTAINABLE MATERIAL DESIGN: A DATA-DRIVEN STATISTICAL APPROACH

**Sthitadhi Das**
Department of Mathematics, Brainware University, Kolkata, India
Corresponding author E-mail: sthdas999@gmail.com

**Abstract**

The increasing generation of industrial waste has created significant environmental and resource-management challenges, while simultaneously providing opportunities for the development of sustainable engineering materials. Industrial waste upcycling offers a promising pathway for converting waste streams into value-added materials for construction, infrastructure, composites, ceramics, and other engineering applications. However, the performance of waste-derived materials is influenced by numerous factors, including waste composition, particle characteristics, replacement level, processing conditions, and curing parameters. This chapter presents a statistical modeling perspective on the development and evaluation of sustainable engineering materials from industrial waste. Established statistical methods, including descriptive analysis, correlation analysis, regression modeling, analysis of variance, response surface methodology, and mixed-effects models, are considered for understanding material behavior and experimental variability. Machine-learning approaches are also discussed as complementary tools for prediction and model comparison. Particular emphasis is placed on using statistical models to identify important factors, predict engineering performance, and optimize material formulations under practical constraints. The chapter further connects statistical prediction with sustainability indicators such as waste utilization, energy consumption, production cost, and environmental impact. A real-data case study will illustrate how statistical modeling can support data-driven material design and contribute to the transition from conventional waste management toward a circular economy.

**Keywords:** Industrial Waste Upcycling, Sustainable Engineering Materials, Statistical Modeling, Regression Analysis, Response Surface Methodology, Machine Learning, Material Optimization, Waste Valorization, Circular Economy, Sustainable Engineering.

**2020 Mathematics Subject Classification:** Primary 62J05, 62J12, Secondary 62P30, 90C90.

## 1. Introduction

Industrialization has contributed substantially to economic development, infrastructure expansion, and technological advancement. However, the production, processing, and consumption of industrial materials also generate substantial quantities of residual materials that require appropriate management. These residuals may arise from energy production,

metallurgical operations, mining, chemical manufacturing, foundry processes, glass production, and construction activities. When such materials are inadequately managed, they may contribute to environmental contamination, resource depletion, and additional economic costs. The United Nations Environment Programme emphasizes the importance of moving beyond conventional waste management toward waste prevention, resource recovery, and circular-economy practices [1]. Although the Global Waste Management Outlook primarily examines municipal solid waste, its broader resource-management principles are relevant to the development of integrated waste valorization strategies.

The environmental significance of waste management extends beyond the disposal stage. The extraction of virgin raw materials, their transportation, industrial processing, and the manufacture of replacement materials can consume energy and generate environmental burdens. Consequently, sustainable material development requires a systematic assessment of both material performance and resource efficiency. Life-cycle assessment (LCA) provides a recognized framework for evaluating environmental aspects and potential impacts throughout the life cycle of a product or process, including the definition of the goal and scope, inventory analysis, impact assessment, and interpretation [2]. Therefore, the environmental advantages of industrial waste utilization should not be assumed solely from the fact that a waste material has been incorporated into a new product. Such advantages depend on factors including waste processing requirements, transportation distance, substitution of conventional materials, product durability, and end-of-life management.

Industrial waste valorization represents a resource-oriented approach in which residual materials are converted into useful secondary resources or value-added products. In contrast to disposaloriented practices, valorization considers the possibility of recovering useful physical, chemical, or functional properties from materials that would otherwise have limited economic value. In construction and materials engineering, this approach is particularly relevant because industrial by-products may serve as supplementary cementitious materials, aggregates, mineral fillers, ceramic constituents, or precursors for alkali-activated materials. For example, coal fly ash has been investigated as a resource for several applications, including cementitious and other construction-related products [3]. Similarly, construction and demolition waste can provide secondary aggregates and other recoverable material fractions, although effective implementation depends on appropriate sorting, processing, quality control, and market acceptance [4, 5]. These applications illustrate the potential of waste valorization to reduce the demand for selected virgin resources while creating additional pathways for material utilization.

The range of industrial residues considered for sustainable material design is broad. It includes fly ash, blast-furnace slag, steel-making residues, red mud, foundry sand, construction and demolition waste, waste glass, quarry dust, mining residues, and rice-husk ash. However, these

materials cannot be treated as interchangeable ingredients. Their properties may vary substantially according to their sources, production processes, chemical composition, mineralogical structure, particle-size distribution, moisture content, and pretreatment conditions. Even materials bearing the same general name may exhibit different engineering characteristics when obtained from different industrial facilities or production batches. Consequently, a waste material that performs satisfactorily in one formulation may not provide the same performance under different processing conditions or when combined with a different binder or matrix. This variability makes systematic characterization and data-driven evaluation important components of sustainable material development.

The successful incorporation of industrial waste into engineering materials depends on several interacting factors. These may include the proportion of waste used, the water-to-binder ratio, particle fineness, chemical composition, additive dosage, mixing procedure, processing temperature, compaction pressure, curing duration, and environmental exposure. The resulting engineering responses may include compressive strength, tensile strength, flexural strength, density, porosity, water absorption, thermal conductivity, durability, and resistance to chemical or physical degradation. In practice, these responses are often interdependent. For instance, a formulation that improves one mechanical property may simultaneously affect density, water absorption, workability, production cost, or long-term durability. The objective of material design is therefore not necessarily to maximize a single response, but to identify a formulation that achieves an appropriate balance among technical, economic, and environmental requirements.

The circular-economy perspective provides a broader context for this problem. Rather than following a linear pattern of resource extraction, manufacturing, use, and disposal, a circular approach seeks to retain the value of materials through reuse, recovery, recycling, and appropriate reintegration into production systems. Reviews of construction and demolition waste management have identified material recovery and circular-economy strategies as important opportunities for improving resource efficiency, while also documenting practical barriers to their implementation [4, 5]. However, circularity alone does not guarantee environmental superiority. The suitability of a waste-derived material must be assessed in relation to its intended application, performance requirements, processing demands, and environmental consequences. For this reason, material characterization and quantitative performance evaluation should be integrated with sustainability assessment rather than treated as separate activities.

A major challenge in industrial waste valorization is that material performance is governed by numerous explanatory variables whose effects may be nonlinear and mutually dependent. Traditional experimental comparisons can identify differences between selected formulations, but they may provide an incomplete understanding when many variables change simultaneously.

Statistical modeling offers a systematic framework for investigating such relationships. Descriptive statistics summarize the distribution and variability of observed measurements, while graphical exploration and correlation analysis help identify preliminary patterns and possible associations. Regression models can quantify relationships between explanatory variables and engineering responses, whereas analysis of variance (ANOVA) can be used to assess differences among experimental conditions under an appropriate statistical design. These methods provide a foundation for interpreting experimental evidence and identifying factors that may warrant further investigation.

A general representation of the relationship between material properties and explanatory variables is

$$Y_i = f(X_{i1}, X_{i2}, \ldots, X_{ip}) + \varepsilon_i, \qquad i = 1,2,\ldots,n, \qquad (1.1)$$

where $Y_i$ denotes an observed engineering-performance response for the $i$th experimental observation, $X_{i1},\ldots,X_{ip}$ represent the corresponding waste characteristics and processing variables, $f(\cdot)$ denotes an unknown response function, and $\varepsilon_i$ represents unexplained variation. The sample size is $n$, and $p$ denotes the number of explanatory variables. Depending on the experimental setting, the response may be a continuous measurement, such as compressive strength or thermal conductivity, or another outcome appropriate to the material-design problem.

The form of $f(\cdot)$ depends on the scientific problem and the available data. A linear regression model may be useful when the response can be adequately approximated by additive linear effects. Polynomial regression can accommodate curvature, while interaction terms can represent situations in which the effect of one variable depends on the level of another. Response surface methodology (RSM) provides a systematic collection of experimental-design and modeling techniques for studying relationships between several controllable factors and one or more responses. It is particularly useful when the objective is to identify operating conditions or material formulations that provide desirable responses within a specified experimental region [6, 7]. For industrial waste-derived materials, such methods can help investigate the combined influence of waste replacement level, binder content, curing conditions, and other formulation variables.

A further consideration is the hierarchical structure of many materials experiments. Measurements may be obtained from multiple specimens prepared within the same batch, from several batches produced on different days, or from different laboratories or industrial facilities. Observations within a common batch may share unmeasured characteristics and therefore may not be statistically independent. Treating all measurements as independent without considering the experimental structure can lead to inappropriate uncertainty estimates. Where the design supports such an analysis, mixed-effects models can distinguish systematic effects associated with measured formulation variables from variation attributable to batches, production runs, or

other grouping factors. This is relevant to the transition from laboratory experimentation to industrial production, where repeatability and batch-to-batch consistency are important considerations.

Machine-learning methods provide additional tools for analyzing complex relationships between material composition and engineering performance. Algorithms such as regression trees, random forests, support vector regression, and artificial neural networks can be used to represent nonlinear associations without requiring the analyst to specify a complete parametric response function in advance. A systematic review by Hassan *et al.* [8] documents the application of machine-learning methods to the prediction of properties across different types of concrete. Such methods can complement conventional statistical models when the available dataset contains sufficiently informative observations and the evaluation procedure is carefully designed. Nevertheless, predictive accuracy alone does not establish that a model is scientifically appropriate or that its predictions will generalize to new industrial settings. Data leakage, small sample sizes, imbalanced representation of formulations, measurement error, and differences between training and deployment conditions can all affect model performance. Accordingly, model evaluation should consider appropriate data partitioning, cross-validation where suitable, prediction errors, uncertainty, and the relevance of the validation data to the intended application.

The relationship between statistical prediction and material optimization is particularly important. A model may identify formulations associated with favorable experimental responses, but the preferred formulation must also satisfy practical constraints. These may include minimum strength requirements, acceptable water absorption, durability criteria, limits on waste content, manufacturing feasibility, and restrictions on production cost or environmental impact. When several responses are considered simultaneously, the problem becomes a multi-criteria or multi-objective optimization task. A formulation with the highest predicted compressive strength may not be the most appropriate choice if it requires excessive energy, increases cost, or performs poorly in another essential property. Moreover, any model-based optimum should be treated as a candidate for experimental confirmation rather than as conclusive evidence of optimal performance. Design of experiments, regression modeling, and response surface techniques provide established approaches for linking controlled experimentation with process and product improvement [7].

Sustainability assessment adds another dimension to this framework. The quantity of waste incorporated into a formulation is a useful resource-utilization indicator, but it is not sufficient on its own to establish an overall environmental benefit. Other indicators may include energy consumption, greenhouse-gas emissions, water use, production cost, transportation requirements, durability, and the potential for reuse or recycling at the end of the product's service life. Life-cycle assessment can provide a structured basis for evaluating environmental impacts across

relevant stages of a product's life cycle, subject to the selected system boundaries, functional unit, inventory data, and assessment assumptions [2]. Consequently, statistical models can contribute to sustainability-oriented material design by estimating engineering responses and supporting comparisons among candidate formulations, while environmental assessment provides a complementary basis for evaluating broader consequences.

The present chapter adopts an application-oriented perspective to demonstrate how established statistical and machine-learning methods can support the evaluation of industrial waste-derived materials. The emphasis is on integrating experimental data, exploratory analysis, regression modeling, ANOVA, response surface methodology, mixed-effects modeling, predictive learning, and optimization within a coherent analytical workflow. The objective is not to introduce new statistical theory, but to explain how established techniques can be selected, interpreted, and applied to materialdesign problems. Particular attention is given to the quality of the available data, the interpretation of model assumptions, the assessment of predictive performance, and the distinction between statistical association and causal conclusions.

The proposed framework can be summarized as:

Industrial Waste Characterization
↓
Experimental Design and Data Collection
↓
Exploratory and Statistical Analysis
↓
Regression and Machine-Learning Models
↓
Model Validation and Uncertainty Assessment
↓
Material Formulation and Multi-Response Optimization
↓
Experimental Confirmation and Sustainability Assessment

This workflow emphasizes that sustainable material design is an iterative process rather than a single prediction exercise. Model-based recommendations should be checked against experimental evidence, engineering requirements, and environmental considerations. The resulting integration of statistical analysis and material characterization can support more transparent comparisons among candidate formulations and provide a quantitative basis for identifying promising uses of industrial residuals. Ultimately, the chapter seeks to demonstrate how data-driven methods can help connect industrial waste recovery with the development of technically suitable and environmentally informed engineering materials.

## 2. Industrial Waste and Sustainable Engineering Materials

### 2.1 Industrial waste as a secondary resource

Industrial waste should not necessarily be regarded solely as an environmental burden; under appropriate technical, economic, and environmental conditions, it can serve as a secondary resource for manufacturing value-added engineering materials. Industrial waste valorization involves recovering useful constituents or functional properties from residual materials and incorporating them into new products. This approach is consistent with circular-economy principles, which emphasize resource efficiency, material recovery, and the reduction of dependence on virgin raw materials [1]. For example, fly ash can be utilized in cementitious applications, while suitable construction and demolition waste can be processed into secondary aggregates and other construction products [3, 4].

Depending on their industrial origin, waste materials may contain silica, alumina, calcium compounds, iron oxides, carbonaceous matter, glassy phases, metallic constituents, or other potentially useful components. Their engineering functions depend not only on chemical composition but also on mineralogical structure, particle morphology, fineness, porosity, moisture content, and surface characteristics. Consequently, the same waste may be suitable for one application but unsuitable for another. Furthermore, the presence of undesirable constituents, soluble compounds, or potentially hazardous substances may restrict its use and necessitate appropriate treatment and safety assessment.

Waste characterization is therefore a fundamental prerequisite for material development. Relevant measurements may include chemical composition, particle-size distribution, specific gravity, moisture content, loss on ignition, and other application-specific properties. Measurements should also be collected across different batches whenever possible, since variations in the source material or production process may affect the consistency of the final product. From a statistical perspective, characterization provides the explanatory variables required to investigate the association between waste properties and engineering performance. It also helps distinguish genuine formulation effects from variability attributable to differences in the waste itself.

### 2.2 Major categories of industrial waste

Industrial waste relevant to sustainable engineering materials can be classified according to its source, composition, and potential application. Important categories include the following:

i. **Fly ash and bottom ash:** Residues from thermal power generation that may be considered for cementitious materials, bricks, and other construction products, subject to their composition and application requirements [3].

ii. **Blast-furnace and steel-making slags:** Metallurgical residues that may provide mineral constituents for cementitious binders, aggregates, and other construction materials, depending on their origin, processing, and material properties.

iii. **Red mud:** A residue from alumina production whose mineral composition may support selected applications in ceramics, construction materials, and other mineral-based products, provided that its alkalinity and potentially problematic constituents are appropriately evaluated.

iv. **Foundry sand:** Used moulding and core sands that may be assessed as partial replacements for natural sand or as constituents of selected construction products, subject to contamination and quality-control requirements.

v. **Construction and demolition waste:** Concrete, masonry, brick, and other recoverable fractions that can be processed into secondary aggregates and other construction materials. Their suitability depends on sorting, contamination, particle grading, and processing quality [4, 5].

vi. **Waste glass:** Glass residues that may be processed for use as aggregate, filler, or a constituent of selected glass-based and cementitious products, depending on particle size and compatibility with the intended application.

vii. **Quarry dust and stone-processing residues:** Fine mineral fractions that may be investigated as fillers or partial replacements for natural aggregates in appropriate construction applications.

viii. **Mining and mineral-processing residues:** Tailings and other mineral residues that may contain useful mineral fractions but require careful assessment of chemical stability, contaminant content, and long-term environmental risks.

ix. **Rice-husk and other biomass-derived ashes:** Ashes that may contain useful mineral constituents, including silica, depending on the feedstock and combustion conditions. Their suitability for cementitious and other applications depends on composition, fineness, and processing history.

x. **Waste polymers and industrial plastic residues:** Selected polymer wastes that may be incorporated into composites, modified construction materials, or other products after appropriate sorting and processing. Compatibility, durability, and end-of-life considerations are important in determining their suitability.

xi. **Other metallurgical and process-derived residues:** Sludges, mineral fines, process powders, and related by-products that may offer recovery opportunities when their composition, variability, and environmental safety are adequately established.

These categories illustrate the diversity of potential secondary resources; however, they should not be interpreted as evidence that every waste stream is suitable for direct reuse. The feasibility

of valorization depends on the material's characteristics, processing requirements, relevant engineering standards, environmental safety, and the availability of a technically appropriate application. Consequently, a systematic assessment of both material quality and variability is essential before selecting a waste stream for further development.

**2.3 Engineering applications**

Industrial wastes can be incorporated into engineering materials through different mechanisms, depending on their physical and chemical properties and the characteristics of the receiving material. A waste may function as a partial replacement for cement, natural aggregate, sand, filler, binder, or another constituent. Some materials may contribute to pozzolanic reactions, whereas others may primarily provide particle packing, reinforcement, or mineral filler effects. Suitable aluminosilicate-rich residues may also be investigated as precursors for alkali-activated or geopolymer materials. The actual mechanism and resulting performance must be established for the particular waste, formulation, and processing conditions rather than assumed from the waste category alone.

Consider a composite in which industrial waste partially replaces a conventional constituent. Let

$$Z = \text{percentage of industrial waste incorporated},$$

and let

$$Y = \text{compressive strength of the resulting material}.$$

The relationship between $Z$ and $Y$ may depend on particle packing, chemical reactivity, porosity, water demand, and the properties of the remaining constituents. A moderate replacement level may improve some aspects of performance, whereas excessive replacement may adversely affect strength or other required properties. The response may therefore be nonlinear and may also depend on variables such as curing time, binder content, and water-to-binder ratio. A simple quadratic model can represent such curvature:

$$Y_i = \beta_0 + \beta_1 Z_i + \beta_2 Z_i^2 + \varepsilon_i, \qquad i = 1,\ldots,n, \tag{2.1}$$

where $\beta_0$, $\beta_1$, and $\beta_2$ are unknown parameters and $\varepsilon_i$ represents unexplained variation. A negative quadratic coefficient, when supported by the data and model assumptions, may indicate a concave response over the observed range. However, the estimated turning point should be interpreted as a candidate optimum only if it lies within the investigated range and the model provides an adequate representation of the data.

When several formulation variables interact, a more general model is appropriate:

$$Y_i = \beta_0 + \sum_{j=1}^{p} \beta_j X_{ij} + \sum_{j=1}^{p} \beta_{jj} X_{ij}^2 + \sum_{j<k} \beta_{jk} X_{ij} X_{ik} + \varepsilon_i, \tag{2.2}$$

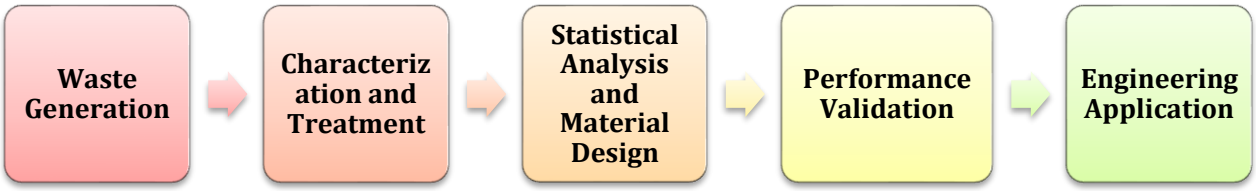
where $X_{ij}$ denotes the $j$th explanatory variable for the $i$th observation, $\beta_j$ represents a linear effect, $\beta_{jj}$ represents a quadratic effect, and $\beta_{jk}$ represents an interaction effect. Such a model provides a basis for response surface analysis and formulation optimization when the experimental design contains sufficient information to estimate the required terms [6, 7].

The same modeling framework can be extended to responses such as water absorption, density, flexural strength, thermal conductivity, and durability indicators. Since the formulation that maximizes one response may not optimize the others, practical material development often requires simultaneous consideration of several performance criteria. Statistical analysis can help identify influential variables, quantify uncertainty, compare candidate formulations, and select promising conditions for experimental confirmation.

**2.4 Circular economy perspective**

The circular economy seeks to retain the value of resources through waste prevention, reuse, recycling, and recovery, thereby reducing dependence on virgin materials and limiting avoidable disposal. Industrial waste valorization can contribute to these objectives by returning suitable residual materials to productive applications. In the construction sector, the recovery of construction and demolition waste illustrates how secondary materials can be incorporated into new production cycles, although implementation remains dependent on material quality, processing infrastructure, economic feasibility, and regulatory requirements [4, 5]. A simplified pathway for industrial waste valorization is:

**Industrial Process**




Statistical modeling can support this pathway by relating waste characteristics and processing conditions to measurable engineering responses. It can also help quantify batch variability, compare alternative formulations, predict performance within a validated domain, and identify promising conditions for further experimentation. Nevertheless, statistical prediction alone cannot establish the overall sustainability of a proposed material. The environmental benefits of replacing conventional resources must be assessed in relation to factors such as energy consumption, transportation, processing requirements, product service life, and end-of-life management. Life-cycle assessment provides a structured framework for evaluating relevant environmental impacts across a defined product system [2].

Accordingly, successful waste valorization requires the integration of material characterization, statistical analysis, engineering validation, and sustainability assessment. This integrated approach can help distinguish technically feasible applications from those that are merely plausible, while providing a quantitative basis for developing reliable and resource-efficient engineering materials.

## 3. Data Collection and Experimental Variables

### 3.1 Data structure

The quality of statistical analysis depends fundamentally on the quality, relevance, and structure of the collected data. In industrial waste valorization, observations may be obtained from laboratory experiments, pilot-scale production, industrial monitoring, or published experimental studies. Each observation should be associated with clearly defined material characteristics, formulation variables, processing conditions, and measured engineering responses. Wherever possible, information about the waste source, production batch, specimen preparation, testing procedure, and measurement units should also be recorded.

A general representation of the dataset is

$$\mathcal{D} = \left\{ \left( Y_i, \boldsymbol{X}_i^\top, \boldsymbol{Z}_i^\top \right) : i = 1, \ldots, n \right\}, \tag{3.1}$$

where $Y_i$ denotes an engineering response, $X_i$ is a vector of $p$ waste characteristics, $Z_i$ is a vector of $q$ processing or formulation variables, and $n$ is the number of experimental observations. When multiple responses are recorded, the response $Y_i$ may be replaced by a vector $Y_i \in \mathrm{R}^m$.

For illustration, consider the partial replacement of a conventional binder with fly ash. The dataset may contain the fly ash replacement percentage, water-to-binder ratio, curing temperature, curing duration, and compressive strength. The primary objective may be to investigate how the formulation and processing variables influence compressive strength while accounting for experimental variability. A hypothetical experimental record is presented below.

**Table 1: Illustrative structure of a waste-upcycling dataset.**

| Obs. | Fly ash (%) | Water/binder ratio | Curing (days) | Temperature (°C) | Strength (MPa) |
|---|---|---|---|---|---|
| 1 | 0 | 0.45 | 28 | 25 | 42 |
| 2 | 10 | 0.45 | 28 | 25 | 45 |
| 3 | 20 | 0.45 | 28 | 25 | 48 |
| 4 | 30 | 0.45 | 28 | 25 | 47 |
| 5 | 40 | 0.45 | 28 | 25 | 44 |
| 6 | 50 | 0.45 | 28 | 25 | 39 |
| 7 | 60 | 0.45 | 28 | 25 | 33 |
| 8 | 70 | 0.45 | 28 | 25 | 27 |

*Note: The values are hypothetical and are used solely to illustrate the statistical procedures. They do not represent experimentally validated fly ash performance.*

The table 1 represents eight formulations evaluated under the same nominal water-to-binder ratio and curing conditions. This controlled comparison illustrates the relationship between replacement level and compressive strength, but it cannot establish the independent effects of

curing conditions because those conditions do not vary. A more comprehensive experiment would vary selected factors systematically and include sufficient replication to estimate experimental error.

An important distinction is that specimens prepared from the same batch are not necessarily equivalent to independently produced experimental batches. If several specimens are obtained from each batch, their shared production conditions may induce dependence. Accordingly, the experimental unit, sampling structure, and replication scheme should be established before selecting a statistical model [7].

**3.2 Waste characteristics**

Waste characteristics describe the composition and physical properties of the material being incorporated into the final product. Depending on the application, the explanatory vector may be written as

$$X_i = (X_{i1}, X_{i2}, \ldots, X_{ip})^\top \tag{3.2}$$

Typical variables include chemical composition, silica and alumina contents, calcium and iron concentrations, particle-size distribution, moisture content, specific gravity, specific surface area, pH, loss on ignition, organic content, and potentially hazardous constituents. Not every variable is required in every study; selection should be guided by material science, the intended application, measurement availability, and relevant safety requirements.

For example, the silica and alumina contents of an aluminosilicate-rich waste may be relevant to its potential use in cementitious or alkali-activated materials. Particle fineness may influence packing, surface area, and reaction rates, whereas moisture content can affect the effective water content of a formulation. Such relationships provide scientific reasons for including these variables in the analysis rather than selecting predictors solely through automated statistical procedures.

Measurements should, whenever feasible, be collected from multiple batches or sources. The resulting variability can then be summarized and incorporated into subsequent models. Where chemical composition is expressed as percentages of total composition, the components are also subject to a sum constraint. Consequently, increases in one component may necessarily correspond to decreases in others, creating dependencies that must be considered during regression modeling.

**3.3 Processing and formulation variables**

Processing variables describe the conditions under which a material is formulated, manufactured, cured, and tested. They may be represented by

$$Z_i = (Z_{i1}, Z_{i2}, \ldots, Z_{iq})^\top \tag{3.3}$$

Relevant examples include

$Z_{i1}$ = waste replacement percentage, $Z_{i2}$ = water-to-binder ratio,

$Z_{i3}$ = curing temperature, $Z_{i4}$ = curing duration, $Z_{i5}$ = compaction pressure.

Other variables may include additive dosage, mixing time, particle pretreatment, processing pressure, and drying conditions. The choice depends on the material and production method.

Careful experimental design is essential because formulation variables may interact. For instance, the effect of increasing waste replacement may differ according to curing duration or water-to-binder ratio. Consequently, varying one factor at a time may fail to reveal important interactions. Factorial designs and response surface methodology provide systematic approaches to investigating such effects and identifying promising operating conditions [6, 7].

The experimental range should be selected using scientific knowledge, safety considerations, engineering specifications, and practical manufacturing constraints. Predictions beyond the observed range should be treated cautiously because an apparently adequate model within the experimental domain may behave unrealistically under extrapolation.

**3.4 Engineering responses**

The response variables quantify the performance of the resulting material. Depending on the application, a multivariate response may be represented by

$$Y_i = (Y_{i1}, Y_{i2}, \ldots, Y_{im})^\top, \tag{3.4}$$

where the components may include

$Y_{i1}$ = compressive strength, $Y_{i2}$ = flexural strength, $Y_{i3}$ = tensile strength, $Y_{i4}$ = water absorption, $Y_{i5}$ = density, $Y_{i6}$ = thermal conductivity,

$Y_{i7}$ = durability indicator.

These responses represent different aspects of material performance and should be interpreted according to their engineering significance. Higher strength may be desirable, whereas lower water absorption may be preferred in some applications. The desirable direction for thermal conductivity depends on whether the intended product is a thermal insulator or a heat-conducting material. Durability also requires a clearly specified measurement procedure, exposure condition, and observation period.

Thus, material selection should not ordinarily be based on a single response in isolation. A formulation that performs well mechanically may be less satisfactory in terms of cost, durability, or environmental impact. The response variables should therefore be chosen to reflect the intended application and the practical criteria against which candidate materials will be evaluated.

**4. Exploratory Statistical Analysis**

Exploratory statistical analysis is the initial stage of quantitative investigation. Its purpose is to understand the structure of the collected data before fitting predictive or explanatory models. Descriptive summaries, graphical displays, and diagnostic checks can reveal variability, skewness, unusual observations, missing measurements, and preliminary relationships among

variables [9, 7]. These procedures do not replace formal modeling; rather, they help determine which models and diagnostic methods are appropriate.

**4.1 Descriptive statistics**

For observations $X_1,\ldots,X_n$, the sample mean is

$$\bar{X} = \frac{1}{n}\sum_{i=1}^{n} X_i, \tag{4.1}$$

and the sample variance is

$$s_X^2 = \frac{1}{n-1}\sum_{i=1}^{n}(X_i - \bar{X})^2. \tag{4.2}$$

The sample standard deviation is $s_X = \sqrt{s^2_X}$. The mean summarizes the central location of the observations, whereas the standard deviation measures their dispersion around the sample mean.

For a positive variable with a nonzero mean, the coefficient of variation is

$$CV_X = \frac{s_X}{|\bar{X}|} \times 100\%. \tag{4.3}$$

It expresses variability relative to the magnitude of the mean and can assist comparisons among positive measurements recorded on different scales. However, it becomes unstable when the mean is close to zero and is generally inappropriate for variables whose meaningful zero or ratio-scale interpretation is absent.

For the illustrative compressive-strength observations in Table 1, the mean is

$$\bar{Y} = \frac{325}{8} = 40.625 \text{ MPa}.$$

Using the sample-variance formula gives

$$s_Y^2 \approx 53.41 \text{ MPa}^2, \qquad s_Y \approx 7.31 \text{ MPa}.$$

Consequently,

$$CV_Y = \frac{7.31}{40.625} \times 100\% \approx 18.0\%.$$

These calculations summarize the strength values across the eight different formulations. The observed variability combines the differences among replacement levels with any other variation present in the measurements. It should not be interpreted as a pure estimate of measurement error because the formulations themselves differ.

For an experimental study, a descriptive table should normally report the sample size, mean, standard deviation, median, interquartile range, and minimum and maximum values, as appropriate. Where replication is available, summaries should also distinguish variability within a formulation from variability between formulations or production batches.

**4.2 Distributional analysis**

Histograms, empirical distribution plots, density estimates, and boxplots provide complementary information about the distribution of a variable. Histograms reveal broad distributional features, while boxplots help identify unusual observations relative to the bulk of the data. Quantile–quantile plots can be useful when assessing whether a distribution is approximately consistent with a proposed reference distribution.

For example, compressive-strength observations may exhibit skewness, particularly when several formulations or material sources are combined. A transformation may be useful if it improves model adequacy or stabilizes the variability. Common transformations include

$$Y_i^* = \log(Y_i), \qquad Y_i > 0, \tag{4.4}$$

and

$$Y_i^* = \sqrt{Y_i}, \qquad Y_i \geq 0. \tag{4.5}$$

The logarithmic transformation is suitable only for strictly positive observations, whereas the squareroot transformation can be applied to nonnegative observations. The choice should be based on the scientific meaning of the response, the observed distribution, and the assumptions of the intended model. Transformation should not be performed merely because the raw observations fail a normality test; in regression, the relevant distributional assumptions generally concern the model errors rather than requiring every predictor and response to be normally distributed.

**4.3 Graphical exploration**

Scatterplots provide a useful graphical tool for examining the relationship between an explanatory variable and an engineering response. For the present illustrative example, Figure 1 displays the relationship between fly ash replacement percentage and compressive strength using the eight observed pairs $(Z_i, Y_i)$, $i = 1,\ldots,8$, where $Z_i$ denotes the replacement percentage and $Y_i$ denotes compressive strength. The scatterplot indicates that compressive strength initially increases and then decreases, with the largest observed value of 48 MPa occurring at a replacement level of 20%.

The observed pattern suggests that a linear model may not adequately represent the relationship between fly ash replacement and compressive strength. However, the largest observed response should not be interpreted as a validated optimum. The dataset contains only eight illustrative observations, without independent replication or estimates of uncertainty at each replacement level. Consequently, the apparent maximum is descriptive and requires further experimental investigation.

For datasets involving multiple explanatory variables, scatterplot matrices, correlation heatmaps, and plots stratified by waste source or production batch can reveal associations that may not be apparent from individual summaries. Such graphical displays should be interpreted in conjunction with the experimental design, since an apparent association may arise from differences in other explanatory variables or from variations in the composition of the sampled batches.

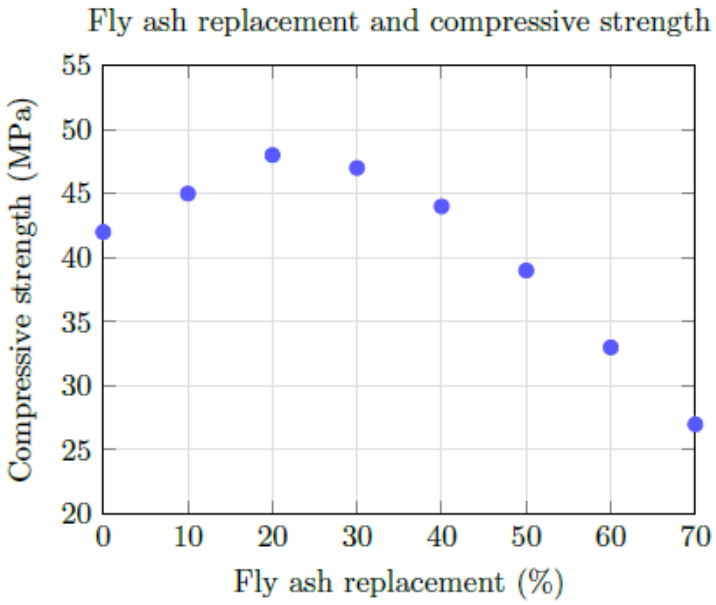



**Figure 1: Scatterplot of fly ash replacement percentage against compressive strength for the illustrative dataset**

### 4.4 Outlier assessment and data quality

An unusual observation may arise from a recording error, instrument malfunction, specimen damage, protocol deviation, or genuine heterogeneity in the waste material. Consequently, an observation should not be removed merely because it is far from the sample mean or appears as an outlier in a boxplot.

Potentially influential observations should be checked against laboratory records, instrument calibration, sample identification, and specimen-preparation procedures. If the observation is valid, it may contain important information about the range of material behavior. If an error is confirmed, the correction or exclusion should be documented transparently.

Data-quality assessment should also examine missing values, inconsistent units, duplicate records, impossible measurements, and differences in testing procedures. Missing observations should be investigated before choosing a deletion or imputation method. In particular, the analysis should preserve the distinction between a genuinely unobserved measurement and a measurement that is absent because a specimen failed or a material did not meet a testing criterion.

## 5. Correlation and Variable Selection

### 5.1 Pearson correlation

The Pearson correlation coefficient measures the strength and direction of the linear association between two quantitative variables. For paired observations $(X_i, Y_i)$, it is defined as

$$r_{XY} = \frac{\sum_{i=1}^{n}(X_i - \bar{X})(Y_i - \bar{Y})}{\sqrt{\sum_{i=1}^{n}(X_i - \bar{X})^2 \sum_{i=1}^{n}(Y_i - \bar{Y})^2}}. \quad (5.1)$$

Its value lies between −1 and 1. Values near 1 indicate strong positive linear association, whereas values near −1 indicate strong negative linear association. A value near zero indicates little linear association, but it does not rule out a nonlinear relationship.

For the eight illustrative observations, let $X$ denote fly ash replacement percentage and $Y$ denote compressive strength. The sample Pearson correlation is approximately $r_{XY} \approx -0.78$. This indicates a negative overall linear association across the observed replacement levels. However, the scatterplot shows that strength first increases and then decreases. The correlation coefficient therefore does not fully describe the response pattern. This example illustrates why correlation should be interpreted alongside graphical exploration and, when appropriate, nonlinear modeling.

### 5.2 Spearman's Rank correlation

When the relationship is monotonic but may not be linear, Spearman's rank correlation provides a complementary measure. It is the Pearson correlation computed using the ranks of the observations.

When there are no tied ranks, it can be written as

$$r_s = 1 - \frac{6\sum_{i=1}^{n} d_i^2}{n(n^2-1)}, \quad (5.2)$$

where $d_i$ is the difference between the ranks of $X_i$ and $Y_i$.

Spearman's coefficient is less dependent on the original measurement scales and can detect monotonic associations that are not linear. However, it does not generally identify a nonmonotonic relationship such as a response that increases and then decreases. Neither Pearson nor Spearman correlation establishes causation; the interpretation must account for the experimental design and potential confounding variables.

### 5.3 Correlation matrix

For $p$ explanatory variables, the pairwise correlations can be organized into the matrix

$$\boldsymbol{R} = (r_{jk})_{p\times p}, \quad (5.3)$$

where $r_{jk}$ denotes the correlation between predictors $X_j$ and $X_k$. A heatmap of this matrix can help identify groups of strongly associated variables and possible redundancy in the predictor set.

For example, silica and alumina contents may be associated because they arise from related mineralogical constituents. Likewise, particle size and specific surface area may be strongly related. Such relationships are scientifically plausible but must be assessed using the actual data rather than assumed in advance.

A further issue arises when chemical composition is recorded as percentages that sum to a fixed total. In such cases, the variables are compositionally constrained, and ordinary correlation can be difficult to interpret independently of that constraint. Depending on the research objective, compositional-data methods or scientifically justified transformations may be more appropriate than including every component as an unrestricted predictor.

**5.4 Multicollinearity**

Multicollinearity occurs when two or more explanatory variables contain overlapping linear information. It can make regression coefficients unstable, increase their standard errors, and complicate the interpretation of individual effects, even when the model retains useful predictive performance. The variance inflation factor for predictor $X_j$ is

$$VIF_j = \frac{1}{1 - R_{j,}^2} \tag{5.4}$$

where $R_j^2$ is the coefficient of determination obtained by regressing $X_j$ on the remaining explanatory variables. A value near 1 indicates little linear inflation from the other predictors, whereas larger values indicate increasing redundancy. Values such as 5 or 10 are sometimes used as diagnostic reference points, but neither constitutes a universal threshold for excluding a variable. In waste-derived material studies, multicollinearity may arise from related chemical components, correlated processing conditions, or variables that are calculated from one another. The appropriate response depends on the objective. For explanatory modeling, scientifically justified simplification or carefully chosen predictor sets may improve interpretation. For prediction, regularization methods such as ridge regression can stabilize estimates without requiring the automatic deletion of scientifically relevant variables [10].

**5.5 Variable selection**

Variable selection aims to identify a useful set of explanatory variables for the scientific or predictive objective. The process should begin with domain knowledge: variables known to influence material performance should be considered even when their individual correlations with the response are modest. A variable may contribute through an interaction or nonlinear effect that is not captured by a simple pairwise correlation.

Common approaches include scientifically guided selection, comparison of candidate models using information criteria, stepwise procedures, regularization methods such as the lasso, and

variableimportance measures from machine-learning algorithms. These approaches differ in their assumptions, stability, and interpretability [7, 10]. Automated selection should not be treated as a substitute for experimental understanding, and stepwise selection in particular can produce unstable models and overstate the apparent certainty of selected coefficients.

For predictive applications, variable selection should be performed within the training and validation procedure. If predictors are selected using the entire dataset before cross-validation, information from the validation observations can leak into the modeling process, leading to an overly optimistic estimate of predictive performance. Where sufficient data are available, the complete selection and model-fitting procedure should be repeated within each training fold.

For the illustrative fly ash example, replacement percentage is an obvious candidate predictor because it is the experimental factor under investigation. However, the eight observations do not support a reliable assessment of a large predictor set, nor can they establish the independent effects of curing, water-to-binder ratio, or waste composition because these variables were held fixed or were not recorded as varying factors. A more informative study would vary the relevant factors systematically, include suitable replication, and evaluate candidate models using diagnostic checks and independent validation where feasible.

Ultimately, the selected variables should provide a defensible balance between scientific relevance, interpretability, data availability, and predictive performance. The purpose is not simply to retain the largest possible number of statistically associated predictors, but to develop a model that adequately represents the material system and supports reliable conclusions within the domain for which data are available.

## 6. Regression Models for Material Performance

Regression analysis quantifies the relationship between material performance and formulation or processing variables. For waste-derived materials, the response may represent compressive strength, particle size, thermal stability, durability, or pollutant-removal efficiency. The following numerical illustrations demonstrate the methodology; the coefficients and observations are hypothetical and should not be interpreted as results from an actual experiment.

### 6.1 Multiple linear regression

Suppose the compressive strength $Y_i$ depends on waste replacement percentage $W_i$, curing temperature $T_i$, curing duration $C_i$, and water-to-binder ratio $R_i$. The multiple linear regression model is

$$Y_i = \beta_0 + \beta_1 W_i + \beta_2 T_i + \beta_3 C_i + \beta_4 R_i + \varepsilon_i, \qquad i = 1, \ldots, n, \tag{6.1}$$

where $\varepsilon_i$ represents random variation not explained by the included predictors. The coefficient $\beta_j$ measures the expected change in strength associated with a one-unit increase in the corresponding predictor, holding the other predictors fixed.

For illustration, consider the hypothetical fitted equation

$$\widehat{Y} = 25 + 0.18W + 0.12T + 0.08C - 18R. \tag{6.2}$$

Here, $W$ is measured in percentage points, $T$ in degrees Celsius, $C$ in days, and $R$ is dimensionless. For $W = 30$, $T = 40$, $C = 28$, and $R = 0.45$, the predicted strength is

$$\begin{aligned}\widehat{Y} &= 25 + 0.18(30) + 0.12(40) + 0.08(28) - 18(0.45) \\ &= 29.34 \text{ MPa}.\end{aligned}$$

Thus, the model predicts a strength of 29.34 MPa for this illustrative combination. This prediction is meaningful only within the context of the assumed equation and the range of experimental conditions used to fit a real model. In practice, the coefficients are estimated by least squares, which minimizes

$$\text{SSE}(\boldsymbol{\beta}) = \sum_{i=1}^{n} (Y_i - \widehat{Y}_i)^2. \tag{6.3}$$

The fitted model should also be assessed using residual diagnostics and appropriate measures of predictive performance.

**6.2 Polynomial regression**

A linear model may be inadequate when increasing the waste content initially improves performance but eventually reduces it. A quadratic model allows curvature:

$$Y_i = \beta_0 + \beta_1 Z_i + \beta_2 Z_i^2 + \varepsilon_i, \tag{6.4}$$

where $Z_i$ denotes waste replacement percentage. If $\beta_2 < 0$, the fitted curve is concave and may possess an interior maximum. Its stationary point is

$$Z^* = -\frac{\beta_1}{2\beta_2}. \tag{6.5}$$

This point represents a maximum only when $\beta_2 < 0$ and it lies within the feasible experimental range.

For example, consider the illustrative equation

$$\widehat{Y} = 42 + 0.45Z - 0.0125Z^2. \tag{6.6}$$

The estimated stationary point is

$$Z^* = -\frac{0.45}{2(-0.0125)} = 18\%.$$

The predicted response there is

$$\widehat{Y}(18) = 42 + 0.45(18) - 0.0125(18)^2 = 46.05 \text{ MPa}.$$

This example illustrates how a quadratic model can describe an interior maximum. The value 18% is not an empirical optimum; it follows solely from the hypothetical coefficients in (6.6).

A cubic model,

$$Yi = \beta 0 + \beta 1 Zi + \beta 2 Zi2 + \beta 3 Zi3 + \varepsilon i, \qquad (6.7)$$

can accommodate more complex curvature. However, additional polynomial terms increase model flexibility and may cause overfitting, especially when observations are few. Model order should therefore be guided by experimental design, residual analysis, and validation rather than by goodness of fit alone.

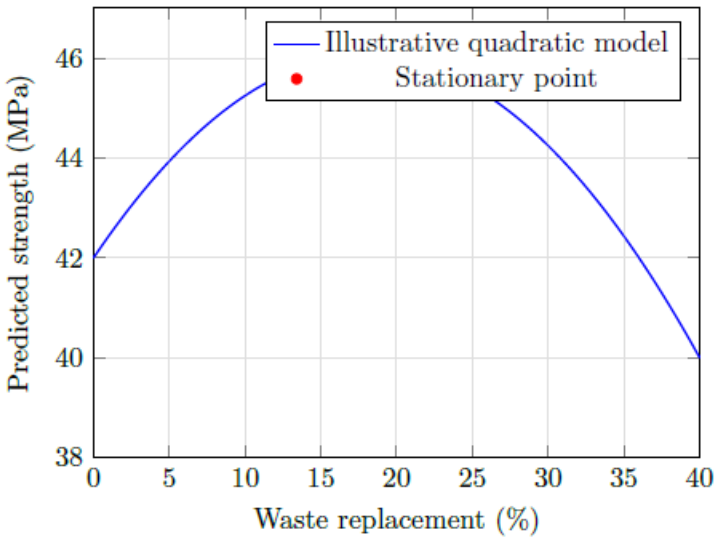



**Figure 2: Illustrative quadratic response curve and its stationary point. The curve is generated from hypothetical coefficients**

### 6.3 Interaction models

The effect of one processing variable may depend on the level of another. For example, the effect of waste replacement may differ between curing temperatures. An interaction model is

$$Yi = \beta 0 + \beta 1 Zi1 + \beta 2 Zi2 + \beta 3 Zi1 Zi2 + \varepsilon i, \qquad (6.8)$$

where $Z_{i1}$ and $Z_{i2}$ denote the two explanatory variables. The interaction coefficient $\beta_3$ describes how the effect of one predictor changes with the other, subject to the model's scale and specification.

For a numerical illustration, let $x_1 = (W - 30)/10$ and $x_2 = (T - 40)/10$ be coded waste content and curing temperature, and consider

$$\hat{Y} = 45 + 2x_1 + 1.5x_2 + 1.2x_1x_2. \qquad (6.9)$$

At $x_2 = -1$, the slope with respect to $x_1$ is $2+1.2(-1) = 0.8$. At $x_2 = 1$, it is $2+1.2(1) = 3.2$. Thus, the predicted change per unit of coded waste content is larger at the higher coded temperature. This illustrates an interaction; it does not establish that such an interaction exists in a real material system.

### 6.4 Model diagnostics

A regression model should be examined for violations of its assumptions and for systematic patterns that it fails to capture. The residuals are

$$e_i = Y_i - \widehat{Y}_i. \qquad (6.10)$$

Important diagnostic checks include residual normality when required for inferential procedures, constant error variance, independence, influential observations, and correct functional specification. Residual-versus-fitted plots can reveal curvature or changing variance, while normal Q–Q plots can indicate departures from normality. Leverage and influence measures, such as Cook's distance, can identify observations that exert disproportionate influence.

For example, if residual magnitudes tend to increase with fitted strength, the constant-variance assumption may be questionable. A transformation, a variance model, or a more appropriate regression structure may then be considered. Diagnostic findings should be interpreted jointly rather than using a single plot as a definitive test.

## 7. ANOVA and Comparative Analysis

Analysis of variance (ANOVA) compares mean engineering responses across material types, replacement levels, or processing conditions. It separates total observed variability into components associated with specified experimental factors and unexplained variation. Reliable inference requires an appropriate design and attention to independence, error variance, and model assumptions.

### 7.1 One-way ANOVA

Suppose three waste-derived formulations, *A*, *B*, and *C*, are tested, with four independent strength measurements per formulation. The one-way ANOVA model is

$$Y_{ij} = \mu + \alpha_i + \varepsilon_{ij}, \qquad i = 1,\ldots,k, \qquad j = 1,\ldots,n_i, \qquad (7.1)$$

where $\mu$ is the overall mean and $\alpha_i$ is the effect of formulation $i$. The hypotheses are

$$H_0 : \mu_1 = \mu_2 = \cdots = \mu_k, H_1 : \text{at least one group mean differs.} \qquad (7.2)$$

Consider the following hypothetical observations, measured in MPa, given by Table 2:

**Table 2: Hypothetical compressive-strength observations (MPa) for three formulations, based on four experimental replicates, with the corresponding mean strength**

| Formulation | 1 | 2 | 3 | 4 | Mean |
|---|---|---|---|---|---|
| A | 42 | 44 | 43 | 45 | 43.5 |
| B | 46 | 48 | 47 | 49 | 47.5 |
| C | 44 | 45 | 46 | 43 | 44.5 |

The overall mean is $\bar{Y}_{..} = 45.17$ MPa (rounded). The between-group and within-group sums of squares are

$$SS_B = \sum_{i=1}^{k} n_i(\bar{Y}_{i.} - \bar{Y}_{..})^2 \approx 34.67, \qquad (7.3)$$

$$SS_W = \sum_{i=1}^{k}\sum_{j=1}^{n_i}(Y_{ij} - \bar{Y}_{i.})^2 = 15. \qquad (7.4)$$

Consequently,

$$SS_T = SS_B + SS_W \approx 49.67.$$

With $k = 3$ groups and $N = 12$ observations, the degrees of freedom are 2 between groups and 9 within groups. Hence,

$$MS_B = \frac{34.67}{2} \approx 17.33, \qquad MS_W = \frac{15}{9} \approx 1.67,$$

and the test statistic is

$$F = \frac{MS_B}{MS_W} \approx 10.40.$$

Under the usual one-way ANOVA assumptions, this value provides evidence against equality of all three population means at the 5% significance level. The calculation is illustrative; actual inference requires genuine independent experimental observations. A significant ANOVA result establishes that not all means are equal, but it does not by itself identify which pairs differ.

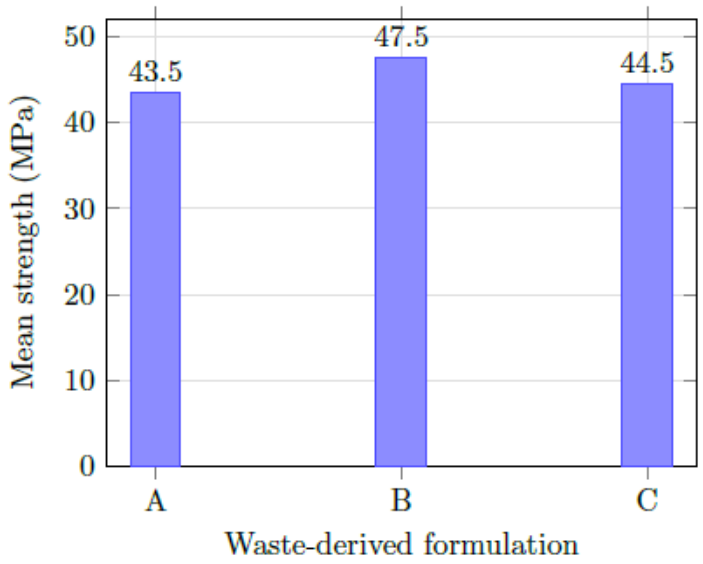



**Figure 3: Illustrative group means for three waste-derived formulations.**

### 7.2 Two-way ANOVA

When both waste type and replacement level are studied, a two-way ANOVA model can separate their main effects and their interaction:

$$Y_{ijk} = \mu + \alpha_i + \beta_j + (\alpha\beta)_{ij} + \varepsilon_{ijk}, \qquad (7.5)$$

where $\alpha_i$ is the waste-type effect, $\beta_j$ is the replacement-level effect, and $(\alpha\beta)_{ij}$ is their interaction. A meaningful interaction indicates that differences among replacement levels are not the same for all waste types. For instance, a replacement level that performs well with fly ash may not perform equally well with slag or rice-husk ash. Replication within factor combinations is generally needed to estimate experimental error and support interaction testing.

### 7.3 Post-hoc comparisons

When the overall ANOVA test rejects the null hypothesis, a multiple- comparison procedure can be used to investigate specific group differences. Tukey's honestly significant difference procedure is one option for comparing all pairs of means while controlling the family-wise error rate under its assumptions. Comparisons should include uncertainty estimates, such as confidence intervals, rather than reporting only rankings of the sample means. When variances differ substantially, alternative procedures such as Welch's ANOVA and suitable unequal-variance post-hoc comparisons may be more appropriate.

## 8. Response Surface Methodology

Response Surface Methodology (RSM) combines designed experiments and regression modeling to characterize the effects of controllable variables and identify favorable operating conditions. It is particularly useful when the response depends on several factors and curvature or interactions are expected.

Let

$$x_1 = \frac{W - 30}{10}, \; x_2 = \frac{T - 40}{10},$$

where $W$ is waste replacement percentage and $T$ is curing temperature in degrees Celsius. These transformations define dimensionless coded variables centred at $W$ = 30% and $T$ = 40°C. A second-order response surface is

$$\widehat{Y}(x_1, x_2) = \beta_0 + \beta_1 x_1 + \beta_2 x_2 + \beta_{11} x_1^2 + \beta_{22} x_2^2 + \beta_{12} x_1 x_2. \qquad (8.1)$$

The linear terms represent local main effects, the squared terms represent curvature, and the product term represents interaction.

### 8.1 Response surface visualization

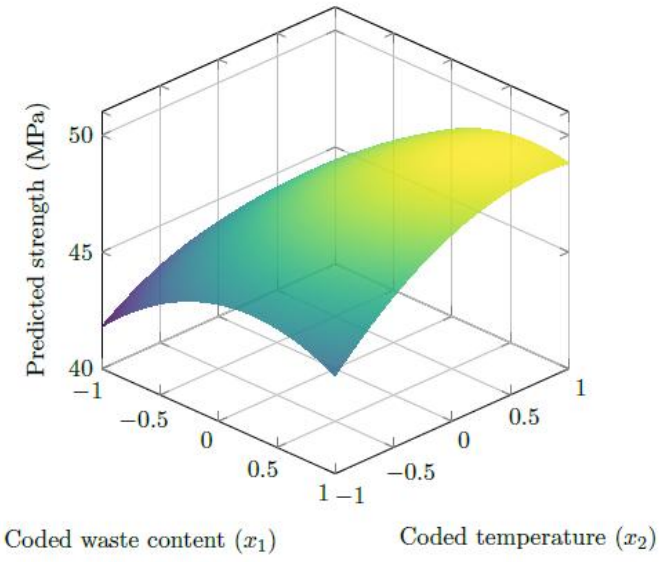



**Figure 4: Three-dimensional response surface for the illustrative second-order model in (8.2)**

For illustration, consider the hypothetical fitted surface

$$\widehat{Y}(x_1, x_2) = 48 + 2x_1 + 1.5x_2 - 2x_1^2 - 1.5x_2^2 + 0.8x_1x_2, \qquad -1 \le x_1, x_2 \le 1. \tag{8.2}$$

The surface is concave because the quadratic terms are negative and the Hessian matrix

$$H = \begin{pmatrix} -4 & 0.8 \\ 0.8 & -3 \end{pmatrix}$$

is negative definite: its first leading entry is negative and $\det(H) = 12 - 0.64 = 11.36 > 0$. Therefore, the stationary point is the unique maximum of this quadratic surface, provided it lies inside the specified feasible region.

**8.2 Optimization through RSM**

The estimated optimum is obtained by solving

$$(\widehat{x}_1, \widehat{x}_2) = \arg \max_{(x_1, x_2) \in \mathcal{R}} \widehat{Y}(x_1, x_2), \tag{8.3}$$

where R denotes the feasible experimental region. For the illustrative surface in (8.2), the stationary point solves

$$\frac{\partial \widehat{Y}}{\partial x_1} = 2 - 4x_1 + 0.8x_2 = 0 \,, \frac{\partial \widehat{Y}}{\partial x_2} = 1.5 + 0.8x_1 - 3x_2 = 0 \,.$$

Solving these equations gives approximately $\widehat{x}_1 = 0.634, \ \widehat{x}_2 = 0.669$. Returning to the original units,

$$\widehat{W} = 30 + 10(0.634) = 36.34\%, \qquad \widehat{T} = 40 + 10(0.669) = 46.69^{\circ}\mathrm{C}.$$

The predicted response at this point is approximately

$$\widehat{Y}(0.634, 0.669) \approx 49.14 \text{ MPa}.$$

These values illustrate the optimization procedure, not a validated industrial formulation. In an actual study, the candidate optimum should be checked against operational constraints, prediction uncertainty, and independent confirmation experiments. If the stationary point lies outside the feasible region, optimization must instead be carried out over the permitted region, including its boundaries.

In sustainable material design, maximizing strength alone may not be sufficient. A practical optimization may also impose limits on cost, energy consumption, emissions, durability, or the proportion of waste incorporated. These requirements can be represented as constraints or combined in a multi-response desirability function. The final recommendation should balance predicted performance with environmental and operational feasibility.

**9. Mixed-Effects Models for Batch Variability**

Industrial waste streams often vary in chemical composition, particle size, moisture content, and contaminant concentration. Consequently, observations from the same production batch may be more similar than observations from different batches. Mixed-effects models account for this hierarchical structure while estimating the effects of formulation and processing variables.

### 9.1 Random-intercept model

Let $Y_{ij}$ denote the engineering response for observation $i$ from batch $j$. A random-intercept model is

$$Y_{ij} = \beta_0 + \sum_{r=1}^{p} \beta_r X_{ijr} + b_j + \varepsilon_{ij}, \tag{9.1}$$

where $b_j$ is the batch-specific random intercept and $\varepsilon_{ij}$ is the observation-level error. A standard assumption is

$$b_j \sim N(0, \sigma_b^2), \qquad \varepsilon_{ij} \sim N(0, \sigma^2),$$

with independent batch effects and errors. The variance $\sigma_b^2$ quantifies between-batch variability, whereas $\sigma^2$ represents residual variability within batches after accounting for the predictors.

For example, suppose the estimated variance components are $\sigma_b^2 = 9$ and $\sigma^2 = 4$, in MPa$^2$.

The

$$\widehat{\sigma}^2_{\text{total}} = 9 + 4 = 13.$$

total variance for observations with the same predictor values is then

The intraclass correlation coefficient (ICC) is

$$\widehat{\rho} = \frac{\widehat{\sigma}_b^2}{\widehat{\sigma}_b^2 + \widehat{\sigma}^2} = \frac{9}{13} \approx 0.692. \tag{9.2}$$

Thus, approximately 69.2% of the modeled variance is attributable to differences between batches. This hypothetical result would indicate substantial batch heterogeneity and support monitoring batch-level properties during industrial production.

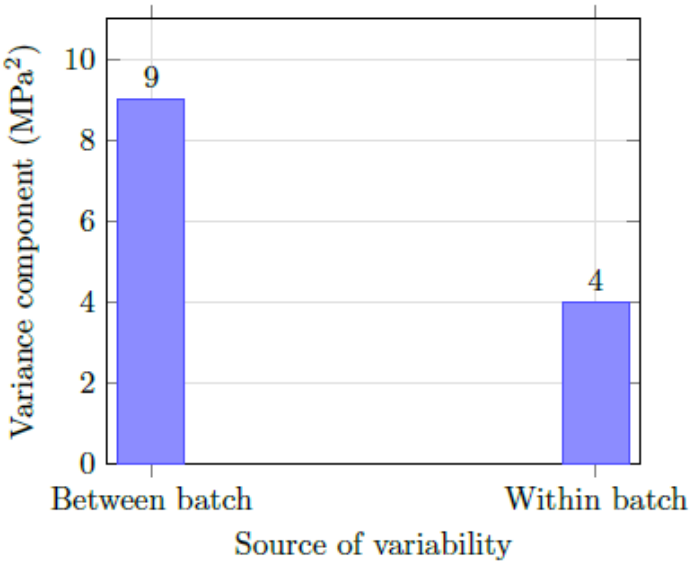



**Figure 5: Hypothetical variance components in a random-intercept model for material strength**

### 9.2 Batch-specific predictions and repeated measurements

The estimated batch effect can be used to obtain batch-specific predictions:

$$\widehat{Y}_{ij} = \widehat{\beta}_0 + \sum_{r=1}^{p} \widehat{\beta}_r X_{ijr} + \widehat{b}_j$$

.

The estimates $\widehat{b_j}$ are commonly obtained using empirical best linear unbiased prediction (BLUP) under the fitted model. They are typically shrunk towards zero, especially for batches with limited observations. This avoids treating a noisy batch mean as if it were estimated without uncertainty.

Mixed-effects models can also accommodate measurements taken at multiple curing ages. For example,

$$Yij = \beta 0 + \beta 1 tij + b0j + b1jtij + \varepsilon ij, \qquad (9.3)$$

where $t_{ij}$ is curing age, $b_{0j}$ is a batch-specific intercept, and $b_{1j}$ is a batch-specific slope. The random slope allows strength development to vary between batches. If observations are repeated on the same specimen, their within-specimen dependence must also be considered when specifying the model.

**10. Machine-Learning Models for Prediction**

Regression models are useful for interpretation and inference, but industrial-material relationships may involve nonlinear effects, thresholds, and complex interactions. Machine-learning methods can provide flexible predictions when sufficient representative data are available. Their usefulness depends on sample size, data quality, validation design, and the intended application.

**10.1 Random forest**

A random forest averages predictions from an ensemble of decision trees:

$$\widehat{Y}(\boldsymbol{X}) = \frac{1}{B} \sum_{b=1}^{B} T_b(\boldsymbol{X}) \qquad (10.1)$$

,

where $T_b$ denotes tree $b$ and $B$ is the number of trees. Random forests can represent nonlinearities and interactions without specifying a polynomial model in advance. Variable-importance measures can assist exploratory analysis, although importance does not establish causality and may be biased when predictors differ in scale or correlation structure.

**10.2 Support vector regression**

Support Vector Regression (SVR) estimates a function while balancing prediction errors against model complexity. With a nonlinear kernel, the fitted predictor can be expressed as

$$\widehat{Y}(\boldsymbol{X}) = \sum_{i=1}^{n} (\alpha_i - \alpha_i^*) K(\boldsymbol{X}_i, \boldsymbol{X}) + b, \qquad (10.2)$$

where $K$ is the chosen kernel and $\alpha_i, \alpha_i^*$ are estimated coefficients. The kernel and tuning parameters should be selected using training data and cross-validation. SVR can be useful for small or moderate datasets, but its performance depends on appropriate scaling and tuning.

### 10.3 Artificial neural networks

A feed-forward neural network represents a sequence of transformations of the input variables. A single-hidden-layer regression network may be written as

$$\widehat{Y} = \beta_0 + \sum_{h=1}^{H} \beta_h \, g\left(a_{h0} + \boldsymbol{a}_h^{\top} \boldsymbol{X}\right), \tag{10.3}$$

where $g$ is an activation function and $H$ is the number of hidden units. Neural networks can approximate complex nonlinear relationships, but large numbers of parameters can lead to overfitting when only a limited number of material formulations have been tested.

### 10.4 Gradient boosting

Gradient boosting builds an ensemble sequentially by adding learners to improve the current fit:

$$\widehat{f}_M(\boldsymbol{X}) = \widehat{f}_0(\boldsymbol{X}) + \sum_{m=1}^{M} \eta \gamma_m h_m(\boldsymbol{X}), \tag{10.4}$$

where $h_m$ is the learner added at iteration $m$, $\gamma_m$ is its fitted contribution, and $\eta$ is a learning-rate parameter. Boosted trees can provide strong predictive performance for structured tabular data, but tree depth, learning rate, and number of iterations require careful tuning.

### 10.5 Interpretability

Predictive accuracy alone is insufficient when a model will inform material formulation or industrial process control. Partial dependence plots can summarize the average predicted response as one predictor varies, while accumulated local effects can be useful when predictors are correlated. Feature importance and SHAP-type attributions can help describe model behavior, but their results depend on the fitted model and data distribution. These methods should be interpreted as explanations of predictions rather than proof of physical mechanisms.

## 11. Model Validation and Performance Comparison

Predictive performance must be evaluated using observations that were not used to fit the model. Let $D_{train}$ denote the training data and $D_{test}$ the held-out test data. The test set should remain separate from model selection and hyperparameter tuning to avoid optimistic performance estimates.

### 11.1 Prediction-error measures

For $n$ test observations, the root mean squared error (RMSE) and mean absolute error (MAE) are

$$\mathrm{RMSE} = \sqrt{\frac{1}{n}\sum_{i=1}^{n}(Y_i - \widehat{Y}_i)^2}, \tag{11.1}$$

$$\mathrm{MAE} = \frac{1}{n}\sum_{i=1}^{n}|Y_i - \widehat{Y}_i|. \tag{11.2}$$

RMSE penalizes large errors more strongly, whereas MAE summarizes the typical absolute error in the response's measurement units. The test-set coefficient of determination is

$$R^2_{\text{test}} = 1 - \frac{\sum_{i=1}^{n}(Y_i - \widehat{Y}_i)^2}{\sum_{i=1}^{n}(Y_i - \bar{Y}_{\text{test}})^2}, \qquad (11.3)$$

where $\bar{Y}_{\text{test}}$ is the mean of the observed test responses. A negative test-set $R^2$ is possible and indicates that the predictions perform worse, under this metric, than predicting the test-set mean. Consider five hypothetical test responses: $Y = (40,45,50,55,60)$ MPa. The following table 3 uses illustrative predictions to demonstrate the calculation. These are not fitted results from a real dataset.

**Table 3: Comparison of predictive performance of statistical and machine-learning models for concrete compressive strength**

| Model | $\widehat{Y}_1$ | $\widehat{Y}_2$ | $\widehat{Y}_3$ | $\widehat{Y}_4$ | $\widehat{Y}_5$ | RMSE | MAE | *R2* |
|---|---|---|---|---|---|---|---|---|
| Linear regression | 42 | 46 | 49 | 57 | 58 | 1.673 | 1.600 | 0.944 |
| Random forest | 41 | 46 | 51 | 54 | 61 | 1.000 | 1.000 | 0.980 |
| SVR | 43 | 44 | 49 | 56 | 59 | 1.612 | 1.400 | 0.948 |
| Gradient boosting | 40 | 47 | 49 | 56 | 60 | 1.095 | 0.800 | 0.976 |

For the random forest, the squared errors are $1,1,1,1,1$, giving

$$\text{RMSE} = \sqrt{\frac{5}{5}} = 1 \text{ MPa}, \qquad \text{MAE} = \frac{5}{5} = 1 \text{ MPa}.$$

The test-response mean is 50 MPa and the total sum of squares is 250 $\text{MPa}^2$. Hence,

$$R^2_{\text{test}} = 1 - \frac{5}{250} = 0.98.$$

In this illustration, the random forest has the smallest RMSE, whereas gradient boosting has the smallest MAE. The ranking therefore depends partly on the performance measure. With only five test observations, however, these rankings would be highly uncertain, as seen in Figure 6.

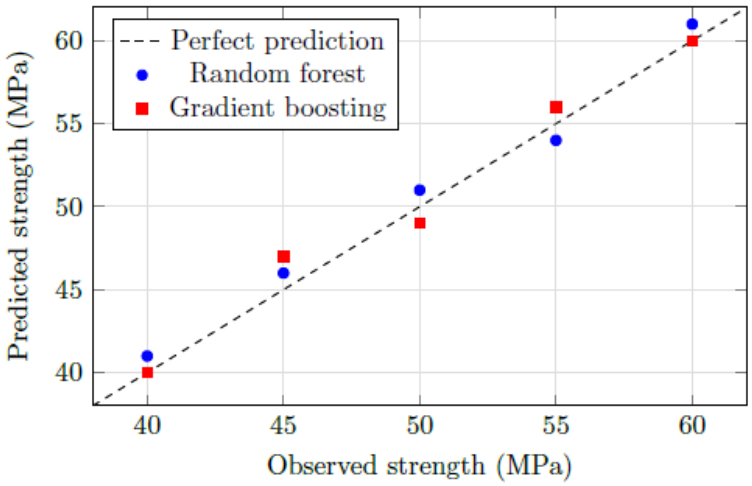



**Figure 6: Observed versus predicted values for two illustrative models. Points closer to the dashed line have smaller prediction errors for these observations**

### 11.2 Cross-validation and fair comparison

In *K*-fold cross-validation, the training data are partitioned into *K* folds. Each fold is used once for validation while the remaining folds are used for fitting. The fold-specific errors can be summarized to compare candidate models and tune hyperparameters. Preprocessing, including imputation, scaling, and feature selection, must be learned within each training fold rather than from the full dataset.

For industrial data, random splitting may be inappropriate if observations from the same batch occur in both training and test sets. When the intended application is prediction for a new production batch, group-based validation should hold out entire batches. Where predictions concern future production, a time-ordered split may be more suitable. These choices prevent information leakage and give a more realistic assessment of deployment performance.

### 11.3 Model selection

The preferred model should combine predictive accuracy with interpretability, robustness, computational cost, and suitability for the intended engineering decision. A model with a slightly larger RMSE may be preferable if its effects are easier to explain, its predictions are more stable across batches, or it supports reliable uncertainty quantification. The table above is a calculation example only; a real model comparison should report metrics calculated from the same validation design.

## 12. Statistical Optimization of Material Formulation

After model development and validation, the fitted response function can be used to identify promising formulations. Let $Z = (Z_1,...,Z_q)^\top$ denote controllable formulation and processing variables, and let $\widehat{f}(\boldsymbol{Z})$ be the predicted engineering response. A single-response optimization problem is

$$\max_{\boldsymbol{Z}\in\mathcal{R}} f(\boldsymbol{Z}), \tag{12.1}$$

where R is the feasible region defined by engineering, safety, and operational constraints.

For example, suppose $Z$ is the waste replacement percentage and the feasible range is $0\% \le Z \le 50\%$. Consider the hypothetical prediction function

$$\widehat{Y}(Z) = 42 + 0.45Z - 0.0125Z^2. \tag{12.2}$$

Its stationary point is $Z = 18\%$, which lies within the feasible range and maximizes the fitted quadratic because the coefficient of $Z^2$ is negative. Nevertheless, this conclusion is conditional on the model being appropriate over the specified range. An independent experiment should be conducted near the proposed optimum before implementation.

### 12.1 Multiple engineering objectives

A sustainable formulation may need to maximize strength while minimizing water absorption, cost, and carbon footprint. These objectives can conflict, so a single maximum may not exist that

simultaneously optimizes every response. One approach is to define desirability functions $d_r(Y_r) \in [0,1]$ that encode the acceptable range and target for each response. A weighted geometric aggregate is

$$D(\boldsymbol{Z}) = \left\{ \prod_{r=1}^{m} [d_r(\widehat{Y}_r(\boldsymbol{Z}))]^{w_r} \right\}^{1/\sum_{r=1}^{m} w_r}, \qquad w_r \geq 0 \tag{12.3}$$

where $w_r$ expresses the relative importance of response $r$. The formulation is selected by maximizing $D(Z)$ over the feasible region. If any positively weighted desirability is zero, the aggregate is zero. Weights and desirability functions should be justified before examining the final optimum, not chosen solely to favor a preferred formulation.

A second approach is Pareto optimization, which identifies formulations for which no objective can be improved without worsening at least one other objective. The resulting Pareto frontier makes trade-offs explicit and can be particularly useful when engineering performance, cost, and environmental impact are all important.

## 13. Sustainability and Circular-Economy Assessment

Statistical performance should be connected to material utilization, environmental impact, energy demand, and cost. A formulation with high strength is not necessarily more sustainable if it requires energy-intensive processing, long-distance transport, or hazardous pretreatment. Environmental comparisons should therefore use consistent system boundaries and a clearly specified functional unit, following life-cycle assessment principles.

### 13.1 Waste utilization

A simple waste-utilization indicator is

$$WU = \frac{m_{\text{waste}}}{m_{\text{material}}} \times 100\%, \tag{13.1}$$

where $m_{\text{waste}}$ is the mass of industrial waste incorporated and $m_{\text{material}}$ is the total mass of the resulting material, both measured on a consistent basis.

For example, incorporating 30 kg of waste into 100 kg of final material gives

$$WU = \frac{30}{100} \times 100\% = 30\%.$$

This metric measures the waste fraction; it does not by itself demonstrate environmental benefit or product safety.

### 13.2 Carbon-emission reduction

Let $C_{\text{conv}}$ and $C_{\text{up}}$ denote emissions per equivalent functional unit for conventional and upcycled materials. The percentage reduction is

$$CR = \frac{C_{\text{conv}} - C_{\text{up}}}{C_{\text{conv}}} \times 100\%. \tag{13.2}$$

If the conventional option emits 500 kg $CO_2$-equivalent and the upcycled option emits 380 kg $CO_2$equivalent per equivalent functional unit, then

$$CR = \frac{500 - 380}{500} \times 100\% = 24\%.$$

A negative value would indicate greater emissions for the upcycled option. Such comparisons should include relevant processing, transportation, pretreatment, and end-of-life stages where these fall within the chosen system boundary.

**13.3 Energy consumption and production cost**

Energy demand may be modeled as a function of formulation and processing conditions:

$$E = E(Z_1, \ldots, Z_q), \qquad \widehat{E} = \widehat{E}(\boldsymbol{Z}).$$

The total production cost may similarly be decomposed as

$$C_{\text{total}} = C_{\text{raw}} + C_{\text{processing}} + C_{\text{transport}} + C_{\text{energy}}. \qquad (13.3)$$

For illustration, if these cost components are respectively 40, 25, 10, and 15 monetary units per functional unit, then the total is 90 monetary units. Such a calculation is meaningful only when the components share the same cost basis and production quantity. Costs associated with waste collection, quality control, emissions treatment, and disposal should also be included when relevant.

**13.4 Illustrative sustainability comparison**

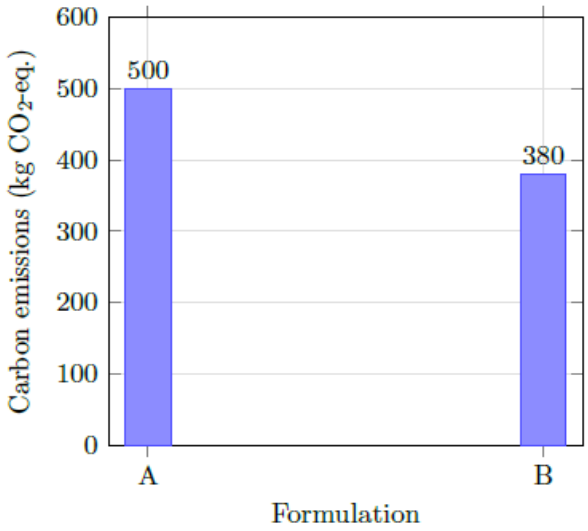



**Figure 7: Hypothetical carbon-emission comparison on an equivalent functional basis**

Consider two hypothetical formulations assessed on the same functional basis. The following values demonstrate how engineering and environmental indicators can be presented together, as in Table 4. Formulation B incorporates more waste and has lower illustrative carbon emissions, but its predicted strength is slightly lower and its cost is higher. Whether B is preferable depends on minimum strength requirements, cost limits, environmental boundaries, and the relative importance assigned to each outcome.

**Table 4: Hypothetical comparison of engineering, waste-utilization, environmental, and economic indicators for two alternative formulations**

| Indicator | Formulation A | Formulation B |
|---|---|---|
| Waste utilization (%) | 20 | 30 |
| Strength (MPa) | 45 | 44 |
| Carbon emissions (kg $CO_2$-eq.) | 500 | 380 |
| Production cost (monetary units) | 90 | 94 |

### 13.5 Integrated sustainability score

For preliminary screening, normalized indicators may be combined into a composite score:

$$S = w_1 S_{\text{engineering}} + w_2 S_{\text{environmental}} + w_3 S_{\text{economic}} + w_4 S_{\text{waste}}, \qquad \sum_{r=1}^{4} w_r = 1, \tag{13.4}$$

where each component is scaled consistently so that a higher value represents better performance. For example, strength may be scored higher when it increases, whereas cost and emissions should be transformed so that lower values correspond to higher desirability.

The weights should reflect transparent engineering priorities or a justified decision-making procedure. Because normalization and weighting can materially affect rankings, sensitivity analysis should examine whether the preferred formulation changes under plausible alternative weights. A composite score is a decision aid, not a substitute for reporting the individual indicators and their uncertainties.

## 14. Case Study: Statistical Analysis of a Real IndustrialWaste Dataset

### 14.1 Dataset and research objectives

This case study uses the Concrete Compressive Strength dataset originally developed by Yeh (1998)[11] and distributed through the UCI Machine Learning Repository (https://archive.ics.uci.edu/ dataset/165/concrete+compressive+strength). The dataset contains 1,030 observations, with eight quantitative explanatory variables and one quantitative response variable. The explanatory variables are cement, blast-furnace slag, fly ash, water, superplasticizer, coarse aggregate, fine aggregate, and curing age. The constituent quantities are measured in kg/m$^3$, curing age is measured in days, and compressive strength is measured in MPa. The accompanying dataset documentation reports no missing attribute values.

The dataset is relevant to industrial-waste valorization because blast-furnace slag and fly ash are industrial by-products that can be incorporated into cementitious materials. Their use in concrete formulations provides a practical setting for examining the relationship between by-product incorporation, mixture composition, and mechanical performance. Nevertheless, the dataset does not contain production-batch identifiers, detailed waste chemistry, curing temperature, production costs, energy consumption, or life-cycle environmental indicators. Therefore, the

analysis investigates the statistical relationships between concrete composition and compressive strength rather than claiming a comprehensive assessment of environmental or economic sustainability.

The principal objectives are to characterize the distribution of compressive strength, investigate its association with mixture constituents, compare alternative regression specifications, examine the observed difference between mixtures with and without fly ash, and explore nonlinear response patterns involving fly ash content and curing age. The numerical results reported below are obtained from the analysis files contained in the accompanying case-study archive.

**14.2 Descriptive and graphical analysis**

Let $Y_i$ denote the measured compressive strength of the $i$th concrete mixture. Across the 1,030 observations, the mean compressive strength is 35.818 MPa, with a standard deviation of 16.706 MPa. The observed strengths range from 2.332 to 82.599 MPa. The first and third quartiles are 23.707 and 46.136 MPa, respectively, while the median is 34.443 MPa. Thus, the interquartile range is approximately 22.429 MPa, indicating substantial variation in mechanical performance across the recorded mixtures.

The mean is slightly greater than the median, suggesting some right-sided asymmetry in the empirical distribution. The histogram and boxplot provide complementary views of this variability. In particular, the wide observed range indicates that concrete mixtures with different compositions and curing ages can exhibit markedly different compressive strengths. Consequently, a single average strength would not adequately characterize the dataset.

**Table 5: Descriptive statistics for compressive strength in the UCI Concrete Compressive Strength dataset**

| Variable | Mean | SD | Min. | $Q_1$ | Median | $Q_3$ | Max. |
|---|---|---|---|---|---|---|---|
| Compressive strength (MPa) | 35.818 | 16.706 | 2.332 | 23.707 | 34.443 | 46.136 | 82.599 |

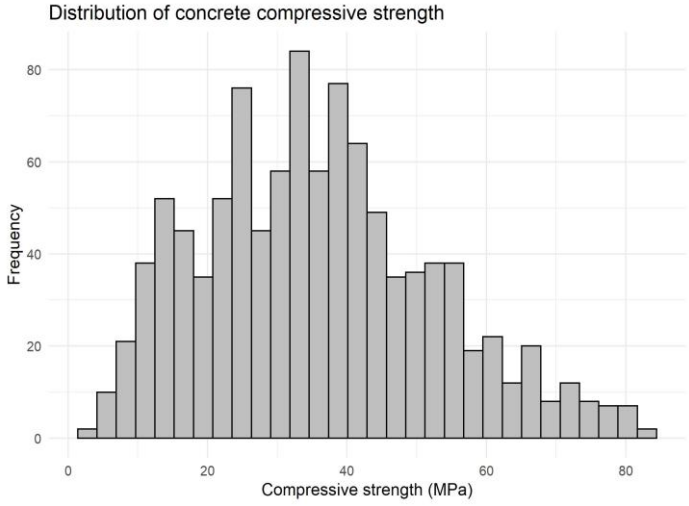



**Figure 8: Empirical distribution of concrete compressive strength in the 1,030 observations**

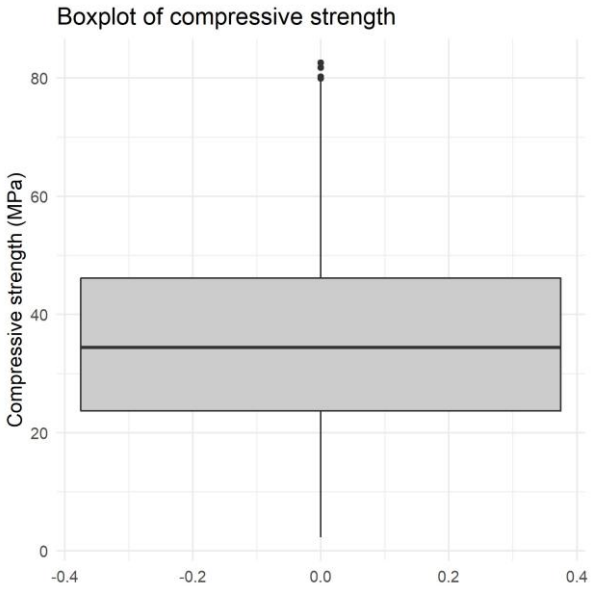



**Figure 9: Boxplot of concrete compressive strength, showing the median, interquartile range, and observations beyond the central spread**

Figure 9 presents the histogram and boxplot of compressive strength. These graphics help identify the spread of observations and the presence of relatively low or high strength values. Such observations should not automatically be treated as erroneous, since they may represent genuine differences in mixture composition or curing age.

**14.3 Correlation analysis**

Pearson correlation coefficients were calculated to summarize the linear associations between the explanatory variables and compressive strength. The largest positive correlation with strength is observed for cement content, with $r = 0.498$. Superplasticizer content has a positive correlation of $r = 0.366$, while curing age has a positive correlation of $r = 0.329$. Blast-furnace slag has a weaker positive correlation with strength ($r = 0.135$).

In contrast, water content has a negative Pearson correlation of $r = -0.290$ with compressive strength. Fine aggregate and coarse aggregate also exhibit negative correlations, equal to $-0.167$ and $-0.165$, respectively. Fly ash has a weak negative linear correlation with strength ($r = -0.106$). These coefficients describe the observed mixtures and should not be interpreted as isolated causal effects. For example, the association between fly ash and strength may partly reflect differences in cement content, water content, curing age, and other formulation characteristics. The correlation matrix also reveals relationships among the explanatory variables. In particular, water and superplasticizer have a Pearson correlation of $-0.657$, while water and fine aggregate have a correlation of $-0.451$. Cement and fly ash are negatively correlated ($r = -0.397$), and fly ash and superplasticizer are positively correlated ($r = 0.377$). These relationships indicate that mixture constituents do not vary independently, which is important when interpreting individual regression coefficients.

**Table 6: Pearson correlations between selected explanatory variables and compressive strength**

| Variable | Pearson correlation with strength |
|---|---|
| Cement | 0.498 |
| Superplasticizer | 0.366 |
| Curing age | 0.329 |
| Blast-furnace slag | 0.135 |
| Fly ash | −0.106 |
| Coarse aggregate | −0.165 |
| Fine aggregate | −0.167 |
| Water | −0.290 |

The Spearman correlation between curing age and strength is 0.596, which is considerably greater than the corresponding Pearson correlation of 0.329. This difference is consistent with the possibility that the association between curing age and strength is not adequately summarized by a simple linear relationship. Spearman's coefficient measures rank-based monotonic association and does not require the relationship to be linear. The Pearson and Spearman correlations between cement and strength are similar, at 0.498 and 0.478, respectively. For fly ash, the corresponding values are −0.106 and −0.078, indicating a weak marginal association with strength under both measures.

The correlation heatmap in Figure 10 provides a compact visualization of the relationships among all nine variables. The results support the use of multivariable models because the observed strength is associated with several mixture characteristics, while the explanatory variables themselves also exhibit appreciable correlations.

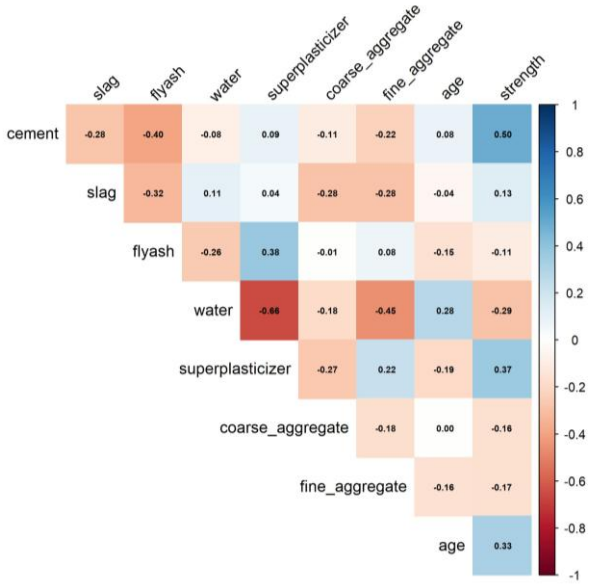



**Figure 10: Pearson correlation heatmap for mixture constituents, curing age, and compressive strength**

### 14.4 Regression and response-surface analysis

The baseline multiple linear regression model is specified as

$$Y_i = \beta_0 + \beta_1 \text{Cement}_i + \beta_2 \text{Slag}_i + \beta_3 \text{FlyAsh}_i + \beta_4 \text{Water}_i + \beta_5 \text{Superplasticizer}_i + \beta_6 \text{CoarseAggregate}_i + \beta_7 \text{FineAggregate}_i + \beta_8 \text{Age}_i + \varepsilon_i, \quad (14.1)$$

where $Y_i$ is compressive strength and $\varepsilon_i$ denotes the unexplained component.

To investigate potential nonlinear relationships, a quadratic regression model adds squared terms for fly ash content and curing age. A response-surface specification further includes an interaction between fly ash and curing age. The corresponding additional terms can be written as

$$\gamma_1 \text{FlyAsh}_i^2 + \gamma_2 \text{Age}_i^2 + \gamma_3 \text{FlyAsh}_i \text{Age}_i.$$

These terms allow the fitted relationship to exhibit curvature and permit the association between fly ash and strength to vary with curing age.

**Table 7: Training-data modelselection criteria for the three regression specifications**

| Model | Adjusted $R^2$ | AIC | BIC |
|---|---|---|---|
| Multiple linear regression | 0.616 | 6222.697 | 6269.838 |
| Quadratic regression | 0.758 | 5844.700 | 5901.270 |
| Responsesurface model | 0.759 | 5840.476 | 5901.761 |

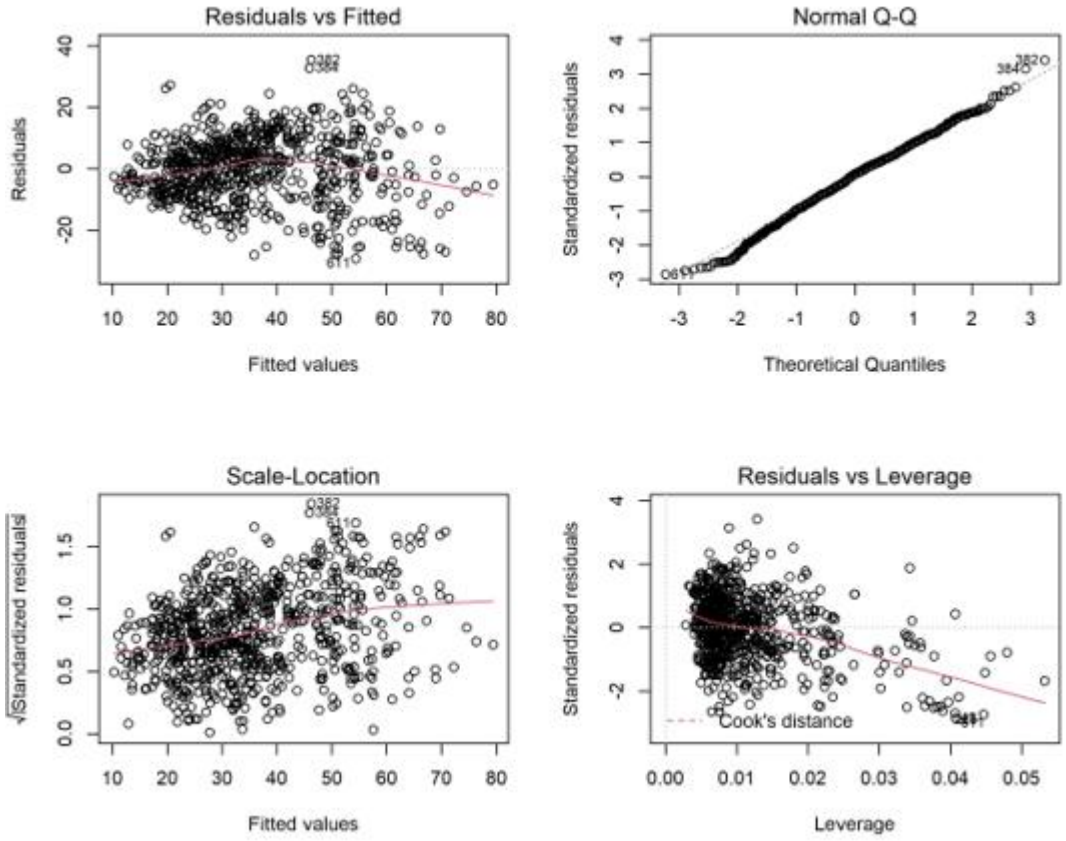



**Figure 11: Regression diagnostic plots for the linear model**

The training-data model-selection results are summarized in Table 7. The adjusted coefficient of determination for the linear regression is 0.616, whereas the quadratic and response-surface models achieve adjusted $R^2$ values of 0.758 and 0.759, respectively. Thus, the two nonlinear specifications account for a greater proportion of the variation in the training response after adjustment for the number of fitted parameters. The Akaike information criterion (AIC) decreases from 6222.697 for the linear regression to 5844.700 for the quadratic model and 5840.476 for the response-surface model. The Bayesian information criterion (BIC) is 6269.838, 5901.270, and 5901.761, respectively. Accordingly, the response-surface model has the smallest AIC, whereas the quadratic model has a marginally smaller BIC. The difference in BIC between the two nonlinear models is approximately 0.490, so this criterion does not provide strong separation between them. Taken together, the results suggest that allowing curvature improves the in-sample representation of compressive strength, although these criteria alone do not establish superior predictive performance on unseen data.

The diagnostic figure in Figure 11 is used to assess the adequacy of the linear model. Residualversus-fitted plots help identify systematic patterns or nonconstant residual variance, while normal Q–Q plots assess departures from normality. Such diagnostics are important because a high adjusted $R^2$ does not, by itself, guarantee that the regression assumptions are appropriate.

For a complete predictive comparison, the candidate models should be evaluated on the same held-out observations using root mean squared error (RMSE), mean absolute error (MAE), and testset $R^2$. These quantities should be reported separately from adjusted $R^2$, AIC, and BIC, which are training-data criteria in the supplied analysis. The latter are useful for comparing fitted regression specifications but cannot replace an independent evaluation of predictive accuracy.

**14.5 Exploratory analysis of fly ash incorporation**

To examine the observed differences between mixtures with and without fly ash, the data were divided into two groups: mixtures with zero fly ash and mixtures with positive fly ash content. There are 566 observations in the zero-fly-ash group and 464 observations in the positive-fly-ash group.

The mean compressive strength is 36.772 MPa for mixtures without fly ash and 34.654 MPa for mixtures containing positive amounts of fly ash. The corresponding standard deviations are 18.445 and 14.234 MPa, while the medians are 35.301 and 33.743 MPa, respectively. Thus, the zero-fly-ash group has a higher observed mean by approximately 2.117 MPa. The positive-fly-ash group also exhibits a smaller sample standard deviation, indicating less observed dispersion in strength in this particular grouping.

A one-way analysis of variance was used to test $\mathbf{H_0}: \mu_{\text{zero}} = \mu_{\text{positive}}$ against the alternative that the two group means differ. The reported ANOVA gives $F(1,1028) = 4.108$ with $p = 0.0429$. At the

conventional 5% significance level, the null hypothesis is rejected. The observed difference between the two group means is therefore statistically significant under this one-way ANOVA analysis.

**Table 8: Descriptive comparison of compressive strength by fly ash presence**

| Group | *n* | Mean (MPa) | SD (MPa) | Median (MPa) |
|---|---|---|---|---|
| Zero fly ash | 566 | 36.772 | 18.445 | 35.301 |
| Positive fly ash | 464 | 34.654 | 14.234 | 33.743 |

**Table 9: One-way ANOVA comparing mean compressive strength between mixtures with zero and positive fly ash content**

| Source | Df | Sum of squares | F | p-value |
|---|---|---|---|---|
| Fly ash group | 1 | 1143.1 | 4.108 | 0.0429 |
| Residuals | 1028 | 286030.0 | | |

This finding, provided by tables 8 and 9 must be interpreted cautiously. The grouping does not control for cement, water, slag, superplasticizer, aggregate proportions, or curing age. The result therefore does not imply that adding fly ash necessarily reduces compressive strength. It indicates only that the average strengths of the two observed groups differ in this dataset. A more informative assessment of the role of fly ash would adjust for the other mixture constituents and examine possible interactions and nonlinear effects. Figure 12 displays the group comparison. The substantial overlap between the two distributions is consistent with the modest difference in their means relative to the observed within-group variation. Hence, fly ash presence alone does not provide a complete explanation of compressive strength.

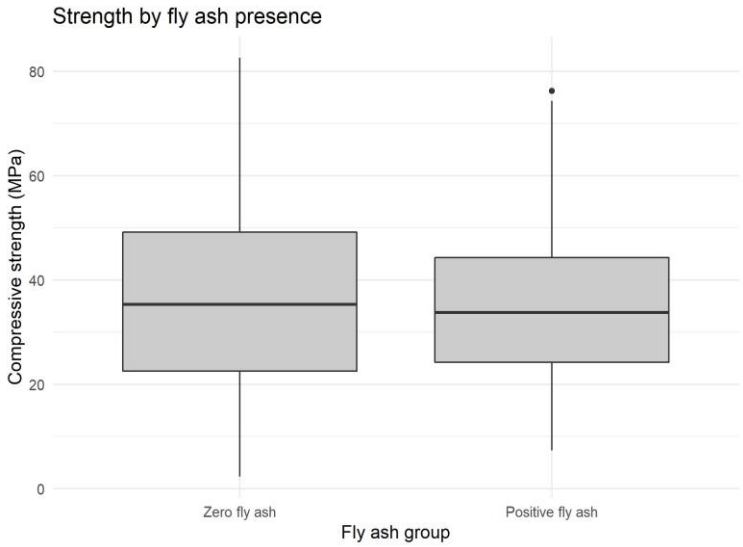



**Figure 12: Compressive strength for mixtures with zero and positive fly ash content**

### 14.6 Exploratory formulation screening

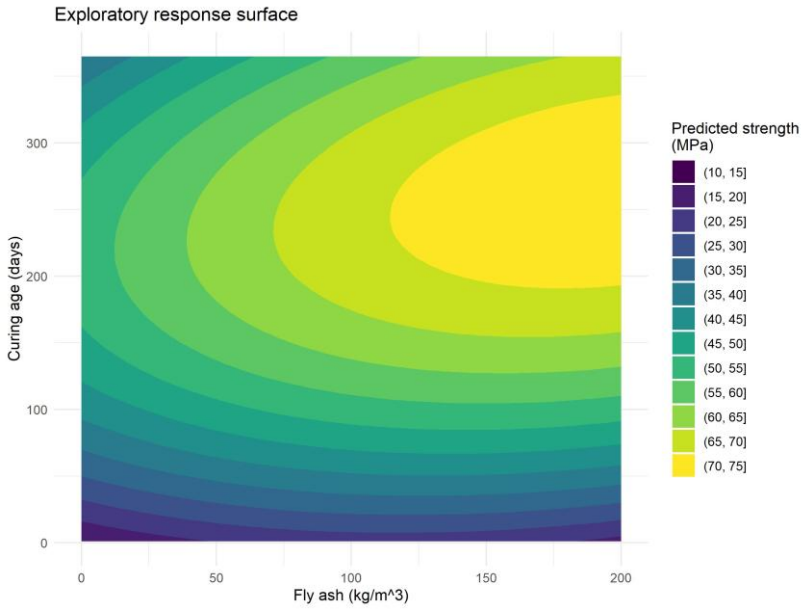



**Figure 13: Exploratory response surface for predicted concrete compressive strength as a function of fly ash content and curing age, conditional on the reference values of the remaining constituents**

The response-surface analysis was also used to examine predicted strength over a grid of fly ash contents and curing ages, while holding the other mixture constituents at specified reference values. The resulting contour plot, shown by Figure 13, illustrates the fitted model's conditional predictions and provides a visual summary of the nonlinear response pattern. The supplied grid-search output identifies a candidate with fly ash content of 200 kg/m$^3$ and curing age of approximately 263.633 days. At this point, the other constituents are fixed at cement content 266 kg/m$^3$, blast-furnace slag content 24 kg/m$^3$, water content 185 kg/m$^3$, superplasticizer content 6.625 kg/m$^3$, coarse aggregate content 968 kg/m$^3$, and fine aggregate content 780.09 kg/m$^3$. The fitted model predicts a compressive strength of approximately 74.092 MPa for this combination.

This candidate is an exploratory model-based result, not a validated optimum. In particular, the prediction is conditional on the chosen reference composition and the fitted response surface. The available grid-search output does not establish that this combination satisfies all practical mixturedesign constraints, nor does it demonstrate that an experimental specimen prepared at this composition would achieve the predicted strength. Confirmation would require a feasible mixture-design assessment and independent experimental validation. The result should therefore be interpreted as a candidate for further investigation rather than a final formulation recommendation. The results are presented in Table 10.

Although the response-surface analysis can help screen potential formulations for mechanical performance, it cannot directly identify the most environmentally sustainable formulation. The dataset does not contain carbon emissions, energy consumption, cost, or life-cycle assessment

indicators. Accordingly, the candidate cannot be described as the environmental or economic optimum. Such an assessment would require additional measurements and a multi-objective optimization framework that incorporates both mechanical performance and sustainability criteria.

**Table 10: Exploratory response-surface candidate recorded in the analysis archive, including the selected mixture proportions, curing age, and predicted compressive strength**

| Quantity | Value |
|---|---|
| Cement (kg/m³) | 266.000 |
| Blast-furnace slag (kg/m³) | 24.000 |
| Fly ash (kg/m³) | 200.000 |
| Water (kg/m³) | 185.000 |
| Superplasticizer (kg/m³) | 6.625 |
| Coarse aggregate (kg/m³) | 968.000 |
| Fine aggregate (kg/m³) | 780.090 |
| Curing age (days) | 263.633 |
| Predicted strength (MPa) | 74.092 |

### 14.7 Reproducibility and limitations

The analysis archive contains the analysis-ready dataset, descriptive statistics, Pearson and Spearman correlation matrices, ANOVA output, regression-model selection criteria, the exploratory responsesurface candidate, and the figures used in this case study. These materials provide a basis for reproducing the reported numerical summaries and graphical analyses. The original dataset documentation identifies 1,030 observations, nine variables, and no missing attribute values.

Several limitations should be considered when interpreting the findings. First, the data represent concrete mixture records and do not provide production-batch identifiers; therefore, the analysis cannot quantify between-batch variability or establish performance under a batch-based validation design. Second, correlations and the unadjusted fly ash group comparison are observational and do not establish causal effects. Third, the regression criteria available in the archive describe trainingdata fit, while a complete numerical table of held-out predictive performance for all candidate models is not included. Consequently, the available results do not support declaring one of the seven candidate prediction methods the definitive best model. Finally, environmental and economic superiority cannot be established without direct sustainability measurements.

Overall, this case study demonstrates how descriptive statistics, correlation analysis, analysis of variance, nonlinear regression, and response-surface screening can be combined to investigate the mechanical performance of concrete containing industrial by-products. The numerical results

show substantial variation in compressive strength, a stronger marginal association with cement and curing age than with fly ash alone, and improved training-data fit when nonlinear terms are introduced. These findings illustrate the usefulness of data-driven statistical analysis for preliminary formulation screening while highlighting the need for independent validation and additional environmental and economic data before drawing broader conclusions about sustainable material design.

**15. Challenges, Future Directions, and Conclusions**

The sustainable utilization of industrial waste in engineering materials presents considerable opportunities for resource conservation, waste minimization, and circular-economy development. However, translating these opportunities into reliable industrial applications requires a systematic understanding of the relationships among waste characteristics, material composition, processing conditions, and final engineering performance. Statistical modeling provides a valuable framework for investigating these relationships, quantifying uncertainty, identifying influential variables, and supporting evidence-based material design. Nevertheless, several methodological and practical challenges must be addressed before data-driven approaches can be applied reliably across different waste streams, material formulations, and industrial environments.

One of the principal challenges is the inherent heterogeneity of industrial waste. Waste materials originating from different industries, production processes, geographical regions, and storage conditions may exhibit substantial differences in chemical composition, particle-size distribution, moisture content, and physical properties. Even materials obtained from the same industrial source may vary considerably between production batches. Such variability can influence both the reproducibility of experimental results and the predictive performance of statistical models. Consequently, future investigations should consider hierarchical and mixed-effects models that explicitly account for batch-to-batch and source-specific variations. Where data are collected from multiple industries or geographical locations, multilevel modeling may help distinguish general relationships from sourcedependent effects. The systematic characterization of waste materials, together with appropriate uncertainty quantification, would further improve the reliability and transferability of the resulting models.

The availability of experimental data represents another important limitation. Materials research frequently involves expensive laboratory procedures, specialized equipment, and time-consuming mechanical or chemical tests, which may restrict the number of observations available for statistical analysis. Although complex machine-learning algorithms can represent highly nonlinear relationships, their use with limited datasets may lead to overfitting and unreliable predictions outside the observed experimental range. Therefore, the complexity of a statistical model should be selected according to the amount, quality, and structure of the

available data. Regression models, regularization techniques, and carefully specified response-surface models may provide effective alternatives when sample sizes are relatively small. Cross-validation should be employed to assess predictive performance, while independent datasets should be used whenever possible to evaluate generalizability. Future studies may also investigate optimal experimental-design strategies to select informative formulations and processing conditions, thereby reducing experimental costs without compromising the quality of statistical inference.

Missing observations and measurement uncertainty require equally careful consideration. Certain chemical properties, microstructural characteristics, or mechanical responses may remain unobserved because the corresponding tests are costly, technically difficult, or unavailable for every experimental specimen. Simply deleting incomplete observations may reduce the effective sample size and introduce bias when the probability of missingness is related to observed or unobserved variables. Future research should therefore examine statistically appropriate missing-data procedures, including multiple imputation, likelihood-based methods, and sensitivity analyses under alternative missingness assumptions. The suitability of any procedure should be evaluated in relation to the data-collection mechanism and the scientific objectives of the investigation. In addition, engineering measurements are subject to experimental error, specimen-to-specimen variation, and laboratory-specific conditions. For example, nominally identical specimens may exhibit different compressive strengths because of variations in preparation, curing, composition, or testing. Accordingly, reporting only a fitted mean response or a point prediction may provide an incomplete description of material performance. Prediction intervals, confidence intervals, and, where appropriate, estimates of measurement and between-specimen variability should accompany statistical predictions. Such information is particularly important when predicted material properties are used to assess engineering suitability or compliance with performance requirements.

A further challenge concerns the transferability of laboratory findings to pilot-scale and industrialscale production. A material formulation that performs satisfactorily under controlled laboratory conditions may behave differently when produced using industrial equipment or under less uniform environmental conditions. Differences in mixing efficiency, temperature regulation, curing procedures, production scale, and raw-material composition may alter the resulting material properties. Therefore, a formulation identified as promising by a laboratory-based statistical model should not automatically be regarded as an industrially validated solution. Future studies should progressively evaluate model performance using laboratory, pilot-scale, and industrial-scale observations. Where datasets from these stages are available, domain-specific effects and changes in the relationships between processing variables and material responses can be investigated explicitly. Periodic model recalibration may also be necessary

when production conditions or the characteristics of the incoming waste stream change over time. This approach would help distinguish formulations that perform well under a particular experimental setting from those that remain reliable under practical manufacturing conditions.

The integration of conventional statistical methods with artificial intelligence offers another important direction for future research. Exploratory data analysis, correlation analysis, regression, analysis of variance (ANOVA), and response-surface methodology provide interpretable tools for understanding experimental relationships and assessing differences among material formulations. However, complex interactions and nonlinear dependencies may not always be adequately represented by simple parametric models. Machine-learning approaches, including random forests, support vector regression, artificial neural networks, and gradient boosting, can complement conventional methods when sufficient high-quality data are available. Rather than treating statistical modeling and machine learning as competing alternatives, future investigations should evaluate their complementary strengths through systematic model comparison and independent validation. Explainable machinelearning methods are particularly relevant because engineering practitioners need to understand not only the predicted performance of a formulation but also the variables and interactions contributing to that prediction. Feature-importance measures and partial-dependence analyses may assist interpretation, although their results should be examined carefully when predictors are strongly correlated. The combined use of interpretable statistical models and flexible predictive algorithms could provide a more comprehensive basis for material characterization, performance prediction, and formulation development.

Industrial digitalization also creates opportunities to extend statistical modeling beyond the analysis of static experimental datasets. Modern production environments increasingly generate information through sensors, automated monitoring systems, and digital manufacturing platforms. Measurements of temperature, moisture, pressure, material composition, mixing duration, and energy consumption could be integrated with laboratory measurements of mechanical and physical performance. These data may support the development of dynamic predictive models that track changes in production conditions and identify deviations from desired material properties. Future research could investigate online monitoring, sequential model updating, and early-warning procedures for detecting changes in raw-material characteristics or manufacturing performance. However, successful implementation would require reliable sensor measurements, appropriate data preprocessing, robust model validation, and consideration of delays between processing conditions and the availability of final quality measurements. When these requirements are satisfied, data-driven monitoring may support timely adjustments to processing conditions and reduce material waste during production.

Beyond predictive accuracy, future studies should place greater emphasis on the optimization and sustainability assessment of waste-derived materials. A formulation that maximizes a single mechanical property may not necessarily provide the most desirable overall solution. Material selection and formulation optimization may involve several competing objectives, including engineering strength, durability, waste utilization, production cost, energy consumption, and environmental impact. Statistical models can be incorporated into multi-objective optimization procedures to identify candidate formulations that provide an appropriate balance among these objectives. The resulting solutions should then be examined through confirmatory experiments and, where feasible, life-cycle and economic assessments. In particular, the use of industrial waste should not be considered environmentally beneficial solely because it reduces the quantity of waste requiring disposal. The environmental implications of collection, transportation, pretreatment, processing, and long-term material performance must also be considered. Integrating statistical prediction with experimental confirmation and sustainability assessment would therefore provide a stronger basis for determining whether a proposed formulation is technically feasible, economically competitive, and environmentally responsible.

The overall framework for the data-driven development of sustainable materials from industrial waste can be summarized as follows:

Industrial Waste Characterization

↓

Experimental Design and Data Collection

↓

Exploratory Statistical Analysis

↓

Regression, ANOVA, and Response-Surface Modeling

↓

Machine-Learning Prediction and Model Interpretation

↓

Uncertainty Quantification and Independent Validation

↓

Material Formulation and Process Optimization

↓

Pilot-Scale and Industrial-Scale Verification

↓

Economic and Environmental Assessment

↓

Sustainable Material Production and Circular Economy

In conclusion, the successful upcycling of industrial waste into sustainable engineering materials requires more than identifying a waste material that can be incorporated into a formulation. It requires a systematic investigation of material variability, experimental uncertainty, processing conditions, engineering performance, and environmental consequences. Exploratory statistical analysis can reveal the distributions and variability of experimental variables, while correlation analysis can identify potentially important associations. Regression models provide interpretable descriptions of material performance, and polynomial and response-surface models can represent nonlinear effects and interactions. ANOVA facilitates comparisons among materials and formulations, whereas hierarchical and mixed-effects models can account for structured variability across batches, sources, and production conditions. Machine-learning methods can extend these analyses when more complex relationships are present, provided that model complexity is appropriate for the available data and predictive performance is assessed rigorously.

Importantly, prediction should be regarded as an intermediate step rather than the ultimate objective of statistical modeling. The practical value of a fitted model lies in its ability to support experimentally verifiable formulation decisions, identify promising processing conditions, quantify uncertainty, and guide the efficient use of industrial waste. Such decisions should be supported by independent validation and evaluated against engineering, economic, and environmental criteria. The integration of statistical inference, predictive modeling, optimization, and sustainability assessment can therefore transform experimental observations into actionable knowledge for materials development. Although challenges associated with heterogeneous waste streams, limited datasets, missing observations, measurement uncertainty, and industrial-scale implementation remain substantial, addressing these issues systematically can improve the reliability and practical relevance of data-driven approaches. Ultimately, statistical modeling provides an important link between experimental materials science and sustainable engineering by supporting the development of waste-derived materials that are technically reliable, economically viable, and environmentally responsible.

**Acknowledgement**

The author gratefully acknowledges the support and facilities provided by the Department of Mathematics, Brainware University, Kolkata, India.

**References**

1. United Nations Environment Programme. (2024). *Global waste management outlook 2024: Beyond an age of waste—Turning rubbish into a resource*. https://www.unep.org/en/resources/global-waste-management-outlook-2024

2. International Organization for Standardization. (2006). *Environmental management—Life cycle assessment—Principles and framework* (ISO Standard No. 14040:2006, 2nd ed.). https://www.iso.org/standard/37456.html
3. Ahmaruzzaman, M. (2010). A review on the utilization of fly ash. *Progress in Energy and Combustion Science, 36*(3), 327–363. https://doi.org/10.1016/j.pecs.2009.11.003
4. Purchase, C. K., Al Zulayq, D. M., O'Brien, B. T., Kowalewski, M. J., Berenjian, A., Tarighaleslami, A. H., & Seifan, M. (2022). Circular economy of construction and demolition waste: A literature review on lessons, challenges, and benefits. *Materials, 15*(1), Article 76. https://doi.org/10.3390/ma15010076
5. Papamichael, I., Voukkali, I., Loizia, P., & Zorpas, A. A. (2023). Construction and demolition waste framework of circular economy: A mini review. *Waste Management & Research, 41*(12), 1728–1740. https://doi.org/10.1177/0734242X231190804
6. Box, G. E. P., & Wilson, K. B. (1951). On the experimental attainment of optimum conditions. *Journal of the Royal Statistical Society: Series B (Methodological), 13*(1), 1–45. https://doi.org/10.1111/j.2517-6161.1951.tb00067.x
7. Montgomery, D. C. (2019). *Design and analysis of experiments* (10th ed.). John Wiley & Sons.
8. Hassan, S. I., Syed, S. A., Ali, S. W., Zahid, H., Tariq, S., Su Ud, M. M., & Alam, M. M. (2024). Systematic literature review on the application of machine learning for the prediction of properties of different types of concrete. *PeerJ Computer Science, 10*, Article e1853. https://doi.org/10.7717/peerj-cs.1853
9. NIST/SEMATECH. (n.d.). *e-Handbook of statistical methods*. National Institute of Standards and Technology. https://www.itl.nist.gov/div898/handbook/
10. James, G., Witten, D., Hastie, T., & Tibshirani, R. (2021). *An introduction to statistical learning: With applications in R* (2nd ed.). Springer. https://doi.org/10.1007/978-1-0716-1418-1
11. Yeh, I.-C. (1998). Modeling of strength of high-performance concrete using artificial neural networks. *Cement and Concrete Research, 28*(12), 1797–1808. https://doi.org/10.1016/S0008-8846(98)00165-3

*Bhumi Publishing, India*
*November 2026*

# UNCERTAINTY MODELLING WITH ADVANCED FUZZY LOGIC SYSTEMS

**Vicky B. Watkar**
Department of Mathematics,
Indira Mahavidyalaya, Kalamb, Dist. Yavatmal, M.S. India
Corresponding author E-mail: vickywatkar24@gmail.com

## Introduction

Fuzzy logic, introduced by Lotfi Zadeh in 1965, has established itself as a powerful tool for modeling uncertainty and imprecision in complex systems. Traditional Boolean logic, which operates on binary values of true or false (0 or 1), often struggles to handle real-world ambiguity and vagueness. Fuzzy logic, on the other hand, allows for intermediate values between 0 and 1, enabling more human-like reasoning and decision-making. Over the past few decades, fuzzy logic has evolved from a theoretical framework to a widely applied tool in artificial intelligence (AI), control systems, machine learning, and decision support systems.

The past decade has seen remarkable advancements in both the theoretical foundations and practical applications of fuzzy logic. From type-2 fuzzy sets and intuitionistic logic to the integration of fuzzy logic with machine learning and neural networks, these developments have enhanced the ability of systems to reason under uncertainty. This chapter explores the latest trends in fuzzy logic, focusing on new theoretical models, computational improvements, and real-world applications. The discussion concludes with an outlook on future research directions and potential challenges.

**Keywords:** Fuzzy Logic, Type-2 Fuzzy Sets, Interval Type-2 Fuzzy Logic Systems, Intuitionistic Fuzzy Sets, Hesitant Fuzzy Sets, Neutrosophic Logic, Fuzzy Neural Networks, Fuzzy Inference Systems, Uncertainty Modeling, Intelligent Decision Systems.

## Introduction

### Fuzzy Sets and Membership Functions

A fuzzy set A in a universe of discourse X is defined by a membership function:

$$\mu_A(x): X \to [0,1] \qquad (1)$$

where:

$x \in X$ = element of the universal set, $\mu A(x)$ = degree of membership of x in fuzzy set A

The value of $\mu A(x)$ indicates how strongly the element x belongs to the fuzzy set. For example, in a fuzzy set representing "tall people," a person with a height of 6 feet may have a membership value of 0.8, indicating that the person is "mostly tall."

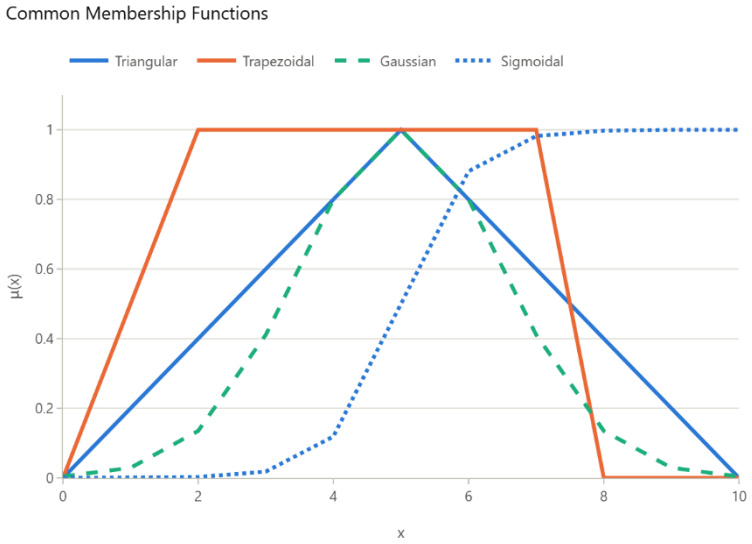
### Example of Membership Function

A common membership function is the triangular function, defined as:

$$\mu A(x) = \left\{ 0, x \le a \; \frac{x-a}{b-a}, a < x \le b \; \frac{c-x}{c-b}, b < x \le c \; 0, x > c \right\}$$

where a, b, c defines the shape of the triangle.

Other widely used membership functions include trapezoidal, Gaussian, and sigmoidal functions.




**Type-2 and Interval Type-2 Fuzzy Logic Systems (IT2-FLS)**

A classical (type-1) fuzzy set A in a universal set X is defined by a membership function:

$$\mu A(x): X \to [0,1] \mu_A(x): X \to [0,1] \quad (2)$$

where $\mu A(x) \mu_A(x)$ represents the degree of membership of element $x \in X$ in the fuzzy set A.

A type-2 fuzzy set $A$ $A^{\sim}$ extends this definition by allowing the membership function itself to be

$$A = \left(x, \mu A\ (x)\right) \mid x \in X, \mu A\ (x) \in [0,1] \quad (3)$$

$$A^{\sim} = \{(x, \mu_{A^{\sim}}(x)) \mid x \in X, \mu_{A^{\sim}}(x) \in [0,1]\} \quad (4)$$

where the membership value $\mu A\ (x) \mu_{A^{\sim}}(x)$ is now a fuzzy set on the unit interval [0,1] [0, 1].

In an Interval Type-2 Fuzzy Set (IT2-FLS), the membership function is defined as an interval:

$$A = (x, [\mu^{-} A\ (x), \mu^{-} A\ (x)]) \mid x \in X \quad (5)$$

$$A^{\sim} = \{(x, [\mu_{-A^{\sim}}(x), \mu{-}_{A^{\sim}}(x)]) \mid x \in X\} \quad (6)$$

where $\mu^{-} A\ (x) \mu_{-A^{\sim}}(x)$ and $\mu^{-} A\ (x) \mu{-}_{A^{\sim}}(x)$ are the lower and upper bounds of the membership function, respectively.

IT2-FLS reduces computational complexity while preserving the ability to handle uncertainty. Recent applications include:

- **Control systems** – Enhanced stability and adaptability in automotive and robotic control.
- **Medical diagnosis** – Better handling of uncertain or conflicting patient data.
- **Financial forecasting** – Improved modeling of stock market volatility and economic indicators.

**Intuitionistic and Hesitant Fuzzy Logic**

An intuitionistic fuzzy set (IFS) introduced by Atanassov is defined as:

$A = (x, \mu A(x), \nu A(x)) \mid x \in XA = \{(x, \mu_A(x), \nu_A(x)) \mid x \in X\}$ (7)

where $\mu A(x)\mu_A(x)$ is the degree of membership and $\nu A(x)\nu_A(x)$ is the degree of non-membership, satisfying:

$0 \leq \mu A(x) + \nu A(x) \leq 10 \leq \mu_A(x) + \nu_A(x) \leq 1$ (8)

The hesitation degree $\pi A(x)\pi_A(x)$ is given by:

$\pi A(x) = 1 - \mu A(x) - \nu A(x)\pi_A(x) = 1 - \mu_A(x) - \nu_A(x)$ (9)

Hesitant fuzzy sets allow for multiple possible membership values, modeled as:

$H(x) = \mu 1, \mu 2, \ldots, \mu nH(x) = \{\mu_1, \mu_2, \ldots, \mu_n\}$ (10)

where $\mu i \in [0,1]\mu_i \in [0,1]$

This allows modelling of conflicting or ambiguous information.

**Neutrosophic Logic**

Neutrosophic sets generalize fuzzy sets by defining truth, falsehood, and indeterminacy degrees simultaneously:

$A = \big(x, TA(x), FA(x), IA(x)\big) \mid x \in X$ (11)

$A = \{(x, T_A(x), F_A(x), I_A(x)) \mid x \in X\}$ (12)

here $TA(x)\, T_A(x)$ is the degree of truth, $FA(x)\, F_A(x)$ is the degree of falsehood, and $IA(x)$ $I_A(x)$ is the degree of indeterminacy, satisfying:

$$0 \leq TA(x) + FA(x) + IA(x) \leq 30$$

$$\leq T_A(x) + F_A(x) + I_A(x) \leq 3 \quad (13)$$

**Computational and Algorithmic Developments**

**Fuzzy Neural Networks (FNN)**

Fuzzy neural networks combine neural network adaptability with fuzzy interpretability. An FNN model typically computes the output as:

$$y = \sum i \ = 1nwi \cdot \mu i(x)$$

$$y = \sum_{i=1}^{n} \quad w_i \cdot \mu_i(x) \quad (14)$$

where:

- $w_i$ = weights learned through backpropagation
- $\mu i(x)\mu_i(x)$ = fuzzy membership functions

**Fuzzy Inference Systems (FIS)**

A fuzzy inference system maps fuzzy inputs to fuzzy outputs using fuzzy rules. For a Mamdani FIS, the output is computed as:

$y = \sum i$

$= 1n\mu i(x) \cdot wi\sum i$

$= 1n\mu i(x)y$

$= \frac{\sum_{i=1}^{n} \ \mu_i(x) \cdot w_i}{\sum_{i=1}^{n} \ \mu_i(x)}$ (15)

where $\mu i(x)\mu_i(x)$ represents the degree of activation of the i[th] fuzzy rule.

**Fuzzy Optimization and Metaheuristics**

In fuzzy optimization problems, the objective function can be defined as:

$x \in Xf(x)\ subject\ to\ gi(x) \leq 0,\ hj(x) = 0$

$f_{x\in X}(x)\ subject\ to\ g_i(x) \leq 0, h_j(x) = 0$

where the constraints are represented as fuzzy inequalities or equalities:

$$\mu gi(x) \geq \alpha, \mu hj(x) = \beta \mu_{g_i}(x) \geq \alpha, \mu_{h_j}(x) = \beta \quad (16)$$

where $\alpha, \beta \in [0,1] \alpha, \beta \in [0,1]$ represent the degree of satisfaction.

**Applications and Industry Impact**

**Control Systems and Robotics**

Fuzzy controllers are defined using rules like:

$$R: if\ (x\ isA_1) \wedge (x\ isA_2) \wedge (y\ isB_{A1}) \wedge (y\ isA_2) \wedge (y\ is\ B)\ then\ (z\ is\ C) \quad (17)$$

Where,

$A_1A_2 \subseteq X \qquad B_{A1,}\ A_{2,}\ B \subseteq Y \qquad C \subseteq Z$

The corresponding membership functions are

$\mu A_1: X \to [0\ ,1],\ \ \mu A_2: X \to [0\ ,1]$

$\mu BA_1: Y \to [0\ ,1],\ \ \mu A_2: Y \to [0\ ,1],\ \ \mu B: Y \to [0\ ,1]$

And $\mu c: Z \to [0\ ,1]$

For an input pair $(x, y)$, the firing strength of the rule using a t -norm T is

$\alpha = T(\mu A_1(x), \mu A_2(x), \mu BA_1(y), \mu A_2(y), \mu B(y))$

With

$$0 \leq \alpha \leq 1$$

For the commonly used minimum -norm,

$\alpha = min\{\mu A_1(x), \mu A_2(x), \mu BA_1(y), \mu A_2(y), \mu B(y)\}$

The resulting fuzzy output set C' is then

$$\mu c'(z) = \{\alpha, \mu c(z)\}, z \in Z \quad (18)$$

**Conclusion**

Fuzzy logic continues to play a pivotal role in AI and decision-making systems. Recent advancements in type-2 fuzzy sets, fuzzy neural networks, and hybrid models have enhanced the ability to reason under uncertainty and handle complex real-world problems. Future research will focus on improving computational efficiency, expanding the applicability of fuzzy systems, and exploring new hybrid approaches with deep learning and probabilistic models.

**References**

1. Zadeh, L. A. (1965). Fuzzy sets. *Information and Control, 8*(3), 338–353.

2. Zadeh, L. A. (1975). The concept of a linguistic variable and its application to approximate reasoning—I. *Information Sciences, 8*(3), 199–249.
3. Zadeh, L. A. (1975). The concept of a linguistic variable and its application to approximate reasoning—II. *Information Sciences, 8*(4), 301–357.
4. Zadeh, L. A. (1978). Fuzzy sets as a basis for a theory of possibility. *Fuzzy Sets and Systems, 1*(1), 3–28.
5. Mamdani, E. H., & Assilian, S. (1975). An experiment in linguistic synthesis with a fuzzy logic controller. *International Journal of Man-Machine Studies, 7*(1), 1–13.
6. Takagi, T., & Sugeno, M. (1985). Fuzzy identification of systems and its applications to modeling and control. *IEEE Transactions on Systems, Man, and Cybernetics, 15*(1), 116–132.
7. Zadeh, L. A. (1975). The concept of a linguistic variable and its application to approximate reasoning. *Information Sciences, 8*, 43–80.
8. Mendel, J. M. (2001). *Uncertain rule-based fuzzy logic systems: Introduction and new directions*. Prentice Hall.
9. Mendel, J. M., & John, R. I. (2002). Type-2 fuzzy sets made simple. *IEEE Transactions on Fuzzy Systems, 10*(2), 117–127.
10. Karnik, N. N., Mendel, J. M., & Liang, Q. (1999). Type-2 fuzzy logic systems. *IEEE Transactions on Fuzzy Systems, 7*(6), 643–658.
11. Liang, Q., & Mendel, J. M. (2000). Interval type-2 fuzzy logic systems: Theory and design. *IEEE Transactions on Fuzzy Systems, 8*(5), 535–550.
12. Atanassov, K. T. (1986). Intuitionistic fuzzy sets. *Fuzzy Sets and Systems, 20*(1), 87–96.
13. Torra, V. (2010). Hesitant fuzzy sets. *International Journal of Intelligent Systems, 25*(6), 529–539.
14. Torra, V., & Narukawa, Y. (2009). On hesitant fuzzy sets and decision. In *Proceedings of the 2009 IEEE International Conference on Fuzzy Systems*.

# STATISTICAL ANALYSIS OF POPULATION GROWTH USING DIFFERENTIAL EQUATIONS: A MATHEMATICAL AND STATISTICAL MODELLING APPROACH

**S. Revathi**
Department of Mathematics,
Krishnasamy College of Science, Arts & Management for Women,
Senjikumarapuram, Cuddalore, Tamil Nadu 607109
Corresponding author E-mail: srevthi@gmail.com

**Abstract**
Population growth is a central concern in demography, mathematical biology, public administration and resource planning. Population size changes over time as a result of births, deaths, immigration and emigration. Differential equations provide a framework for representing the rate of population change, while statistical methods connect the mathematical models with observed population data. This chapter presents two classical continuous-time models: the exponential growth model and the logistic growth model. The exponential model assumes a constant per-capita growth rate, whereas the logistic model incorporates a finite carrying capacity and a declining per-capita growth rate as population size increases. The chapter explains the derivation and interpretation of both models, parameter estimation through regression, residual analysis, goodness-of-fit assessment and the use of fitted models for forecasting. A worked numerical illustration is included to demonstrate the calculations; the values are hypothetical and are not observations from a real population. The chapter also discusses model assumptions, limitations and the importance of using reliable demographic data. It is intended to show how differential equations and statistical analysis can be combined to investigate population dynamics and support evidence-informed planning.

**Keywords:** Population Dynamics, Differential Equations, Exponential Growth, Logistic Growth, Regression Analysis, Parameter Estimation, Model Validation, Population Forecasting.

## 1. Introduction

Population growth refers to the change in the number of individuals in a defined population over time. At the simplest level, the change is determined by the balance between additions to and losses from the population. Births and immigration increase population size, whereas deaths and emigration decrease it. Consequently, population growth is influenced by demographic, economic, social, environmental and policy-related factors.

Understanding population change is important for planning housing, education, healthcare, transport, food, water and other public services. Mathematical models help describe possible

patterns of change and provide a structured way to examine assumptions about future population size. Differential equations are particularly useful when population change is represented as a continuous process.

Two foundational models are commonly introduced in population modelling. The exponential model represents growth at a constant per-capita rate and is often useful over periods when conditions remain relatively stable. The logistic model extends this idea by allowing the per-capita growth rate to decrease as the population approaches a limiting level, called the carrying capacity. The logistic model is associated with the work of Verhulst (1838, 1845).

Mathematical models do not automatically provide reliable forecasts. Their parameters must be estimated from suitable data, and the resulting model must be checked against observations. Regression analysis, residual diagnostics, uncertainty assessment and validation are therefore essential parts of a statistical study of population growth (Keyfitz & Caswell, 2005; Tsoularis & Wallace, 2002).

## 2. Aim and Objectives

The main aim of this chapter is to explain how differential equation models and statistical techniques can be integrated to analyse population growth.

- To formulate the exponential and logistic population growth models.
- To explain the meaning and role of the parameters in each model.
- To describe methods for estimating model parameters from historical population data.
- To discuss regression, residual analysis and goodness-of-fit measures for evaluating model performance.
- To explain how fitted models can be used for population forecasting and why forecasts should be interpreted cautiously.

## 3. Population Change and Differential Equations

Let P(t) denote the population size at time t. A general accounting expression for population change over a time interval is:

$$\textbf{Change in population} = \textbf{Births} - \textbf{Deaths} + \textbf{Immigration} - \textbf{Emigration}$$

In a continuous-time representation, the rate of change can be expressed as:

$$\frac{dP}{dt} = B(t) - D(t) + I(t) - E(t)$$

Here, B(t), D(t), I(t) and E(t) represent the corresponding rates of births, deaths, immigration and emigration. Specific mathematical models arise by making assumptions about how these rates depend on population size and time. The exponential and logistic models are simplified representations; they do not explicitly describe every demographic mechanism.

## 4. Exponential Growth Model

### 4.1 Mathematical formulation

The exponential growth model assumes that the instantaneous rate of population change is proportional to the current population size. Its differential equation is:

$$\mathbf{dP/dt = rP}$$

where P(t) is the population at time t and r is the constant per-capita growth rate. If r is positive, the model describes growth; if r is negative, it describes decline; and if r is zero, the population remains constant.

### 4.2 Derivation of the solution

Separating variables gives:

$$\mathbf{(1/P)\, dP = r\, dt}$$

Integrating both sides:

$$\mathbf{\ln P = rt + C}$$

Exponentiating and applying the initial condition $P(0) = P_0$ gives the exponential solution:

$$\mathbf{P(t) = P_0\, e^{(rt)}}$$

The parameter $P_0$ is the initial population. The parameter r is the continuous per-capita growth rate, and t is elapsed time in the same time unit used to define r.

### 4.3 Interpretation and assumptions

The model produces a J-shaped curve when r is positive. It assumes that the per-capita growth rate remains constant over the period considered. In practice, this assumption may be reasonable for a limited time interval, but it is unlikely to remain valid indefinitely because birth rates, death rates, migration and environmental conditions can change.

### 4.4 Estimating the growth rate by linear regression

Taking natural logarithms of the exponential solution gives:

$$\mathbf{\ln P(t) = \ln P_0 + rt}$$

Let $Y = \ln P(t)$. The expression is linear in time and can be written as $Y = a + bt$, where $a = \ln P_0$ and $b = r$. A linear regression of log population on time can therefore estimate the continuous growth rate, provided the assumptions of the transformation and error model are suitable. The slope estimates r and the intercept estimates $\ln P_0$.

For two observations $(P_1, t_1)$ and $(P_2, t_2)$, a simple two-point estimate is:

$$\mathbf{\hat{r} = [\ln(P_2/P_1)] / (t_2 - t_1)}$$

When more than two observations are available, regression using all observations is generally preferable to relying on only two points. The analyst should also consider whether errors are more appropriately described on the original population scale or on the logarithmic scale.

## 5. Logistic Growth Model

### 5.1 Mathematical formulation

The logistic model represents population growth under a limiting environmental capacity. Its differential equation is:

$$\mathbf{dP/dt = rP(1 - P/K)}$$

Here, r is the intrinsic growth-rate parameter and K is the carrying capacity. The carrying capacity represents the limiting population level implied by the model under the assumed conditions. It is not necessarily a fixed or directly observable physical maximum in a changing real-world environment.

### 5.2 Solution of the logistic equation

For an initial population $P(0) = P_0$, the solution is:

$$\mathbf{P(t) = K / [1 + A\ e^{(-rt)}]}$$

where:

$$\mathbf{A = (K - P_0) / P_0}$$

The curve is typically S-shaped when $0 < P_0 < K$ and $r > 0$. Growth is relatively slow when the population is small, becomes faster over an intermediate range, and then slows as P(t) approaches K. Under the standard model, the population approaches K asymptotically.

### 5.3 Interpretation and assumptions

The logistic model assumes that the per-capita growth rate decreases linearly with population size and that the carrying capacity is constant during the period being modelled. It is more flexible than the exponential model with respect to resource limitation, but it remains a simplified model. Sudden migration, epidemics, policy changes, environmental shocks and age-structure effects may require additional variables or a different modelling framework.

The classical logistic model is historically associated with Verhulst (1838, 1845). Reviews of logistic growth models discuss a wider family of related growth curves and the restrictions involved in their use (Tsoularis & Wallace, 2002).

## 6. Statistical Methodology and Data Requirements

### 6.1 Data collection

An empirical study should specify the geographical unit, population definition, observation period, time interval and data source before fitting a model. Population counts should be drawn from a reliable source, such as a national census or an official statistical agency. For international comparisons, the United Nations World Population Prospects provides population estimates and projections for countries and areas, together with methodological documentation (United Nations, 2024). The data source, access date, population definition and any revisions should be reported.

The current supplied manuscript does not identify a particular country, state, district or town, and it does not include an observed population dataset. Therefore, the numerical examples in this revised chapter are explicitly illustrative. They must not be described as findings from an actual population study.

**6.2 Data preparation**

i. Arrange observations in chronological order and express time consistently, for example as years since the first observation.
ii. Check for missing values, duplicate records, changes in geographical boundaries and changes in population definitions.
iii. Record whether the data are census counts, estimates or projections; these categories should not be treated as interchangeable.
iv. Plot population against time before fitting a model to inspect the broad pattern and identify unusual observations.
v. Document any data adjustments and retain the original values for transparency.

**6.3 Parameter estimation**

For the exponential model, the growth rate can be estimated by linear regression after taking logarithms of the observed population values. For the logistic model, the parameters r and K generally require nonlinear regression because the solution is nonlinear in these parameters. Nonlinear least squares estimate parameters by minimizing the sum of squared differences between observed and model-predicted population values. Maximum likelihood estimation may also be used when a probability model for the observations has been specified.

$$S(r, K) = \Sigma_i [P_i - \hat{P}(t_i; r, K)]^2$$

In this expression, $P_i$ is the observed population at time $t_i$ and $\hat{P}(t_i; r, K)$ is the value predicted by the logistic model. Parameter constraints and starting values should be selected carefully, and uncertainty in the estimates should be reported where possible.

**7. Illustrative Numerical Example**

The following example demonstrates the estimation of an exponential growth rate. It is a hypothetical dataset created for teaching purposes and is not an empirical population record.

| Year | Illustrative Population | ln (Population) |
|---|---|---|
| 2020 | 1,000 | 6.9078 |
| 2021 | 1,100 | 7.0031 |
| 2022 | 1,210 | 7.0986 |
| 2023 | 1,331 | 7.1937 |
| 2024 | 1,464 | 7.2889 |

The values approximately follow an annual multiplication factor of 1.10. Taking the first and last observations, with a four-year interval:

$$\hat{r} = \ln(1464/1000) / 4 \approx 0.0953 \text{ per year}$$

The fitted continuous-time exponential model is approximately:

$$\hat{P}(t) = 1000\, e^{(0.0953t)}$$

where t is the number of years after 2020. The continuous growth-rate estimate of approximately 0.0953 corresponds to a yearly multiplication factor of e^0.0953, which is approximately 1.10. Thus, the equivalent discrete annual increase is approximately 10%. Small differences in the table arise from rounding.

This example illustrates parameter estimation only. A real study should use the complete observed dataset, estimate parameters with an appropriate regression procedure, examine residuals and assess predictions on data not used for fitting whenever possible.

**8. Model Evaluation and Comparison**

A model should not be selected solely because its fitted curve appears visually close to the observed data. Quantitative diagnostics and the purpose of the analysis should also be considered.

| Measure | Interpretation |
|---|---|
| Residuals | Differences between observed and fitted population values; patterns may indicate model inadequacy. |
| RMSE | Square root of the mean squared prediction errors; expressed in the same units as the response variable. |
| R-squared | A measure of explained variation for a specified response scale and model; interpretation depends on the fitting method. |
| Confidence intervals | Describe uncertainty in estimated parameters. |
| Prediction intervals | Describe uncertainty around future predicted values and are generally wider than confidence intervals for the mean response. |

For a fair comparison, the analyst must consider the scale on which each model is fitted. Regression on log population emphasizes proportional deviations, whereas fitting population on its original scale emphasizes absolute deviations. Consequently, goodness-of-fit statistics calculated on different response scales should not be compared without qualification.

A practical comparison should examine residual plots, prediction errors and performance on a validation period or hold-out observations. A model that fits historical data well may still forecast poorly if demographic conditions change.

**9. Population Forecasting**

Once a model has been fitted and checked, its estimated parameters can be substituted into the corresponding solution to generate conditional forecasts. Under the exponential model:

$$\hat{P}(t) = \hat{P}_0 \, e^{(\hat{r}t)}$$

Under the logistic model:

$$\hat{P}(t) = \hat{K} / [1 + \hat{A} \, e^{(-\hat{r}t)}]$$

These expressions produce projections conditional on the model assumptions and estimated parameters. They should not be interpreted as certain predictions. Forecast uncertainty increases with the forecast horizon, and changes in migration, fertility, mortality, public policy, economic conditions and environmental circumstances may alter the observed trajectory.

For practical planning, it is useful to report a forecast together with its assumptions, forecast horizon and uncertainty range. Alternative scenarios may also be considered when future demographic conditions are uncertain.

**10. Discussion**

The exponential and logistic models provide complementary starting points for population analysis. The exponential model is mathematically simple and can describe short-term growth when a nearly constant per-capita rate is plausible. The logistic model incorporates a limiting level and may be useful when the observed trajectory shows a clear slowing of growth. Neither model should be assumed to be universally appropriate.

The choice of model should be guided by the study objective, the characteristics and length of the dataset, the demographic context and diagnostic evidence. In particular, the carrying capacity in a logistic model can be difficult to estimate reliably when the observed data do not show a clear approach to a plateau. In such circumstances, the estimate may be highly uncertain.

Population counts may also be affected by census undercount, revisions, boundary changes and differences in estimation methods. These issues should be acknowledged because statistical precision cannot compensate for poor or inconsistent input data. More detailed demographic studies may need age-structured, sex-structured, migration or stochastic models. Mathematical demography provides broader approaches for analysing fertility, mortality, population structure and projection (Keyfitz & Caswell, 2005).

**11. Limitations**

- The exponential model assumes a constant per-capita growth rate and does not include a carrying capacity.
- The standard logistic model assumes a constant carrying capacity and a particular form of density dependence.
- Both models simplify complex demographic processes and may not explicitly represent age structure, migration patterns or sudden external events.
- Parameter estimates depend on the quality, length and consistency of the available data.
- A good fit to historical observations does not guarantee accurate long-term forecasts.

- The present chapter contains illustrative calculations rather than an analysis of a named population dataset.

**Conclusion and Future Scope**

Differential equations provide a clear mathematical framework for describing population change, while statistical methods allow model parameters to be estimated from observed data and model performance to be evaluated. The exponential growth model represents a constant per-capita growth rate, whereas the logistic model incorporates a carrying capacity and a reduction in growth as population size increases. Linear regression on log-transformed population data can be used to estimate the exponential growth rate, while nonlinear regression is commonly used for the logistic model.

Reliable population analysis requires careful data selection, transparent parameter estimation, residual diagnostics, model validation and clear communication of uncertainty. The models discussed in this chapter are useful introductory tools, but their assumptions must be considered before they are applied to real populations.

Future work should apply the methods to a clearly identified geographical population using verified census or official statistical data. It could compare exponential and logistic fits over a specified time period, report parameter uncertainty, validate forecasts against later observations and investigate whether models incorporating migration, changing vital rates or age structure provide improved performance.

**References**

1. Keyfitz, N., & Caswell, H. (2005). *Applied mathematical demography* (3rd ed.). Springer. https://doi.org/10.1007/b139042
2. Tsoularis, A., & Wallace, J. (2002). Analysis of logistic growth models. *Mathematical Biosciences, 179*(1), 21–55. https://doi.org/10.1016/S0025-5564(02)00096-2
3. United Nations, Department of Economic and Social Affairs, Population Division. (2024). *World population prospects 2024*. https://population.un.org/wpp/
4. Verhulst, P.-F. (1838). Notice sur la loi que la population suit dans son accroissement. *Correspondance Mathématique et Physique, 10*, 113–121.
5. Verhulst, P.-F. (1845). Recherches mathématiques sur la loi d'accroissement de la population. *Nouveaux Mémoires de l'Académie Royale des Sciences et Belles-Lettres de Bruxelles, 18*, 1–40.

# ON THE SOLVABILITY OF AN INFINITE SYSTEM OF THREE POINT BOUNDARY VALUE PROBLEM IN THE SEQUENCE SPACES m(Φ) AND $m^B(\Phi)$ USING MEIR-KEELER CONDENSING OPERATORS

**Washmin Ara Begum[1] and Rituparna Das[2]**

[1]Department of Mathematics, Gauhati University, Guwahati -781014, Assam, India.

[2]Department of Mathematics, Pandu College, Pandu, Guwahati -781012, Assam, India.

Corresponding author E-mail: washminbegum72013@gmail.com, ri2p.das@gmail.com, rituparna.das@panducollege.ac.in

**Abstract**

In this paper, we study the existence of solutions of an infinte system of third order three point boundary value problem in the sequence spaces $m(\phi)$ and $m^{\beta}(\phi)$. The problem is studied using Hausdorff measure of noncompactness along with the idea of Meir-Keeler condensing operator. We have also provided suitable examples to illustrate our results.

**Keywords:** Infinite System of Differential Equations, Meir-Keeler Condensing Operator, Sequence Space, Fixed Point Theory, Measure of Noncompactness.

**2020 Mathematics Subject Classification:** 47H08, 47H09, 47H10, 34A34.

## 1. Introduction

The concept of measure of noncompactness (MNC) is a very important branch of nonlinear analysis with many applications specially in functional analysis, operator theory, fixed point theory, fractional calculus, differential equations, integral equations, integrodifferential equations etc. The concept of MNC was first introduced by Kuratowski [1] in the year 1930. Since then, many authors have used the concept of MNC in various branches of mathematics. Bana´s and Lecko [10] examined the solvability of infinite systems of differential equations in some Banach sequence spaces. Mursaleen and Mohiuddine [12] studied the solvability of an infinite system of differential equations in the sequence space $\ell_p$. Mursaleen and Rizvi [19] proved existence of infinite systems of second order differential equations in the sequence spaces $c_0$ and $\ell_1$ by Meir-Keeler condensing operators. Srivastava *et al.* [20] studied the existence of solutions of infinite systems of differential equations of general order with boundary conditions in the spaces $c_0$ and $\ell_1$ via the MNC. Alotaibi *et al.* [17] used the concept of MNC to examine the existence of solutions of an infinite system of linear equations in different sequence spaces. Saadati *et al.* [21] discussed the solvability of infinite systems of third order differential equations in $c_0$ space by Meir-Keeler condensing operators. Apart from these, various applications of MNC can be obtained in different literatures [13,15,16, 18, 22].

Recently Sapkota *et al.* [26,27] discussed the existence of solutions of an infinite system of third order three point boundary value problems in the sequence spaces $bv_0, c_0$ and $\ell_1$. Motivated from this, in this paper, we investigate the solvability of an infinite system of third order three point differential equations in the sequence spaces $m(\phi)$ and $m^{\beta}(\phi)$. The sequence space $m(\phi)$ was first introduced by Sargent [4] in 1960. Later Mursaleen [11] discussed some geometric properties of this sequence space. Mehravaran *et al.* [25] introduced and studied different properties of the tempered sequence space $m^{\beta}(\phi)$.

**2. Preliminaries and Background**

Let $\mathrm{B}_H$ be the family of all non-empty and bounded subsets of the Banach space $(H,\|.\|)$ over the set of real numbers. Also, let $\mathfrak{B}_H^C \subseteq \mathfrak{B}_H$ be the sub-family of all bounded closed sets. Further, let $\mathfrak{C}_H$ be the collection of all non-empty and relatively compact subsets of $H$. If $S \subseteq H$, then $S$ and Conv($S$), are the closure and convex closure of $S$ respectively.

In 1980, Bana´s and Goebel [8] defined the axiomatic definition of measure of noncompactness (MNC) as follows:

**Definition 2.1.** *For a Banach space H, a function* $\psi : \mathfrak{B}_H \to \mathrm{R}+ \cup \{0\}$ *is called a measure of noncompactness (MNC) in H if it satisfies the following axioms:*

*(i)* *The family* $\ker \psi = \{E \in \mathfrak{B}_X : \psi(E) = 0\}$ *is non-empty and* $\ker \psi \subset \mathfrak{C}_H$.

*(ii)* $E_1 \subset E_2 \Rightarrow \psi(E_1) \leq \psi(E_2)$.

*(iii)* $\psi(\bar{E}) = \psi(E)$.

*(iv)* $\psi(\mathrm{Conv}(E)) = \psi(E)$.

*(v)* $\psi(\lambda E + (1-\lambda)F) \leq \lambda\psi(E) + (1-\lambda)\psi(F)$, *for all* $\lambda \in (0,1)$.

*(vi)* *If* $(S_n)$ *is a decreasing sequence in* $\mathfrak{B}^C{}_H$ *and if* $(\psi(S_n))$ *is in* $c_0$, *then there exists at least one* $s \in H$ *such that* $s \in S_n$, *for all* $n \in \mathrm{N}$.

Let us recall some well known definitions and results which will be helpful for preparing the results of this paper.

**Definition 2.2. [14]** *Let* $\psi$ *be a MNC in a Banach space H. Suppose that E,* $E_1$ *and* $E_2$ *are bounded subsets of H. Then,*

*(i)* $\psi$ *is said to be homogeneous if* $\psi(\lambda(E)) = |\lambda|\mu(E)$, *for all scalar* $\lambda$.

*(ii)* $\psi$ *is said to be subadditive if* $\mu(E_1 + E_2) \leq \mu(E_1) + \mu(E_2)$.

*(iii)* $\psi$ *is said to have maximum property if* $\psi(E_1 \cup E_2) = \max\{\psi(E_1), \psi(E_2)\}$.

*(iv)* $\psi$ *is said to be sublinear if it is both homogeneous and subadditive.*

*(v)* $\psi$ *is said to be regular if it is sublinear, has the maximum property and* $\ker \psi = \mathrm{C}_X$. *The MNC* $\psi$ *such that* $\ker \psi = \mathrm{C}_X$ *is called the full measure or the measure with full kernel.*

**Definition 2.3. [9]** *Let* $H_1$ *and* $H_2$ *be two Banach spaces. Suppose that* $\psi_1$ *and* $\psi_2$ *be two MNC's on* $H_1$ *and* $H_2$ *respectively. An operator F from* $H_1$ *to* $H_2$ *is called* $(\psi_1, \psi_2)$ *condensing operator if*

*(i)* *F is continuous,*

*(ii)* $\psi_2(F(A)) < \psi_1(A)$ *, where A is bounded as well as non compact subset of* $H_1$.

A $(\psi_1,\psi_2)$-condensing operator becomes $\psi$-condensing operator when $\psi_1 = \psi_2 = \psi$ and is defined on the same Banach space.

**Theorem 2.1. [2]** *Let H be a Banach space with an arbitrary MNC* $\psi$*. Suppose that A is in* $\mathfrak{B}^C_H$*. A continuous mapping* $\mathcal{F}$: $A \to A$ *contains a fixed point in A if*

*(i) A is convex,*

*(ii)* $\psi(\mathcal{F}(A)) \leq \lambda\psi(A)$ *for some* $\lambda \in [0,1)$.

**Definition 2.4. [7]** *Let* $(X,\rho)$ *be a metric space. A mapping* $\mathcal{F}$ *on* $\mathfrak{X}$ *is said to be a Meir-Keeler contraction if for each* $\epsilon > 0$*, there exists* $\delta > 0$ *with* $d(\mathcal{F}u,\mathcal{F}v) < \epsilon$ *whenever* $\epsilon \leq \rho(u,v) < \epsilon + \delta$*, for all* $u,v \in \mathfrak{X}$.

**Theorem 2.2. [7]** *A Meir-Keeler contraction mapping* $\mathcal{F}$ *on a complete metric space* $(\mathbf{x},\rho)$ *always has a unique fixed point.*

**Definition 2.5. [15]** *Let H be a Banach space,* $\psi$ *be an arbitrary MNC on it and C be a non-empty subset of H. A Meir-Keeler condensing operator acting upon C is an operator* $\mathcal{F} : C \to C$ *such that for each* $\epsilon > 0$*, there exists* $\delta > 0$ *with* $\psi(F(B)) < \epsilon$ *whenever* $\epsilon \leq \psi(B) < \epsilon + \delta$ *for every bounded subset B of C.*

**Theorem 2.3. [15]** *Let H be a Banach space,* $\psi$ *be an arbitrary MNC and A be a non-empty, bounded, closed and convex subset of it. Suppose* $\mathcal{F}$ *be a continuous and Meir-Keeler condensing operator on A , then* F *has at least one fixed point and the set of all these fixed points of* $\mathcal{F}$ *in A are compact.*

## 3. The Hausdorff Measure of Noncompactness(H-MNC) on Banach Spaces

The Hausdorff measure of noncompactness is a very important mathematical tool in non-linear analysis with several applications. It was first introduced by Golden˘stein and Markus [6] in 1965.

**Definition 3.1.** *Let S be a bounded subset of a metric space* $(\mathbf{x},\rho)$*. Then the Hausdorff measure of noncompactness (H-MNC) of S, denoted by* $\chi(S)$*, is defined as*

$$\chi(S) = \inf\left\{\epsilon > 0 : S \subset \bigcup_{i=1}^{n} B(x_i, r_i),\ x_i \in \mathfrak{X},\ r_i < \epsilon, 1 \leq i \leq n, n \in \mathbb{N}\right\}$$

*where,* $B(x_i,r_i)$ *is an open ball in* $\mathbf{x}$.

The function $\chi$ is called the Hausdorff measure of noncompactness.

For the following results, one may refer to [14].

**Lemma 3.1.** *Let B,* $B_1$ *and* $B_2$ *be bounded subsets of a complete metric space* $(\mathbf{x},\rho)$*. Then*

*(i)* $\chi(B) = 0$ *if and only if B is totally bounded.*

*(ii)* $\chi(B) = \chi(\overline{B})$.

*(iii)* $B_1 \subset B_2 \Rightarrow \chi(B_1) \leq \chi(B_2)$.

*(iv)* $\chi(B_1 \cup B_2) = \max\{\chi(B_1),\chi(B_2)\}$.

*(v)* $\chi(B_1 \cap B_2) \leq \min\{\chi(B_1), \chi(B_2)\}$.

**Lemma 3.2.** *Let B, $B_1$ and $B_2$ be bounded subsets of a normed space* X. *Then*

*(i)* $\chi(B_1 + B_2) \leq \chi(B_1) + \chi(B_2)$.

*(ii)* $\chi(B + x) = \chi(B)$ *for every* $x \in \mathbf{x}$.

*(iii)* $\chi(\lambda B) = |\lambda|\chi(B)$, *for all scalar* $\lambda$.

*(iv)* $\chi(B) = \chi(\text{Conv}(B))$.

**Lemma 3.3.** *Let x be an infinite-dimensional normed space and* $\mathcal{B}_x$ *be the closed unit ball of* X. *Then* $\chi(\mathcal{B}_x) = 1$.

## 4. The H-MNC on Sequence Spaces

For each $n \in \mathbb{N}$, let $e^{(n)} = \{e_1^{(n)}, e_2^{(n)}, e_3^{(n)}, \cdots\}$, be the sequence such that

$$e_k^{(n)} = \begin{cases} 1, & \text{if } k = n \\ 0, & \text{if } k \neq n. \end{cases}$$

For any sequence $x = (x_k)$, its $n$-section is given by

$$x^{[n]} = \sum_{k=1}^{n} x_k e^{(k)}.$$

**Definition 4.1.** *Let X be a sequence space of real or complex valued sequences. Then,*

*(i) X is said to be an FK-space if*

- *X is a complete linear metric space,*
- *each of the maps* $p_n : X \to \mathbb{C}$ *defined by* $p_n(x) = x_n$ *is continuous for each* $n \in \mathbb{N}$.

*(ii) A FK-space together with a norm is called a BK-space.*

*(iii) An FK-space X is said to have AK if every sequence* $x = (x_n) \in X$ *has a unique representation* $x = \sum_{k=1}^{\infty} x_k e^{(k)}$ *that is,* $x = \lim_{n\to\infty} x^{[n]}$.

For the following results regarding the H-MNC on sequence spaces, please refer to [14].

**Lemma 4.1.** *Let X be a BK space with Schauder basis* $(b_n)$, $Q \in \mathcal{B}_X$, $P_n : X \to X$, $(n \in \mathbb{N})$ *be the projection onto the linear span of* $\{e_1, e_2, \cdots, e_n\}$ *and I be the identity operator on X. Then*

$$\frac{1}{a} \limsup_{n\to\infty} \left( \sup_{x\in Q} ||(I - P_n)(x)|| \right) \leq \chi(Q) \leq \inf_n \left( \sup_{x\in Q} ||(I - P_n)(x)|| \right) \leq \limsup_{n\to\infty} \left( \sup_{x\in Q} ||(I - P_n)(x)|| \right)$$

*Where*

$$a = \limsup_{n\to\infty} ||I - P_n||.$$

**Lemma 4.2.** *Let X be a BK space with AK and monotone norm. Suppose that* $Q \in \mathcal{B}_X$. *Let* $P_n : X \to X$, $(n \in \mathbb{N})$ *be the operator (projection) defined by* $P_n(x_1, x_2, \cdots) = x^{[n]} = (x_1, x_2, \cdots, x_n, 0, 0, \cdots)$ *for all* $x = (x_1, x_2, \cdots) \in X$. *Then*

$$\chi(Q) = \lim_{n\to\infty}\left(\sup_{x\in Q}||(I-P_n)(x)||\right).$$

**5. The Sequence Spaces $m(\phi)$ and $m^{\beta}(\phi)$**

Let $\ell^0$ is a set of all real sequences and let C be the space consisting finite sets of distinct positive integers. For any $\sigma \in$ C, $c(\sigma)$ denote the sequence $(c_n(\sigma))$ such that

$$c_n(\sigma) = \begin{cases} 1, \text{if } n \in \sigma \\ 0, \text{if } n \notin \sigma. \end{cases}$$

Further, suppose that

$$\mathcal{C}_\zeta = \{\sigma \in \mathcal{C} : \sum_{n=1}^{\infty} c_n(\sigma) \leq \zeta\}$$

and

$\Phi = \{\phi = (\phi_n) \in \ell^0 : 0 < \phi_1 \leq \phi_n \leq \phi_{n+1},\ (n+1)\phi_n \geq n\phi_{n+1}\}$

For $\phi \in \Phi$, Sargent [4] defined the sequence space

$$m(\phi) = \left\{x = (x_n) \in \ell^0 : \sup_{\zeta\geq 1}\sup_{\sigma\in\mathcal{C}_\zeta}\left(\frac{1}{\phi_\zeta}\sum_{n\in\sigma}|x_n|\right) < \infty\right\}$$

and proved that the sequence space $m(\phi)$ is a BK-space with respect to the norm

$$||x||_{m(\phi)} = \sup_{\zeta\geq 1}\sup_{\sigma\in\mathcal{C}_\zeta}\left(\frac{1}{\phi_\zeta}\sum_{n\in\sigma}|x_n|\right)$$

5 .

Mursaleen [11] proved the H-MNC for any bounded subset $P$ of the sequence space $m(\phi)$ as follows:

$$\chi_{m(\phi)}(P) = \lim_{k\to\infty}\sup_{x\in P}\left(\sup_{\zeta>k}\sup_{\sigma\in\mathcal{C}_\zeta}\frac{1}{\phi_\zeta}\sum_{n\in\sigma}|x_n|\right).$$

Suppose $\beta = (\beta_i)$ is an non-increasing positive term sequence. Mehravaran *et al.* [25] introduced the tempered sequence space $m^{\beta}(\phi)$ which consists of all the real sequences $x = (x_n)$ such that

$$\sup_{\zeta\geq 1}\sup_{\sigma\in\mathcal{C}_\zeta}\left(\frac{1}{\phi_\zeta}\sum_{n\in\sigma}\beta_n|x_n|\right) < \infty$$

and proved that this sequence space is a Banach space with respect to the norm

$$||x||_{m^{\beta}(\phi)} = \sup_{\zeta\geq 1}\sup_{\sigma\in\mathcal{C}_\zeta}\left(\frac{1}{\phi_\zeta}\sum_{n\in\sigma}\beta_n|x_n|\right).$$

For any $B^{\beta} \in B_{m\beta(\phi)}$, Mehravaran *et al.* [25] defined the H-MNC on $m^{\beta}(\phi)$ as follows:

$$\chi_{m^{\beta}(\phi)}(\mathbb{B}^{\beta}) = \lim_{k\to\infty}\sup_{x\in\mathbb{B}^{\beta}}\left(\sup_{\zeta>k}\sup_{\tau\in\mathcal{C}_\zeta}\frac{1}{\phi_\zeta}\sum_{n\in\tau}\beta_n|x_n|\right).$$

**6. Infinite System of Third Order Differential Equations with Three Point Boundary Conditions**

In this study, we consider the following infinite system of third order differential equations

$$\mathcal{D}^3 v_i(x) + f_i(x, v_1, v_2, \cdots) = 0, \quad \forall i \in \mathbb{N}, \quad x \in [a, b] \tag{6.1}$$

with respect to the boundary conditions given by:

$$v_i(a) = 0 = v_i'(a), \; v_i(b) = k v_i(\eta), \forall i \in \mathbb{N}, \quad \eta \in (a, b) \tag{6.2}$$

where $\mathcal{D}^3 \equiv \frac{d^3}{dx^3}, \quad k \in \mathbb{R}$ such that $k(a - \eta)^2 \neq (a - b)^2$ and $f_i \in C(I \times \mathbb{R}^\infty, \mathbb{R})$ with $f_i(x, v_1, v_2, \cdots) \neq 0$, where $I = [a, b]$

From [21], the infinite system of differential equations (6.1) with respect to the boundary conditions (6.2), the Green's function is given by,

$$\mathcal{G}(x,\xi) = \begin{cases} \dfrac{(a-x)^2(\xi-b)^2}{2(a-b)^2} - \dfrac{(\xi-x)^2}{2} + \dfrac{k(a-x)^2}{(a-b)^2 - k(a-\eta)^2}\mathcal{L}(\eta,\xi), & a \le \xi \le x \le b, \\ \dfrac{(a-x)^2(\xi-b)^2}{2(a-b)^2} + \dfrac{k(a-x)^2}{(a-b)^2 - k(a-\eta)^2}\mathcal{L}(\eta,\xi), & a \le x \le \xi \le b. \end{cases}$$

where, $L(x,\xi)$ is Green's function associated with the differential equation

$D^3 v(x) + f(x) = 0; x \in [a,b]$ $v(a) = 0 = v'(a)$; $v(b) = 0$ given by

$$\mathcal{L}(x,\xi) = \begin{cases} \dfrac{(a-x)^2(\xi-b)^2}{2(a-b)^2} - \dfrac{(\xi-x)^2}{2}, & a \le \xi \le x \le b, \\ \dfrac{(a-x)^2(\xi-b)^2}{2(a-b)^2}, & a \le x \le \xi \le b. \end{cases}$$

Also, from [21], we have the following inequality

$$\int_a^b |\mathcal{G}(x,\xi)| d\xi \le \frac{(b-a)^3}{3} + \frac{|k|}{3}\frac{(b-a)^5}{|(b-a)^2 - k(\eta-a)^2|}$$

$$3 \qquad\qquad 5 \qquad\qquad b \tag{6.3}$$

Taking $M = \dfrac{(b-a)}{3} + \dfrac{|k|}{3}\dfrac{(b-a)}{|(b-a)^2 - k(\eta-a)^2|}$, we get $\int_a |\mathcal{G}(x,\xi)| d\xi \le M$.

**7. Solvability of the System of Differential Equations (6.1) in the Sequence Space $m(\phi)$**

For the solvability of the infinte system of differential equations (6.1) with respect to the boundary conditions (6.2) in the sequence space $m(\phi)$, let us consider the following hypotheses:

(H1) The functions $f_i$ are defined on the set $[a,b] \times R^\infty$ and take the real values. The operator $f$ defined on the space $[a,b] \times m(\phi)$ as

$$(x, v) \mapsto (fv)(x) = (f_1(x, v), f_2(x, v), f_3(x, v), \cdots)$$

so that the class $((fv)(x))$ is equi-continuous at each point of the space $m(\phi)$.

(H2) For each $x \in [a,b]$ and $v_i(x) \in m(\phi)$, we have the following inequality:

$$|f_n(x, v_1, v_2, \cdots)| \le s_n(x)|v_n(x)| + t_n(x); \quad n \in \mathbb{N}$$

where $(t_i(x))$, $(s_i(x))$ are real continuous functions defined on $[a,b]$ such that:

(i) $\frac{1}{\phi_\zeta}\sum_{k\in\sigma} t_k(x)$ converges uniformly on $[a,b]$

(ii) each $s_i(x)$ is equi-bounded on $[a,b]$.

We introduce the following notations:

$$\begin{aligned} s(x) &= \sup\{s_n(x) : n \in \mathbb{N}\} \\ S &= \sup\{s(x) : x \in [a,b]\} \end{aligned}$$

**Theorem 7.1.** *Under the hyptheses (H1)-(H2), the infinite system of differential equations (6.1) along with the boundary conditions (6.2) has at least one solution* $v(x) = (v_i(x))$ *in the sequence space* $m(\phi)$ *whenever*

$$S\left(\frac{(b-a)^3}{3} + \frac{|k|}{3}\frac{(b-a)^5}{|(b-a)^2 - k(\eta-a)^2|}\right) < 1.$$

*Proof.* Using the Green's function and the above hypotheses, for an arbitrary $x \in [a,b]$, we have

$$\begin{aligned} ||v(x)||_{m(\phi)} &= \sup_{\zeta\geq 1}\sup_{\sigma\in\mathcal{C}_\zeta}\left(\frac{1}{\phi_\zeta}\sum_{i\in\sigma}\left|\int_a^b \mathcal{G}(x,\xi)f_i(\xi,v(\xi))d\xi\right|\right) \\ &\leq \sup_{\zeta\geq 1}\sup_{\sigma\in\mathcal{C}_\zeta}\left(\frac{1}{\phi_\zeta}\sum_{i\in\sigma}\int_a^b |\mathcal{G}(x,\xi)|\,|f_i(\xi,v(\xi))|\,d\xi\right) \\ &\leq \sup_{\zeta\geq 1}\sup_{\sigma\in\mathcal{C}_\zeta}\left(\frac{1}{\phi_\zeta}\sum_{i\in\sigma}\int_a^b |\mathcal{G}(x,\xi)|\,(t_i(\xi)+s_i(\xi)|v_i(\xi)|)d\xi\right) \\ &\leq \sup_{\zeta\geq 1}\sup_{\sigma\in\mathcal{C}_\zeta}\left(\frac{1}{\phi_\zeta}\sum_{i\in\sigma}\left\{\int_a^b |\mathcal{G}(x,\xi)|\,t_i(\xi)d\xi + \int_a^b |\mathcal{G}(x,\xi)|[s_i(\xi)|v_i(\xi)|]d\xi\right\}\right)! \end{aligned}$$

Considering

$$\sup_{\zeta\geq 1}\sup_{\sigma\in\mathcal{C}_\zeta}\left(\frac{1}{\phi_\zeta}\sum_{i\in\sigma} t_i(\xi)\right) = \overline{T}$$

we get

$$||v(x)||_{m(\phi)} \leq \left(\frac{(b-a)^3}{3} + \frac{|k|}{3}\frac{(b-a)^5}{|(b-a)^2 - k(\eta-a)^2|}\right)(\overline{T} + S\|v\|_{m(\phi)})$$

Hence,

$$||v(x)||_{m(\phi)} \leq \frac{(|(b-a)^2 - k(\eta-a)^2|(b-a)^3 + |k|(b-a)^5)\overline{T}}{|(b-a)^2 - k(\eta-a)^2|(3-(b-a)^3S) + |k|(b-a)^5S} = d$$

Now, we define a closed ball B as B = B($v^0$,$d_0$) with center $v^0(x) = (v_i^0(x))$, and radius $d_0 \leq d$. Additionally $v_i^0(x) = 0$, for each $x \in [a,b]$. Note that B is non-empty, convex and bounded subset of $m(\phi)$.

Consider an operator on $C[a,b]$,B) as follows:

$$(\mathcal{H}v)(x) = \{(\mathcal{H}_i v)(x)\} = \left\{\int_a^b \mathcal{G}(x,\xi)f_i(\xi,v(\xi))d\xi\right\}$$

Where $v(x) = (v_i(x)) \in \mathbb{B}$ with $v_i(x) \in C([a,b], \mathbb{R})$

Next, we will prove that H is continuous. For this, consider *w*, as an arbitrary fixed point in B and let $\epsilon > 0$ be given. By using hypothesis (H1), $\exists\ \delta > 0$ such that if $v \in$ B and $\|v - w\| \leq \delta$, then $||f(v) - f(w)|| \leq \frac{\epsilon}{M}$.

Again,

$$\begin{aligned}
||(\mathcal{H}v)(x) - (\mathcal{H}w)(x)||_{m(\phi)} &= \sup_{\zeta\geq 1}\sup_{\sigma\in\mathcal{C}_\zeta}\left(\frac{1}{\phi_\zeta}\sum_{i\in\sigma}\left|\int_a^b \mathcal{G}(x,\xi)\{f_i(\xi,v(\xi))d\xi - f_i(\xi,w(\xi))d\xi\}\right|\right.\\
&\leq \sup_{\zeta\geq 1}\sup_{\sigma\in\mathcal{C}_\zeta}\left(\frac{1}{\phi_\zeta}\sum_{i\in\sigma}\int_a^b |\mathcal{G}(x,\xi)|\,|f_i(\xi,v(\xi)) - f_i(\xi,w(\xi))|\,d\xi\right)\\
&\leq M\sup_{\zeta\geq 1}\sup_{\sigma\in\mathcal{C}_\zeta}\left(\frac{1}{\phi_\zeta}\sum_{i\in\sigma}|f_i(\xi,v(\xi))d\xi - f_i(\xi,w(\xi))d\xi|\right)\\
&\leq M\|f(v) - f(w)\|_{C([a.b],m(\phi))}\\
&\leq \epsilon
\end{aligned}$$

Taking supremum on the left side over $x \in [a,b]$, we get $\|(\mathrm{H}v) - (\mathrm{H}w)\|_{C[a.b],m(\phi)} \leq \epsilon$, which shows that *H* is continuous.

Now,

$$\begin{aligned}
\sup_{\zeta\geq 1}\sup_{\sigma\in\mathcal{C}_\zeta}\left(\frac{1}{\phi_\zeta}\sum_{i\in\sigma}|(\mathcal{H}_i v)(x)|\right) &= \sup_{\zeta\geq 1}\sup_{\sigma\in\mathcal{C}_\zeta}\left(\frac{1}{\phi_\zeta}\sum_{i\in\sigma}\left|\int_a^b \mathcal{G}(x,\xi)f_i(\xi,v(\xi))d\xi\right|\right)\\
&\leq \sup_{\zeta\geq 1}\sup_{\sigma\in\mathcal{C}_\zeta}\left(\frac{1}{\phi_\zeta}\sum_{i\in\sigma}\int_a^b |\mathcal{G}(x,\xi)|\,|f_i(\xi,v(\xi))|\,d\xi\right)\\
&\leq \sup_{\zeta\geq 1}\sup_{\sigma\in\mathcal{C}_\zeta}\left(\frac{1}{\phi_\zeta}\sum_{i\in\sigma}\int_a^b |\mathcal{G}(x,\xi)|\,(t_i(\xi) + s_i(\xi)|v_i(\xi)|)d\xi\right)\\
&\leq \sup_{\zeta\geq 1}\sup_{\sigma\in\mathcal{C}_\zeta}\left(\frac{1}{\phi_\zeta}\sum_{i\in\sigma}\left\{\int_a^b |\mathcal{G}(x,\xi)|\,t_i(\xi)d\xi\right.\right.\\
&\quad \left.\left.+\int_a^b |\mathcal{G}(x,\xi)|s_i(\xi)|v_i(\xi)|d\xi\right\}\right)\\
&\leq \left(\frac{(b-a)^3}{3} + \frac{|k|}{3}\frac{(b-a)^5}{|(b-a)^2 - k(\eta-a)^2|}\right)(\overline{T} + S\|v\|_{m(\phi)})
\end{aligned}$$

i.e., for each $x \in [a,b]$; $(\mathrm{H}v)(x) = (\mathrm{H}_i v)(x)\} \in m(\phi)$. Again for boundary conditions,

$$\mathcal{G}(a,\xi) = \frac{(a-a)^2(\xi-b)^2}{2(a-b)^2} + \frac{k(a-a)^2}{(a-b)^2 - k(a-\eta)^2}\mathcal{L}(\eta,\xi) = 0$$

and so,

$$(\mathcal{H}_i v)(a) = \int_a^b \mathcal{G}(a,\xi)f_i(\xi,v(\xi))d\xi = 0$$

Also,

$$(\mathcal{H}_i'v)(x) = \int_a^b \left\{ \frac{-2(a-x)(\xi-b)^2}{2(a-b)^2} - \frac{-2k(a-x)}{(a-b)^2 - k(a-\eta)} \mathcal{L}(\eta,\xi) \right\} . f_i(\xi, v(\xi)) d\xi$$

and so,

$$(\mathcal{H}_i'v)(a) = 0$$

Again,

$$\begin{aligned}
&(\mathcal{H}_i v)(b) \\
&= \int_a^b \left\{ \frac{(a-b)^2(\xi-b)^2}{2(a-b)^2} - \frac{(\xi-b)^2}{2} + \frac{k(a-b)^2 \mathcal{L}(\eta,\xi)}{(a-b)^2 - k(a-\eta)^2} \right\} . f_i(\xi, v(\xi)) d\xi \\
&= \int_a^b \frac{k(a-b)^2}{(a-b)^2 - k(a-\eta)^2} \mathcal{L}(\eta,\xi) . f_i(\xi, v(\xi)) d\xi
\end{aligned}$$

But,

$$\begin{aligned}
(\mathcal{H}_i v)(\eta) &= \int_a^b \mathcal{G}(\eta,\xi) . f_i(\xi, v(\xi)) d\xi \\
&= \int_a^b \left\{ \mathcal{L}(\eta,\xi) + \frac{k(a-\eta)^2}{(a-b)^2 - k(a-\eta)^2} \mathcal{L}(\eta,\xi) \right\} . f_i(\xi, v(\xi)) d\xi \\
&= \int_a^b \frac{(a-b)^2 - k(a-\eta)^2 + k(a-\eta)^2}{(a-b)^2 - k(a-\eta)^2} \mathcal{L}(\eta,\xi) . f_i(\xi, v(\xi)) d\xi \\
&= \int_a^b \frac{(a-b)^2}{(a-b)^2 - k(a-\eta)^2} \mathcal{L}(\eta,\xi) . f_i(\xi, v(\xi)) d\xi
\end{aligned}$$

Hence,

$$\begin{aligned}
(\mathcal{H}_i v)(b) &= k \int_a^b \frac{(a-b)^2}{(a-b)^2 - k(a-\eta)^2} \mathcal{L}(\eta,\xi) . f_i(\xi, v(\xi)) d\xi \\
&= k((\mathcal{H}_i v)(\eta))
\end{aligned}$$

Therefore, each $(\mathrm{H}_i v)(x)$ satisfies boundary conditions given in (6.2).

Also, $\|(\mathrm{H}v)(x) - v^0(x)\|_{m(\phi)} = \|(\mathrm{H}v)(x)\|_{m(\phi)} \leq d$, thus H self-maps on the closed ball $\mathbb{B}$.

Now we will find $\delta > 0$, for each $\epsilon > 0$ such that $\chi(\mathbb{B}) \in [\epsilon, \epsilon + \delta)$ which implies $\chi(\mathrm{H}(\mathbb{B})) < \epsilon$.

The H-MNC of the range space H(B) is given as

$$\begin{aligned}
\chi(\mathcal{H}(\mathbb{B})) &= \lim_{k\to\infty} \sup_{v\in\mathbb{B}} \left[ \sup_{\zeta>k} \sup_{\sigma\in\mathcal{C}_\zeta} \left( \frac{1}{\phi_\zeta} \sum_{i\in\sigma} |\mathcal{H}v_i(x)| \right) \right] \\
&= \lim_{k\to\infty} \sup_{v\in\mathbb{B}} \left[ \sup_{\zeta>k} \sup_{\sigma\in\mathcal{C}_\zeta} \left( \frac{1}{\phi_\zeta} \sum_{i\in\sigma} \left| \int_a^b \mathcal{G}(x,\xi) \{ f_i(\xi, v(\xi)) \} d\xi \right| \right) \right] \\
&\leq \lim_{k\to\infty} \sup_{v\in\mathbb{B}} \left[ \sup_{\zeta>k} \sup_{\sigma\in\mathcal{C}_\zeta} \left( \frac{1}{\phi_\zeta} \sum_{i\in\sigma} \int_a^b |\mathcal{G}(x,\xi)| \{ t_i(\xi) + \sup_{s\in I, i\in\sigma} s_i(\xi) |v_i(\xi)| \} \right) \right] \\
&\leq MS \lim_{k\to\infty} \sup_{v\in\mathbb{B}} \left[ \sup_{\zeta>k} \sup_{\sigma\in\mathcal{C}_\zeta} \frac{1}{\phi_\zeta} \sum_{i\in\sigma} |v_i| \right] \\
&\leq MS\chi(\mathbb{B}) < \epsilon \quad (\because \chi(\mathbb{B}) < \frac{\epsilon}{MS})
\end{aligned}$$

Considering $\delta = \left(\frac{1-MS}{MS}\right)\epsilon$, we get $\chi(\mathbb{B}) \in [\epsilon, \epsilon + \delta)$.

Combining all these above, we find out H is a Meir-Keeler condensing operator on the set B which satisfies all the conditions of Theorem (2.3). Therefore H has a fixed point in B which acts as a solution for the system of differential equations (6.1) along with the boundary conditions (6.2).

**Example 7.1.** *To illustrate our result, let we consider an infinite system of third order differential equations:*

$$-\mathcal{D}^3 v_n(x) = \frac{x(b-x)}{(n+1)^4} + \sum_{m=n}^{\infty} \frac{x\cos(x)v_n(x)}{(1+m^3)n^2} \; ; \quad n \in \mathbb{N}, \quad x \in [-1, 1] \tag{7.1}$$

*with the boundary conditions:*

$$v_n(-1) = 0 = v_n'(1), \; v_n(1) = \frac{1}{\pi^2} v_n(0) \tag{7.2}$$

*where* $\mathcal{D}^3 \equiv \frac{d^3}{dx^3}$.

Here,

$$\begin{aligned} a &= -1 \\ \eta &= 0 \\ b &= 1 \\ f_n(x, v(x)) &= \frac{x(b-x)}{(n+1)^4} + \sum_{m=n}^{\infty} \frac{x\cos(x)v_n(x)}{(1+m^3)n^2} \\ t_n(x) &= \frac{x(b-x)}{(n+1)^4} \\ s_n(x) &= \frac{1}{n^2} \sum_{m=n}^{\infty} \frac{x}{(1+m^3)} \qquad \forall \; n \in \mathbb{N}, \; x \in [-1, 1] \end{aligned}$$

Clearly $t_n(x), s_n(x), f_n(x, v(x))$ are continuous and equi-bounded on $[-1, 1]$.

Again, $\frac{1}{\phi_\zeta} \sum_{k \in \sigma} \frac{x(b-x)}{(k+1)^4}$ converges uniformly to $\frac{b^2}{64}$ for any sequence $\phi \in \Phi$ and $(s_n(x))$ is equi-bounded by $\frac{\pi^2}{6} = S$.

Moreover, we have

$$\begin{aligned} |f_n(x, v(x))| &= \left| \frac{x(b-x)}{(n+1)^4} + \sum_{m=n}^{\infty} \frac{x\cos(x)v_n(x)}{(1+m^3)n^2} \right| \\ &\leq \frac{x(b-x)}{(n+1)^4} + \frac{1}{n^2} \sum_{m=n}^{\infty} \frac{x}{(1+m^3)} |v_n(x)| \\ &\leq t_n(x) + s_n(x)|v_n(x)| \end{aligned}$$

Now, we will prove that $f(x,v(x)) \in m(\phi)$. For this, let us choose arbitrary $x \in [-1,1]$ and $v \in m(\phi)$. Then for any sequence $\phi \in \Phi$, we get

$$\begin{aligned}
\sup_{\zeta\geq 1}\sup_{\sigma\in\mathcal{C}_\zeta}\left(\frac{1}{\phi_\zeta}\sum_{k\in\sigma}|f_k(x,v(x))|\right) &= \sup_{\zeta\geq 1}\sup_{\sigma\in\mathcal{C}_\zeta}\left(\frac{1}{\phi_\zeta}\sum_{k\in\sigma}\left|\frac{x(b-x)}{(n+1)^4}+\sum_{k\geq m}^{\infty}\frac{xcos(x)v_n(x)}{(1+m^3)k^2}\right|\right)\\
&\leq \sup_{\zeta\geq 1}\sup_{\sigma\in\mathcal{C}_\zeta}\left(\frac{1}{\phi_\zeta}\sum_{k\in\sigma}\frac{x(b-x)}{(n+1)^4}+\sum_{m=n}^{\infty}\frac{x|v_n(x)|}{(1+m^3)n^2}\right)\\
&\leq \frac{b^2}{64}+S\sup_{\zeta\geq 1}\sup_{\sigma\in\mathcal{C}_\zeta}\left(\frac{1}{\phi_\zeta}\sum_{k\in\sigma}|v_k(x)|\right)\\
&\leq \frac{b^2}{64}+S\|v(x)\|_{m(\phi)}
\end{aligned}$$

Next, we will show that the family of function $(f(v)(x))$ is equi-continuous at each point of $m(\phi)$. For this, suppose $x \in [-1,1]$ , $z \in m(\phi)$ be arbitrary. Taking any $\epsilon > 0$, we get

$$\begin{aligned}
||(fv)(x)-(fz)(x)||_{m(\phi)} &= \sup_{\zeta\geq 1}\sup_{\sigma\in\mathcal{C}_\zeta}\left(\frac{1}{\phi_\zeta}\sum_{k\in\sigma}\left|\frac{x(b-x)}{(n+1)^4}+\sum_{k\geq m}^{\infty}\frac{x\cos(x)v_n(x)}{(1+m^3)k^2}\right.\right.\\
&\quad\left.\left.-\frac{x(b-x)}{(n+1)^4}-\sum_{k\geq m}^{\infty}\frac{x\cos(x)z_n(x)}{(1+m^3)k^2}\right|\right)\\
&= \sup_{\zeta\geq 1}\sup_{\sigma\in\mathcal{C}_\zeta}\left(\frac{1}{\phi_\zeta}\sum_{k\in\sigma}\sum_{k\geq m}^{\infty}\frac{x\cos(x)}{(1+m^3)k^2}|v_k(x)-z_k(x)|\right)\\
&\leq \sup_{\zeta\geq 1}\sup_{\sigma\in\mathcal{C}_\zeta}\left(\frac{1}{\phi_\zeta}\sum_{k\in\sigma}\sum_{m=n}^{\infty}\frac{x}{(1+m^3)n^2}|v_k(x)-z_k(x)|\right)\\
&\leq \frac{\pi^2}{6}\sup_{\zeta\geq 1}\sup_{\sigma\in\mathcal{C}_\zeta}\left(\frac{1}{\phi_\zeta}\sum_{k\in\sigma}|v_k(x)-z_k(x)|\right)\\
&= \frac{\pi^2}{6}\|v(x)-z(x)\|_{m(\phi)}<\epsilon
\end{aligned}$$

where $\|v(x)-z(x)\|_{m(\phi)} < \delta = \frac{6}{\pi^2}\epsilon$.

Further, for $a=-1$ , $b=1$, $k=\frac{1}{\pi^2}$ and $\eta = 0$ the condition

$$S\left(\frac{(b-a)^3}{3}+\frac{|k|}{3}\frac{(b-a)^5}{|(b-a)^2-k(\eta-a)^2|}\right)<1$$

is satisfied in the interval $[a,b]$.

This also gives $S \approx 1.6433$ and $T \approx 0.015625$.

Therefore, in view of the Theorem (7.1), the operator H has a fixed point $v(x) = v_i(x) \in m(\phi)$ which acts as a solution for the infinite system of differential equations (6.1) along with the boundary conditions (6.2).

**8. Solvability of The System of Differential Equations (6.1) in The Sequence Space $m^{\beta}(\phi)$**

For the solvability of the infinte system of differential equations (6.1) with respect to the boundary conditions (6.2) in the sequence space $m^{\beta}(\phi)$, let us consider the following hypotheses:

(C1) The functions $f_i$ are defined on the set $[a,b] \times \mathrm{R}^{\infty}$ and take the real values. The operator $f$ defined on the space $[a,b] \times m^{\beta}(\phi)$ as

$$(x, v) \mapsto (fv)(x) = (f_1(x, v), f_2(x, v), f_3(x, v), \cdots)$$

so that the class $((fv)(x))$ is equi-continuous at each point of the space $m^{\beta}(\phi)$.

(C2) For each $x \in [a,b]$ and $v_i(x) \in m^{\beta}(\phi)$, we have the following inequality:

$$|f_n(x, v_1, v_2, \cdots)| \leq q_n(x)|v_n(x)| + p_n(x); \quad n \in \mathbb{N}$$

where $(p_i(x))$, $(q_i(x))$ are real continuous functions defined on $[a,b]$ such that:

(i) $\frac{1}{\phi_\zeta} \sum_{k\in\sigma} \beta_k p_k(x)$ converges uniformly on $[a,b]$

(ii) each $q_i(x)$ is equi-bounded on $[a,b]$.

We introduce the following notations:

$$\begin{aligned} q(x) &= \sup\{q_n(x) : n \in \mathbb{N}\} \\ Q &= \sup\{q(x) : x \in [a, b]\} \end{aligned}$$

**Theorem 8.1.** *Under the hyptheses (C1)-(C2), the infinite system of differential equations (6.1) along with the boundary conditions (6.2) has at least one solution* $v(x) = (v_i(x))$ *in the sequence space* $m^{\beta}(\phi)$ *whenever*

$$Q\left(\frac{(b-a)^3}{3} + \frac{|k|}{3}\frac{(b-a)^5}{|(b-a)^2 - k(\eta-a)^2|}\right) < 1.$$

*Proof.* Using the Green's function and the above hypotheses, for an arbitrary $x \in [a,b]$, we have

$$\begin{aligned} \|v(x)\|_{m^{\beta}(\phi)} &= \sup_{\zeta\geq 1}\sup_{\sigma\in\mathcal{C}_\zeta}\left(\frac{1}{\phi_\zeta}\sum_{i\in\sigma}\beta_i\left|\int_a^b \mathcal{G}(x,\xi)f_i(\xi, v(\xi))d\xi\right|\right) \\ &\leq \sup_{\zeta\geq 1}\sup_{\sigma\in\mathcal{C}_\zeta}\left(\frac{1}{\phi_\zeta}\sum_{i\in\sigma}\beta_i\int_a^b |\mathcal{G}(x,\xi)f_i(\xi, v(\xi))|\, d\xi\right) \\ &\leq \sup_{\zeta\geq 1}\sup_{\sigma\in\mathcal{C}_\zeta}\left(\frac{1}{\phi_\zeta}\sum_{i\in\sigma}\beta_i\int_a^b |\mathcal{G}(x,\xi)|\,(p_i(\xi) + q_i(\xi)|v_i(s)|)ds\right) \\ &\leq \sup_{\zeta\geq 1}\sup_{\sigma\in\mathcal{C}_\zeta}\left(\frac{1}{\phi_\zeta}\sum_{i\in\sigma}\beta_i\left\{\int_a^b |\mathcal{G}(x,\xi)|\,p_i(\xi)d\xi + \int_a^b |\mathcal{G}(x,\xi)|[q_i(\xi)|v_i(\xi)|]d\xi\right\}\right. \end{aligned}$$

Considering

$$\sup_{\zeta\geq 1}\sup_{\sigma\in\mathcal{C}_\zeta}\left(\frac{1}{\phi_\zeta}\sum_{i\in\sigma}\beta_i p_i(\xi)\right) = \overline{P}$$

we get

$$\|v(x)\|_{m^{\beta}(\phi)} \leq \left(\frac{(b-a)^3}{3} + \frac{|k|}{3}\frac{(b-a)^5}{|(b-a)^2 - k(\eta-a)^2|}\right)(\overline{P} + Q\|v\|_{m^{\beta}(\phi)})$$

Hence,

$$||v||_{m^{\beta}(\phi)} \leq \frac{(|(b-a)^2 - k(\eta-a)^2|(b-a)^3 + |k|(b-a)^5)\overline{P}}{|(b-a)^2 - k(\eta-a)^2|(3-(b-a)^3 S) + |k|(b-a)^5 Q} = d$$

Now, we define a closed ball $\mathbb{B}^{\beta}$, as $\mathbb{B}^{\beta} = \mathbb{B}^{\beta}(v^0, d_0)$ with center $v^0(x) = (v_i^0(x))$ and radius $d_0 \leq d$ such that $v_i^0(x) = 0$, for each $x \in [a,b]$. Note that $\mathbb{B}^{\beta}$ is non-empty, bounded and convex subset of $m^{\beta}(\phi)$.

Next we define an operator on $C[a,b]$, $\mathbb{B}^{\beta}$) as follows:

$$(\mathcal{H}v)(x) = \{(\mathcal{H}_i v)(x)\} = \left\{ \int_a^b \mathcal{G}(x,\xi) f_i(\xi, v(\xi)) d\xi \right\}$$

In order to show that H is continuous, we consider $w$, as an arbitrary fixed point in $\mathbb{B}^{\beta}$ and let $\epsilon > 0$ be given. By using hypothesis (C1), $\exists \delta > 0$ such that if $v \in \mathbb{B}^{\beta}$ and $||v - w|| \leq \delta$, then $||f(v) - f(w)|| \leq \frac{\epsilon}{M}$.

Again,

$$\begin{aligned}
||(\mathcal{H}v)(x) - (\mathcal{H}w)(x)||_{m^{\beta}(\phi)} &= \sup_{\zeta \geq 1} \sup_{\sigma \in \mathcal{C}_\zeta} \left( \frac{1}{\phi_\zeta} \sum_{i \in \sigma} \beta_i \left| \int_a^b \mathcal{G}(x,\xi) \{ f_i(\xi, v(\xi)) d\xi - f_i(\xi, w(\xi)) d\xi \} \right| \right. \\
&\leq \sup_{\zeta \geq 1} \sup_{\sigma \in \mathcal{C}_\zeta} \left( \frac{1}{\phi_\zeta} \sum_{i \in \sigma} \beta_i \int_a^b |\mathcal{G}(x,\xi)| \, |f_i(\xi, v(\xi)) - f_i(\xi, w(\xi))| \, d\xi \right) \\
&\leq M \sup_{\zeta \geq 1} \sup_{\sigma \in \mathcal{C}_\zeta} \left( \frac{1}{\phi_\zeta} \sum_{i \in \sigma} \beta_i \, |f_i(\xi, v(\xi)) d\xi - f_i(\xi, w(\xi)) d\xi| \right) \\
&\leq M \|f(v) - f(w)\|_{C([a.b], m^{\beta}(\phi))} \\
&\leq \epsilon
\end{aligned}$$

Taking supremum on the left side over $x \in [a,b]$, we get $||(\mathrm{H}v) - (\mathrm{H}w)||_{C[a.b], m\beta(\phi)} \leq \epsilon$, which shows that $\mathcal{H}$ is continuous.

Now,

$$\begin{aligned}
\sup_{\zeta \geq 1} \sup_{\sigma \in \mathcal{C}_\zeta} \left( \frac{1}{\phi_\zeta} \sum_{i \in \sigma} \beta_i \, |(\mathcal{H}_i v)(x)| \right) &= \sup_{\zeta \geq 1} \sup_{\sigma \in \mathcal{C}_\zeta} \left( \frac{1}{\phi_\zeta} \sum_{i \in \sigma} \beta_i \left| \int_a^b \mathcal{G}(x,\xi) f_i(\xi, v(\xi)) d\xi \right| \right) \\
&\leq \sup_{\zeta \geq 1} \sup_{\sigma \in \mathcal{C}_\zeta} \left( \frac{1}{\phi_\zeta} \sum_{i \in \sigma} \beta_i \int_a^b |\mathcal{G}(x,\xi)| \, |f_i(\xi, v(\xi))| \, d\xi \right) \\
&\leq \sup_{\zeta \geq 1} \sup_{\sigma \in \mathcal{C}_\zeta} \left( \frac{1}{\phi_\zeta} \sum_{i \in \sigma} \beta_i \int_a^b |\mathcal{G}(x,\xi)| \, (p_i(\xi) + q_i(\xi)|v_i(\xi)|) d\xi \right) \\
&\leq \sup_{\zeta \geq 1} \sup_{\sigma \in \mathcal{C}_\zeta} \left( \frac{1}{\phi_\zeta} \sum_{i \in \sigma} \beta_i \left\{ \int_a^b |\mathcal{G}(x,\xi)| \, p_i(\xi) d\xi \right. \right. \\
&\quad \left. \left. + \int_a^b |\mathcal{G}(x,\xi)| q_i(\xi) |v_i(\xi)| d\xi \right\} \right) \\
&\leq \left( \frac{(b-a)^3}{3} + \frac{|k|}{3} \frac{(b-a)^5}{|(b-a)^2 - k(\eta-a)^2|} \right) (\overline{P} + Q \|v\|_{m^{\beta}(\phi)})
\end{aligned}$$

i.e., for each $x \in [a,b]$; $(\mathcal{H}v)(x) = \{(\mathcal{H}_i v)(x)\} \in m^{\beta}(\phi)$. Again for boundary conditions,

$$\mathcal{G}(a,\xi) = \frac{(a-a)^2(\xi-b)^2}{2(a-b)^2} + \frac{k(a-a)^2}{(a-b)^2 - k(a-\eta)^2}\mathcal{L}(\eta,\xi) = 0$$

and so,

$$(\mathcal{H}_i v)(a) = \int_a^b \mathcal{G}(a,\xi) f_i(\xi, v(\xi))d\xi = 0$$

Also,

$$(\mathcal{H}_i' v)(x) = \int_a^b \left\{ \frac{-2(a-x)(\xi-b)^2}{2(a-b)^2} - \frac{-2k(a-x)}{(a-b)^2 - k(a-\eta)}\mathcal{L}(\eta,\xi) \right\} . f_i(\xi, v(\xi))d\xi$$

and so,

$(\mathcal{H}_i' v)(a) = 0$

Again,

$$\begin{aligned}
&(\mathcal{H}_i v)(b) \\
&= \int_a^b \left\{ \frac{(a-b)^2(\xi-b)^2}{2(a-b)^2} - \frac{(\xi-b)^2}{2} + \frac{k(a-b)^2\mathcal{L}(\eta,\xi)}{(a-b)^2 - k(a-\eta)^2} \right\} . f_i(\xi, v(\xi))d\xi \\
&= \int_a^b \frac{k(a-b)^2}{(a-b)^2 - k(a-\eta)^2}\mathcal{L}(\eta,\xi) . f_i(\xi, v(\xi))d\xi
\end{aligned}$$

But,

$$\begin{aligned}
(\mathcal{H}_i v)(\eta) &= \int_a^b \mathcal{G}(\eta,\xi) . f_i(\xi, v(\xi))d\xi \\
&= \int_a^b \left\{ \mathcal{L}(\eta,\xi) + \frac{k(a-\eta)^2}{(a-b)^2 - k(a-\eta)^2}\mathcal{L}(\eta,\xi) \right\} . f_i(\xi, v(\xi))d\xi \\
&= \int_a^b \frac{(a-b)^2 - k(a-\eta)^2 + k(a-\eta)^2}{(a-b)^2 - k(a-\eta)^2}\mathcal{L}(\eta,\xi) . f_i(\xi, v(\xi))d\xi \\
&= \int_a^b \frac{(a-b)^2}{(a-b)^2 - k(a-\eta)^2}\mathcal{L}(\eta,\xi) . f_i(\xi, v(\xi))d\xi
\end{aligned}$$

Hence,

$$\begin{aligned}
(\mathcal{H}_i v)(b) &= k\int_a^b \frac{(a-b)^2}{(a-b)^2 - k(a-\eta)^2}\mathcal{L}(\eta,\xi) . f_i(\xi, v(\xi))d\xi \\
&= k((\mathcal{H}_i v)(\eta))
\end{aligned}$$

Therefore, each $(\mathcal{H}_i v)(x)$ satisfies boundary conditions given in (6.2).

Also, $\|(\mathcal{H}v)(x) - v^0(x)\|_{m\beta(\phi)} = \|(\mathcal{H}v)(x)\|_{m\beta(\phi)} \leq d$, thus H self-maps on the closed ball $\mathbb{B}^{\beta}$. The operator $\mathcal{H}$ is continuous on $C[a,b]$, $\mathbb{B}^{\beta}$), by our assumption (C1).

We now find a $\delta > 0$ for each $\epsilon > 0$ such that whenever $\chi(\mathbb{B}^{\beta}) \in [\epsilon, \epsilon + \delta)$, then $\chi(\mathcal{H}(\mathbb{B}^{\beta})) < \epsilon$.

The H-MNC of the range space $H(B^{\beta})$ is as follows:

$$\begin{aligned}
\chi(\mathcal{H}(\mathbb{B}^{\beta})) &= \lim_{k\to\infty}\sup_{v\in\mathbb{B}^{\beta}}\left[\sup_{\zeta>k}\sup_{\sigma\in\mathcal{C}_{\zeta}}\left(\frac{1}{\phi_{\zeta}}\sum_{i\in\sigma}\beta_i|(\mathcal{H}_i v)(x)|\right)\right]\\
&\leq \lim_{k\to\infty}\sup_{v\in\mathbb{B}^{\beta}}\left[\sup_{\zeta>k}\sup_{\sigma\in\mathcal{C}_{\zeta}}\left(\frac{1}{\phi_{\zeta}}\sum_{i\in\sigma}\beta_i\left|\int_a^b \mathcal{G}(x,\xi)f_i(\xi,v(\xi))d\xi\right|\right)\right]\\
&\leq \lim_{k\to\infty}\sup_{v\in\mathbb{B}^{\beta}}\left[\sup_{\zeta>k}\sup_{\sigma\in\mathcal{C}_{\zeta}}\left(\frac{1}{\phi_{\zeta}}\sum_{i\in\sigma}\beta_i\int_a^b|\mathcal{G}(x,\xi)f_i(\xi,v(\xi))|d\xi\right)\right]\\
&\leq \lim_{k\to\infty}\sup_{v\in\mathbb{B}^{\beta}}\left[\sup_{\zeta>k}\sup_{\sigma\in\mathcal{C}_{\zeta}}\left(\frac{1}{\phi_{\zeta}}\sum_{i\in\sigma}\beta_i\int_a^b|\mathcal{G}(x,\xi)|\sup_{\xi\in[a,b],i\in\sigma}q_i(\xi)|v_i(\xi)|d\xi\right)\right]\\
&\leq QM\chi(\mathbb{B}^{\beta})<\epsilon \qquad (\because \chi(\mathbb{B}^{\beta})<\frac{\epsilon}{QM})
\end{aligned}$$

Taking, $\delta=\left[\frac{1}{QM}-1\right]\epsilon$, we get $\chi_m\beta_{(\phi)}(\mathbb{B}^{\beta})\in[\epsilon,\epsilon+\delta)$.

Combining all these above, we find out $\mathcal{H}$ is a Meir-Keeler condensing operator on the set $\mathbb{B}^{\beta}$ which satisfies all the conditions of Theorem (2.3). Therefore $\mathcal{H}$ has a fixed point in $\mathbb{B}^{\beta}$ which acts as a solution for the system of differential equations (6.1) along with the boundary conditions (6.2).

**Example 8.1.** *As an example, we consider the following infinite system of third order differential equation:*

$$-\mathcal{D}^3 v_n(x)=\frac{\sqrt{x}}{2^n n^3}+\sum_{m=n}^{\infty}\frac{\cos(x)v_n(x)}{(1+m^2)n^2} \quad ; \quad n\in\mathbb{N},\quad x\in\left[\frac{1}{2},\frac{3}{2}\right] \tag{8.1}$$

*along with the boundary conditions:*

$$v_n\left(\frac{1}{2}\right)=0=v_n'\left(\frac{3}{2}\right),\ v_n\left(\frac{3}{2}\right)=\frac{1}{\pi^2}v_n(1) \tag{8.2}$$

*where* $\mathcal{D}^3\equiv\frac{d^3}{dx^3}$.

Here, for all $n\in\mathbb{N}$, we consider

$$\begin{aligned} a &= \frac{1}{2} \\ \eta &= 1 \\ b &= \frac{3}{2} \\ k &= \frac{1}{\pi^2} \\ f_n(x, v(x)) &= \frac{\sqrt{x}}{2^n n^3} + \sum_{m=n}^{\infty} \frac{\cos(x) v_m(x)}{(1+m^2)n^2},\ x \in \left[\frac{1}{2}, \frac{3}{2}\right] \\ p_n(x) &= \frac{\sqrt{x}}{2^n n^3},\ x \in \left[\frac{1}{2}, \frac{3}{2}\right] \\ q_n(x) &= \frac{1}{n^2} \sum_{m=n}^{\infty} \frac{1}{1+m^2},\ x \in \left[\frac{1}{2}, \frac{3}{2}\right] \\ \beta_n &= 1 \end{aligned}$$

Clearly, for each $n \in \mathrm{N}$, the sequences of functions $f_n(x,v(x)), p_n(x), q_n(x)$ are continuous and equi-bounded in $\left[\frac{1}{2}, \frac{3}{2}\right]$.

Also the series $\frac{1}{\phi_\zeta} \sum_{k \in \sigma} \beta_k p_k(x) = \frac{1}{\phi_\zeta} \sum_{k \in \sigma} \frac{\sqrt{x}}{2^k k^3}$ converges uniformly to $\frac{\sqrt{3}}{2\sqrt{2}}$ in $\left[\frac{1}{2}, \frac{3}{2}\right]$ for any sequence $\phi \in \Phi$.

Moreover, $q_n(x)$ is equi-bounded by $\frac{\pi^2}{6} = Q$.

Also,

$$\begin{aligned} |f_n(x, v(x))| &= \left| \frac{\sqrt{x}}{2^n n^3} + \sum_{m=n}^{\infty} \frac{\cos(x) v_n(x)}{(1+m^2)n^2} \right| \\ &\leq \frac{\sqrt{x}}{2^n n^3} + \frac{1}{n^2} \sum_{m=n}^{\infty} \frac{1}{1+m^2} |v_n(x)| \\ &= p_n(x) + q_n(x)|v_n(x)| \end{aligned}$$

We now show that $f(x,v(x)) \in m^\beta(\phi)$ for which let us assume that $x \in \left[\frac{1}{2}, \frac{3}{2}\right]$ and $v \in m^\beta(\phi)$ be arbitrary. Then for any sequence $\phi \in \Phi$ we get

$$\begin{aligned} \sup_{\zeta \geq 1} \sup_{\sigma \in \mathcal{C}} \left( \frac{1}{\phi_\zeta} \sum_{k \in \sigma} \beta_k |f_k(x, v(x))| \right) &= \sup_{\zeta \geq 1} \sup_{\sigma \in \mathcal{C}_\zeta} \left( \frac{1}{\phi_\zeta} \sum_{k \in \sigma} \beta_k \left| \frac{\sqrt{x}}{2^n n^3} + \sum_{k \geq m}^{\infty} \frac{\cos(x) v_n(x)}{(1+m^2)k^2} \right| \right) \\ &\leq \sup_{\zeta \geq 1} \sup_{\sigma \in \mathcal{C}_\zeta} \left( \frac{1}{\phi_\zeta} \sum_{k \in \sigma} \beta_k \left( \frac{\sqrt{x}}{2^n n^3} + \sum_{m=n}^{\infty} \frac{|v_n(x)|}{(1+m^2)n^2} \right) \right) \\ &\leq \frac{\sqrt{3}}{2\sqrt{2}} + Q||v(x)||_{m^\beta(\phi)} \end{aligned}$$

Next we show that the family of functions $((fv)(x))$ is equi-continuous at each point of

$m^{\beta}(\phi)$. Let $x \in \left[\frac{1}{2}, \frac{3}{2}\right]$ and $z \in m^{\beta}(\phi)$ be arbitrary. For any $\epsilon > 0$ we get

$$\begin{aligned}
||(fv)(x) - (fz)(x)||_{m^{\beta}(\phi)} &= \sup_{\zeta \geq 1} \sup_{\sigma \in \mathcal{C}_{\zeta}} \left( \frac{1}{\phi_{\zeta}} \sum_{k \in \sigma} \beta_k \left| \frac{\sqrt{x}}{2^n n^3} + \sum_{k \geq m}^{\infty} \frac{\cos(x) v_n(x)}{(1+m^2)k^2} - \frac{\sqrt{x}}{2^n n^3} \right.\right. \\
&\quad \left.\left. - \sum_{k \geq m}^{\infty} \frac{\cos(x) z_n(x)}{(1+m^2)k^2} \right| \right) \\
&\leq \sup_{\zeta \geq 1} \sup_{\sigma \in \mathcal{C}_{\zeta}} \left( \frac{1}{\phi_{\zeta}} \sum_{k \in \sigma} \beta_k \left| \sum_{k \geq m}^{\infty} \frac{\cos(x) v_n(x)}{(1+m^2)k^2} - \sum_{k \geq m}^{\infty} \frac{\cos(x) z_n(x)}{(1+m^2)k^2} \right| \right) \\
&\leq \sup_{\zeta \geq 1} \sup_{\sigma \in \mathcal{C}_{\zeta}} \left( \frac{1}{\phi_{\zeta}} \sum_{k \in \sigma} \beta_k \sum_{k \geq m}^{\infty} \frac{\cos(x)}{(1+m^2)k^2} |v_k(x) - z_k(x)| \right) \\
&\leq \frac{\pi^2}{6} \sup_{\zeta \geq 1} \sup_{\sigma \in \mathcal{C}_{\zeta}} \left( \frac{1}{\phi_{\zeta}} \sum_{k \in \sigma} \beta_k |v_k(x) - z_k(x)| \right) \\
&\leq \frac{\pi^2}{6} \|v(x) - z(x)\|_{m^{\beta}(\phi)} < \epsilon
\end{aligned}$$

where $\|v(x) - v'(x)\|_{m^{\beta}(\phi)} < \delta = \frac{6}{\pi^2}\epsilon$.

Further, for $a = \frac{1}{2}$ , $b = \frac{3}{2}$, $k = \frac{1}{\pi^2}$ and $\eta = 1$ the condition

$$Q\left( \frac{(b-a)^3}{3} + \frac{|k|}{3} \frac{(b-a)^5}{|(b-a)^2 - k(\eta - a)^2|} \right) < 1$$

is satisfied in the interval $[a,b]$.

This also gives $Q \approx 1.6433$ and $T \approx 0.61238921$.

Therefore, in view of the Theorem (7.1), the operator H has a fixed point $v(x) = v_i(x) \in m^{\beta}(\phi)$ which acts as a solution for the infinite system of differential equations (6.1) along with the boundary conditions (6.2).

**References**

1. Kuratowski, K. (1930). Sur les espaces complets. *Fundamenta Mathematicae, 15*, 301–309.
2. Darbo, G. (1955). Punti uniti in transformazioni a condominio non compatto. *Rendiconti del Seminario Matematico della Università di Padova, 24*, 84–92.
3. Persidskii, K. P. (1959). Countable systems of differential equations and stability of their solutions. *Izvestiya Akademii Nauk Kazakhskoy SSR, 7*, 52–71.
4. Sargent, W. L. C. (1960). Some sequence spaces related to the HP spaces. *Journal of the London Mathematical Society, 35*, 161–171.
5. Persidskii, K. P. (1961). Countable systems of differential equations and stability of their solutions III. *Izvestiya Akademii Nauk Kazakhskoy SSR, 9*, 11–34.

6. Goldenštein, L. S., & Markus, A. S. (1965). On a measure of noncompactness of bounded sets and linear operators. *Studies in Algebra and Mathematical Analysis, 29*, 45–54.
7. Keeler, E., & Meir, A. (1969). A theorem on contraction mappings. *Journal of Mathematical Analysis and Applications, 28*, 326–329.
8. Banaś, J., & Goebel, K. (1980). *Measures of noncompactness in Banach spaces*. Marcel Dekker.
9. Akhmerov, R. R., Kamenskii, M. I., Potapov, A. S., Rodkina, A. E., & Sadovskii, B. N. (1992). *Measures of noncompactness and condensing operators*. Operator Theory: Advances and Applications, 55.
10. Banaś, J., & Lecko, M. (2001). Solvability of infinite systems of differential equations in Banach sequence spaces. *Journal of Computational and Applied Mathematics, 137*, 363–375.
11. Mursaleen, M. (2003). Some geometric properties of a sequence space related to ℓp. *Bulletin of the Australian Mathematical Society, 67*, 343–347.
12. Mursaleen, M., & Mohiuddine, S. A. (2012). Applications of measures of noncompactness to the infinite system of differential equations in spaces. *Nonlinear Analysis: Theory, Methods & Applications, 75*(4), 2111–2115.
13. Mursaleen, M., & Alotaibi, A. (2012). Infinite system of differential equations in some spaces. *Abstract and Applied Analysis*. Hindawi. Article ID 863483, 1–20.
14. Banaś, J., & Mursaleen, M. (2014). *Sequence spaces and measures of noncompactness with applications to differential and integral equations*. Springer.
15. Aghajani, A., Mursaleen, M., & Haghighi, A. S. (2015). Fixed point theorems for Meir-Keeler condensing operators via measure of noncompactness. *Acta Mathematica Scientia. Series B (English Edition), 35*(3), 552–566.
16. Aghajani, A., & Pourhadi, E. (2015). Application of measure of noncompactness to ℓ1 solvability of infinite systems of second order differential equations. *Bulletin of the Belgian Mathematical Society—Simon Stevin, 22*(1), 105–118.
17. Alotaibi, A., Mursaleen, M., & Mohiuddine, S. A. (2015). Application of measures of noncompactness to infinite system of linear equations in sequence spaces. *Bulletin of the Iranian Mathematical Society, 41*(2).
18. Mohiuddine, S. A., Srivastava, H. M., & Alotaibi, A. (2016). Application of measures of noncompactness to the infinite system of second-order differential equations in ℓp spaces. *Advances in Difference Equations*, 317.
19. Mursaleen, M., & Rizvi, S. (2016). Solvability of infinite systems of second order differential equations in c0 and ℓ1 by Meir-Keeler condensing operators. *Proceedings of the American Mathematical Society, 144*(10), 4279–4289.

20. Srivastava, H. M., Das, A., Hazarika, B., & Mohiuddine, S. A. (2018). Existence of solutions of infinite systems of differential equations of general order with boundary conditions in the spaces c0 and ℓ1 via the measure of noncompactness. *Mathematical Methods in the Applied Sciences, 41*(10), 3558–3569.
21. Smirnov, S. (2019). Green's function and existence of solutions for a third-order three-point boundary value problem. *Mathematical Modelling and Analysis, 24*(2), 171–178.
22. Srivastava, H. M., Das, A., Hazarika, B., & Mohiuddine, S. A. (2019). Existence of solution for non-linear functional integral equations of two variables in Banach algebra. *SIGMA. Symmetry, Integrability and Geometry: Methods and Applications, 11*(5), Article ID 674.
23. Saadati, R., Pourhadi, E., & Mursaleen, M. (2019). Solvability of infinite systems of third-order differential equations in c0 by Meir–Keeler condensing operators. *Journal of Fixed Point Theory and Applications, 21*(2), 64.
24. Banaei, S., Mursaleen, M., & Parvaneh, V. (2020). Some fixed point theorems via measure of noncompactness with applications to differential equations. *Journal of Computational and Applied Mathematics, 39*, 1–12.
25. Mehravaran, H., Kayvanloo, H. A., & Allahyari, R. (2022). Solvability of infinite systems of fractional differential equations in the space of tempered sequence space mβ(ϕ). *International Journal of Nonlinear Analysis and Applications, 13*(1), 1023–1034.
26. Sapkota, N., Das, R., & Savapondit, S. (2023). Consistency of an infinite system of third order three-point boundary value problem in the bv0 space by the theory of measure of noncompactness. *Boletín de la Sociedad Paranaense de Matemática, 41*, 1–10.
27. Das, R., Sapkota, N., & Savapondit, S. (2023). Solvability of an infinite system of three-point BVP in c0 and ℓ1 spaces using measure of noncompactness. *Asian-European Journal of Mathematics, 16*(10), Article ID 2350190, 1–18.

**Research and Reviews in Mathematical and Statistical Science**
**(ISBN: 978-81-69967-27-3)**

## About Editors



Dr. Chakrala Sreelatha is an academician and researcher in Statistics, serving as Assistant Professor and Head of the Department of Statistics at Rajendra University, Balangir, Odisha. She holds M.Sc., MBA, and Ph.D. degrees. Her research interests include Queueing Theory, Biostatistics, Operations Research, Multivariate Analysis, and Stochastic Processes. She has teaching experience at undergraduate and postgraduate levels, covering Probability, Statistical Inference, Regression Analysis, Econometrics, Demography, and Operations Research. She is proficient in R, SPSS, SAS, STATA, C, and C++. Dr. Sreelatha pursues research and supervises two Ph.D. scholars in Queueing Theory, while guiding undergraduate and postgraduate dissertations. She has published 20 research papers in journals, including Scopus-indexed publications, focusing on queueing models and applied statistics. She has participated in conferences, workshops, and faculty development programmes and delivered invited lectures. She served as a Project Scientist at ICMR's NCDIR. Achievements include a UGC fellowship, the Young Achiever Award, and two published patents.



Dr. Sudha Bishnoi is an Assistant Scientist (Statistics) in the Department of Mathematics and Statistics at Chaudhary Charan Singh Haryana Agricultural University, Hisar, Haryana, India. She holds M.Sc. and Ph.D. degrees in Statistics from the same university, completing her doctorate in 2020. She subsequently served as Project Scientist-C at the Indian Council of Medical Research's National Centre for Disease Informatics and Research, Bengaluru, and as a Research Associate at the India Meteorological Department, New Delhi, in 2023. She qualified the ICAR-NET in Agricultural Statistics in 2019. Dr. Bishnoi has published research papers, articles, and book chapters. She has participated in national and international training programmes, seminars, and conferences. Her research interests include multivariate analysis, regression analysis, statistical genetics, and machine learning. Her academic and professional experience reflects her commitment to statistical research and its applications.



Dr. Paban Dhar is an Assistant Professor in the Department of Mathematics at Karimganj College, Sribhumi, Assam. He holds M.Sc. and Ph.D. degrees, along with a Postgraduate Diploma in Computer Applications (P.G.D.C.A.). His academic specialization is Applied Mathematics, with research interests primarily focused on Fluid Dynamics, particularly the study of Newtonian and Non-Newtonian fluids. His research explores important aspects of fluid behaviour and its mathematical applications. Dr. Dhar has published more than 15 research papers in reputed journals, contributing to the advancement of knowledge in applied mathematics and fluid mechanics. He is also actively associated with professional academic organizations and serves as a life member of the Indian Science Congress and the Assam Academy of Mathematics. Through his teaching, research, and professional engagements, he contributes to mathematics education and promotes scholarly activities in his field of specialization.

Bhumi Publishing

Bhumi Publishing,
Kolhapur, Maharashtra, India
bhumipublishing@gmail.com
www.bhumipublishing.com

ISBN 978-81-69967-27-3
9 788169 967273